

# ***POLITECNICO DI TORINO***

## ***Master's degree in Mechanical Engineering***

Mechanical, Aerospace, Automotive and Production Engineering Department



## ***Experimental analysis and modelling of a suspension test bench***

### **Supervisors:**

*Vigliani Alessandro  
Galvagno Enrico  
Vella Domenico Angelo*

### **Candidate:**

*Margherita Petrolo*

*Torino, 26 Luglio 2021*

# Index

Index.....	1
Abstract .....	2
Introduction.....	3
1. Suspensions.....	5
1.1 Suspension's introduction .....	5
1.2 Suspension's classification.....	7
1.3 Suspension's parameters analysis .....	8
1.4 Characteristic angles.....	9
1.5 Double-wishbone suspension.....	14
2. Test bench overview .....	15
2.1 Hardware overview .....	15
2.2 Software overview .....	17
2.2.1 Code analysis .....	17
2.2.2 Data acquisition.....	17
3. Test bench analysis .....	18
3.1 Test plan.....	18
3.2 Test analysis.....	19
3.2.1 First tests: proofs at different steering angles – parameters in reference condition.....	23
3.2.2 Second tests: proofs at different spring potentiometer positions in vertical direction.....	30
3.2.3 Third test: proofs at different spring potentiometer positions in longitudinal direction...	34
3.2.4 Fourth test: proofs at different mounting position .....	38
4. MSC/Adams car.....	50
4.1 Assembly system set-up.....	51
4.2 Simulation parameters.....	57
4.3 Simulation set-up .....	58
4.4 Original vs modified suspension behaviour.....	62
4.5 Simulation's results.....	68
4.6 Roll centre influence .....	73
5. Choice from catalogue for the construction of an electric motor .....	78
5.1 Introduction.....	78
5.2 Electric motor.....	79
6. Conclusions.....	88
7. Reference .....	89

## Abstract

A suspension test bench is used to simulate the behaviour of a real front double-wishbone suspension tested under wheel centre travel along the vertical direction. Different tests were performed by modifying some parameters, allowing to understand the reaction of the suspension in terms of camber, caster, and steer angles.

The acquisition and analysis of the data is obtained by means of the software “*poliTO suspension test bench*”, implemented on Matlab. It is a code that can give as output the wheel centre position and angles behaviour, both as a function of time and wheel centre displacement. The obtained results were then post-processed, analysed and compared to one another and with the theoretical values computed by means of MSC/Adams Car. This latter is a multibody environment which enables the simulation of bodies in a dynamic field, allowing to act on different parameters and using several inputs. The outputs are available both as plots and numerical data, which were later postprocessed on Matlab.

To have clearer ideas about the behaviour of the suspension, MSC/Adams Car shows it also by means of animations.

Once the reliability of the model was confirmed on some fronts, other tests, which could not be conducted on the test bench, were carried out exclusively on MSC/Adams Car. These tests were aimed to find the best inclination of the steering tie-rod for which the steer angle variation is reduced as much as possible.

The final step provides a feasibility study on the design of an electric motor. The goal is to replace the manual work done to handling the jack that rises the suspension, allowing to have a smoother and more regular wheel travel. Furthermore, it would improve the repeatability of the tests, by maintaining unvaried the starting and the ending points and by carrying out tests always with the same velocity.

The results show that the geometry of the suspension replicated on the test bench leads to have a non-optimal camber angle values but, on the contrary, a good behaviour in terms of caster angle. Concerning the steer angle, the geometry that leads to an improvement was found.

## Introduction

The purpose of this thesis is to analyse the behaviour of a real front *double wishbone suspension* from a Sport-Utility Vehicle [1]. Therefore, to introduce this topic, there is a summary about suspensions, about their usefulness and their different geometries. Since the design and the development of the suspensions are related to the study of the kinematics of the mechanism which the suspension is based on, there is also an analysis about the parameters that characterize them, i.e., spring stiffness, suspension stiffness, installation ratio and roll stiffness.

Suspensions are components that link the sprung masses with the unsprung ones, being the first ones the parts supported by springs, and the second ones parts that move up and down following the movement of the wheels over bumps, rebounds, steps, potholes, and other kind of obstacles. Sprung masses therefore include the chassis, the motor, the interior, the body, and the passengers, while unsprung masses account for wheels, tires, differential, brakes and all the other things that are directly linked to the wheel. Suspensions are chosen based on compromise between the needs of road holding, comfort and, most importantly, safety. To improve comfort means to reduce vibrations, noise, and road sickness, which can be uncomfortable for human body. The ride must be smooth, the driver and the passengers should not feel every road irregularity, neither car should tilt right and left. Furthermore, braking must not be noisy, and suspensions should ensure continuous steering wheel adjustment. All these characteristics are analysed when choosing one suspension over another.

There are different types of suspensions:

- Air suspensions, which functionality is based on the ability of the air to be compressed. The big advantage of these suspensions is that air pressure can be modified, by making it more rigid and quicker in response [2].
- Hydropneumatics suspensions, like the previous ones but controlled by means of oil [2].
- Hydraulic suspensions, which operation is based on the use of an incompressible liquid and rubbery containers which, by expanding, absorb shocks [2].
- Elastomer suspensions, which use materials with elasticity properties, like rubber [2].
- Coil spring suspensions, with torsion springs often associated with a shock absorber [2].
- Leaf spring suspensions, where the elastic means are the leaf springs themselves [2].
- Torsion bar suspensions, in which the energy is dissipated by means of a transverse or longitudinal bar [2].

For this thesis, the choice to deal with the behaviour of the suspensions was mainly driven by the fascination for cars and curiosity towards the laws of mechanics that govern them. Moreover, this study is important to understand how, for a certain input, the output changes according to certain parameters. In this way, it will be possible to optimize these components more and more, obtaining increasingly satisfactory results in terms of comfort and safety.

The objective of this thesis is therefore to find the parameters that most influence the camber, the caster, and the steering angles as a consequence of the displacement of the wheel centre along the z-axis.

To do this, two approaches are followed: experimental and virtual tests.

For the first ones, a test bench is used, which, by means of a software implemented on “Matlab”, allows the collection and analysis of data. Different quantities (the displacement of the wheel centre in the three spatial dimensions, the steering angle, the caster and camber angles and the spring motion ratio) are represented both in dependence of the time and of the wheel centre displacement in vertical direction.

Regarding the modelling approach, instead, the simulations are done using MSC/ Adams Car, which is a software that allows to reproduce the geometry of individual car components, both standalone or integrated in a system, leading to the construction of a full vehicle model. It is possible to change not only the geometry but also several parameters (material, encumbrance, mass, inertia, etc.), as well as the inputs, leading to run simulations that represents reality in the best possible way.

The various points are faced in six chapters, organized as follows:

- The first chapter includes an excursus about the suspensions, which are seen from a generic point of view in the first part, and then described more in detail, focusing on the main parameters, also by using mathematical relations. Later, the attention focuses on the suspension under analysis, the double-wishbone, describing its geometry and its advantages and disadvantages.
- The second chapter describes a detailed model of the test bench, both in terms of hardware and software, explaining which components the bench is made of, and how to perform the tests and to acquire data.
- The third chapter is dedicated to the analysis of the tests performed on the bench, by describing the procedure, the parameters chosen for each of them and the reasons behind these choices. Finally, the results and the relative plots are shown.
- To compare the numerical data with the experimental results, the fourth chapter focuses on MSC/Adams Car section, starting from the set-up of the model to the comparison between real and theoretical results.
- The fifth chapter shows the improvement that could be done on the experimental simulations by introducing an electric motor which replaces the manual work and makes tests more realistic.
- Conclusions are listed in the sixth chapter.

The goal is, therefore, to find a good correlation between experimental data and the results of the virtual simulations. In this way, once the correlation is confirmed, it is possible to modify some parameters on the virtual model and to analyse the consequent behaviour only in a virtual field, allowing the study of different geometries, looking for improvements, with the certainty of having reliable results.

# 1. Suspensions

## 1.1 Suspension's introduction

As already anticipated in the previous paragraph, a car suspension is a system of springs, shock absorbers and linkages that allow connecting a vehicle to its wheel, so that it is possible to have a relative motion between the two.

Thanks to the presence of tires, it is possible to smooth out minor irregularities in the ground. In case of significant irregularities, instead, there is a spontaneous loss of contact and consequently driving difficulties. Furthermore, failing to absorb vibrations, comfort is lost too. The latter is not a simple concept to define, since it is subjective, but it is important since it is what customers search for. From a physical point of view, it depends on the vibrations that arrive to the passengers. However, SAE (Society of Automotive Engineers), made a classification according to the frequencies [3]:

- Motion sickness:  $0.1 < \text{Hz} < 0.5$  [3]
- Ride: low frequencies  $< 5 \text{ Hz}$  [3]
- Shake: intermediate frequencies  $5 < \text{Hz} < 25$  (subsystems: cooling parts or some devices, not the whole vehicle) [3]
- Harshness: high frequencies  $25 < \text{Hz} < 100$  (components) [3]
- Noise: acoustic phenomenon  $100 < \text{Hz} < 22000$  (vibrations are heard by humans) [3]

According to the human body perception, the frequencies between 4 Hz and 8 Hz is troublesome. The ISO 2361 divides vibrations according to the frequency range and according to what they cause. Frequencies in the range between 0.5 Hz and 80 Hz cause discomfort and fatigue, while frequencies between 0.1 Hz and 0.5 Hz can cause motion sickness.

As shown in the following picture, not only the exposure time and the frequency are problematic, but also the acceleration the human body is subjected to.

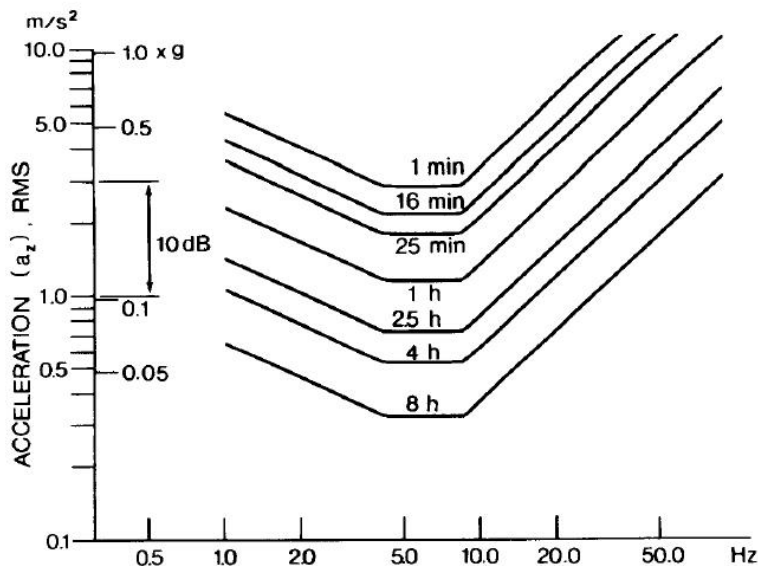


Figure 1.1.1 - Physical efficiency as a function of the acceleration and of the frequency [3]

Natural frequencies of both sprung and unsprung masses should stay far from the frequencies which provoke discomfort. Lower natural frequencies are due to sprung masses and should be between 1 Hz and 4 Hz. Unsprung masses are instead linked to higher natural frequencies, which must be higher than 10 Hz.

The sources of vibrations can be:

- External = roughness of the road profile, wind, aerodynamics [3]. In detail, the road profile is the responsible of the vertical load that the road applies to the tire. The higher is its variation, the lower is the ability to develop forces in longitudinal and lateral direction.
- Internal = wheels, ICE, cooling devices, bears. These components lead to vibrations because of imbalance. The engine contributes largely with the driving torque variation and the inertial forces of the rotating parts. [3]

All these problems compromise drivability and therefore suspensions were developed.

The idea was to separate the sprung mass (including the chassis, the motor, the interior, the body, and the passengers) which remains rigid, from the unsprung mass (composed by wheels, tires, differential, and brakes). The latter supports the irregularities of the ground without losing adhesion.

The main tasks of the suspensions are the following:

- To allow the vehicle to follow the road profile without losing grip, through the development and the transmission of longitudinal forces, during acceleration and braking, and lateral forces when cornering.
- To increase comfort, handling, and safety, by reducing vibrations and bouncing in the vertical direction.

In a few words, the first aim of the suspension system is to exchange static and dynamic forces with the ground.

However, the two points listed above are in contradiction from a technical and design point of view. For example, one of the main parameters is the spring stiffness, which should be reduced to increase comfort, in such a way that the natural frequency of the vehicle is small compared to the excitatory frequency dictated by the irregularity of the ground. The downside is that spring stiffness reduction leads to instability problems [3].

The choice of spring stiffness is therefore usually the result of a trade-off between comfort and performance. It is therefore necessary to differentiate the design of the suspension basing on the use for which the vehicle is intended to.

For this reason, there are different types of suspensions, and the choice is mainly based on spring stiffness and on the damping capacity [3].

## 1.2 Suspension's classification

From a kinematics point of view, frontal suspensions can be classified as:

- Wishbone suspensions: they are composed by some transversal elements, each of which is called *wishbone*. To keep the suspension in position there are also a spring and a damper, linked to the lower arm. Between the two wheels there is a roll bar and a steering axle, linked to the steering mechanism [3]. The suspension analysed in this thesis, the *double wishbone*, belongs to this category. According to the distance between the two arms, they are distinguished in high and low quadrilateral. This kind of suspension is often used in sports vehicles [2].
- Mac-Pherson suspensions: its main characteristics is that the upper arm is replaced by the shock absorber, which has also a structural task since the entire load passes through it [3]. To reduce the hysteresis and so to improve the comfort, the damper and the spring are not coaxial, but they create a small angle which leads to a reduction of the shearing stresses [2].
- Sliding suspensions: in this type of suspensions, the wheels slide on a support connected to the chassis by means of a rigid constraint [2].

Rear suspensions can also be classified according to the kinematics of the elements:

- Rigid axle suspensions: in these suspensions there is a rigid bar connecting the differential and the two wheels [2].
- “Ponte de Dion” suspensions: they have semi-independent wheels, and the axle acts as anti-roll bar. Its advantage is the ability in reducing the unsprung masses [2].
- Torsion bar suspensions: they have two longitudinal arms connected one each other by means of a tube and also linked to the chassis [2].
- Longitudinal wishbone suspensions: they are composed by two arms, parallel to the longitudinal axis, each of them connected to one wheel and both connected to the body by means of a hinge. Between the arms and the body there are the spring and the damper [2].
- Transversal wishbone suspensions: the difference in respect to the previous one is that they develop transversally and that they are connected to the vehicle centre [2].
- Multilink suspensions: there are at most five arms, each of them constraining one degree of freedom of the wheel, allowing only the movement in the vertical direction [2].

From a kinetic point of view, instead, suspensions are in general classified as:

- Independent: each wheel is linked to the chassis with linkages that allow only 1 degree of freedom.
- Rigid axle: the two wheels of the same axle are rigidly connected and linked to the chassis with a 2 degrees of freedom mechanism.

### 1.3 Suspension's parameters analysis

According to the geometry of the system, there is a correlation between the stiffness of the spring and the stiffness of the suspension. In detail, indicating with  $\Delta z$  the deformation of the suspension and with  $\Delta x$  the spring deformation, it is possible to define the *installation ratio*,  $IR$ , which represents the ratio between how much the spring and damper move with respect to the wheel displacement. So, it follows [3]:

$$IR = \frac{\Delta x}{\Delta z} \quad (1.3.1)$$

It allows to understand the amount of deflection the spring and the damper will be subjected to as a consequence of any displacement of the wheel [3].

By defining the *suspension stiffness*,  $K_S$ , and the *spring stiffness*,  $K^*$ , they are related as below [3]:

$$K_S = K^* \cdot IR^2 \quad (1.3.2)$$

The latter equation highlights the correlation between the stiffness of the spring and the stiffness of the suspension, which is an important characteristic [3].

The suspension geometry also influences the *roll centre*, which is the point at which the cornering forces meet the reaction of the vehicle body. It is therefore possible to describe the *roll motion* as the angular displacement of the car around the roll centre, and, consequently, around the roll axis, which is, in general, not parallel to the ground.

By defining the *roll stiffness*,  $K_R$ , it can be found that, as shown by the following equation, it is a function of the suspension stiffness and of the track,  $t$ , of the vehicle. In detail [3]:

$$K_R = K_S \cdot \frac{t^2}{2} \quad (1.3.3)$$

Usually,  $K_R$  is a small quantity, hence the roll angle would be large under certain lateral accelerations. To avoid this, the roll stiffness can be increased by means of an additional component, the *roll bar*, which acts as a torsional spring [3].

## 1.4 Characteristic angles

Suspension geometry is characterized by four characteristic angles: *toe angle*, *camber angle*, *caster angle* and *king-pin angle*. The first two parameters are useful to describe the wheel position (with no steering angle) with respect to the ground, while the last ones spot the position of the steering axis with respect to the ground [4].

- *Toe angle*, showed in figure 1.4.1, is the angle that each wheel spots with the longitudinal axis of the vehicle, from the upper point of view [4]. It is the static steer angle. It is symmetric, and it can be positive, nil, or negative. Its value should be low, otherwise there would be a steering opposition between right and left wheel. This would lead to an increase in roll resistance and to a higher tyres wear. It is used to improve braking stability and handling of the vehicle since it enhances the response while cornering [5]. Toe-in angle on the rear axle will reduce the oversteer on exit and causes a slip angle, which increases the grip on a straight line. Furthermore, it improves the ability of tyre to transmit torque to the ground. On the other hand, rear tyres will suffer more for heat and wear. Also toe-in on the front axle increases stability on a straight line since, if there would be an outward steering of the wheel, this would lead to a straightening of the wheel and to develop zero toe. In this way the vehicle will continue going straight on. On the other hand, because of the toe-in, the vehicle will be less responsive while cornering.

This problem can be solved with the Ackerman angle steering geometry.

Toe angle variation because of vertical wheel travel is measured with the *bump steer*. Instead, *roll steer* refers to a toe angle variation caused by a roll angle. If bump steer is positive, the bumping motion of the suspension, leads to a toe-in tendency. The other way around, if bump steer is negative, there will be a toe-out tendency. Generally, bump steer is positive in the front axle and negative in the rear one. If the wheel centre is subjected to a longitudinal force, there will be a toe variation. This variation is measured with the *traction steer*. In the ideal scenario, it should be small but, since it is related to braking steer, which has the priority, this is not always possible.

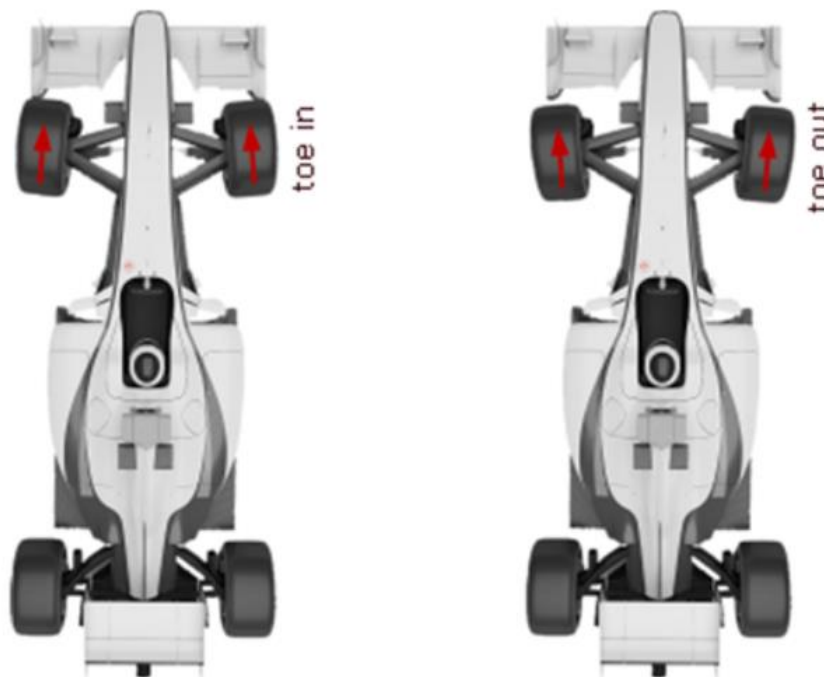


Figure 1.4.1 – Toe angle [4]

- *Camber angle*, showed in figure 1.4.2, is the angle between the plane on which the wheel rolls and the vertical axis of the vehicle, when viewed from the front or from the rear view. Ideally, the suspension should allow wheel movement only in vertical direction without variation in toe and camber angles. On the other hand, the roll angle changing leads to a camber angle variation. As it would be advisable not to have variation of these angles, it is appropriate to consider camber recovery to compensate the roll angle.

Camber angle can be positive, neutral, or negative. Its aim is to improve the adherence. During the driving, this angle changes a lot because of suspension and steering movement [4]. If it is equal to zero, when going on a straight line, forces on the tyres are symmetrically distributed. This leads to a higher grip when accelerating or braking. While cornering, instead, zero camber leads to an unequal distribution of the load on the tyres and a consequent loss of grip. If it is negative, instead, there is an opposite situation. There is not an equal load distribution when going straight on, but a better grip on the external tyres when cornering. This latter situation is preferable in respect to the previous one. For this reason, its value is generally negative and on passengers' vehicles it is between -0.5 degrees and 1.5 degrees [5]. The downside of a negative camber is, however, more degradation, unequal wear of the tyre and additional heat.

It is one of the key parameters which influence tyre performances, and it is the result of a combination between static camber, bump camber, camber compliance and steering geometry [5].

*Bump camber* is the camber variation because of wheel travel. It is always negative since it is the result of the negative camber which a wheel is subjected to during bouncing. It is useful because thanks to it, it is possible to recover the loss a tyre camber is subjected to when cornering. So, adding bump camber improves cornering ability of a vehicle. On the other hand, it cannot be too much higher since it can compromise performances during traction and braking [5].

*Camber compliance*, instead, expresses the reliability of a suspension when it is subjected to lateral forces in the contact point between tyre and ground, during cornering. The lower its value is, the lower camber variation is. Low camber compliance means high contact patch stiffness, and this is an important aspect for the front axle, because it ensures the steering feels [5].



Figure 1.4.2 – Camber angle [4]

- *Caster angle*, showed in figure 1.4.3, is the angle identified by the steering axis and the vertical one, from a lateral point of view. It can be positive, nil, or negative. It highlights how quickly the wheel will recover the straight position [4]. This angle influences the camber angle. If it is positive, when cornering, the outside wheel will gain negative camber and the opposite wheel will lose it. It is a benefit, because in cornering the outside wheel is the one with the higher load and a more negative camber will improve cornering capacity [5]. Its optimal range is  $+3 \div +5$  degrees, values for which the vehicle shows a better driving feeling. Anyway, if it is too high, turning becomes harder and camber angle assumes excessive values. Caster angle variation because of wheel travel gives as result the *bump caster*. Each suspension has a *caster pole*. On a double wishbone suspension, it is the point in which two planes going through the upper and the lower control arms intersect. Bump caster is the consequence of a rotation of the wheel around the caster pole.

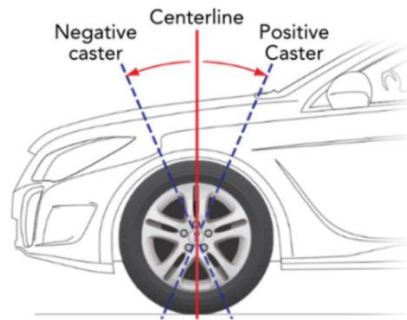


Figure 1.4.3 – Caster angle [4]

- *King-pin angle*, showed in figure 1.4.4, is the angle that the suspension steer axis spots with respect to the vertical one, in a frontal point of view. On a double-wishbone suspension, kingpin axis is the line that connects ball joints of the lower and the upper control arms. By increasing the king-pin angle, it increases also the returnability of the wheel, which is its ability in self-centring while driving. So, the response of the strut in taking back the wheel in straight position depends on it [5]. This angle must be small since also the camber angle is related to it, giving a positive contribute while curving [4].

The distance between the centre of the tyre and the steer axis is the so-called *scrub radius*. It is the arm for forces during braking. If it is positive, while braking, there will be a toe out tendency on the front wheels. If braking takes place when cornering, the positive scrub radius will lead to a better stability because of the understeer effect. A negative scrub radius, instead, would improve stability when braking forces are not equally distributed between the two wheels. In this scenario, the vehicle will tend to turn toward the wheel which is braking more. The negative scrub radius will counteract by increasing stability.

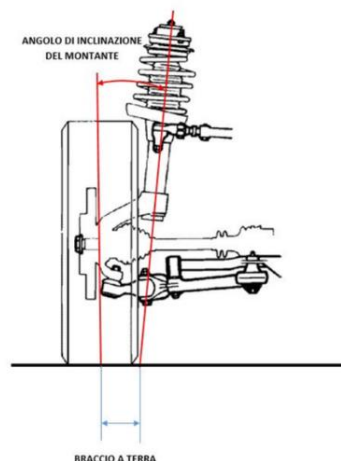
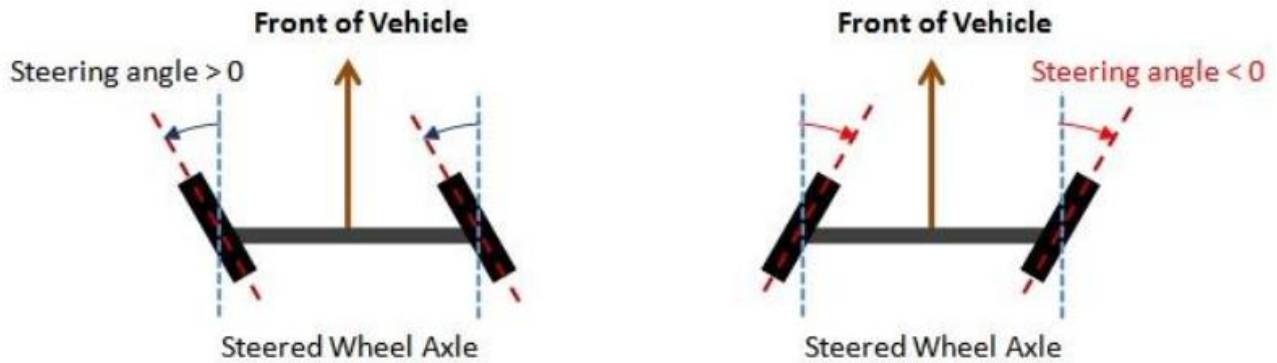


Figure 1.4.4 – King-pin angle [4]

Another important parameter is the *steering angle*, which is the angle between the wheel direction and the front of the vehicle. It is present in the front wheels while in the rear ones, instead, it is negligible [3].



Definition of Steering Angle

Figure 1.4.5 – Steering angle [6]

The ratio between this angle and the toe angle variation is called *steering ratio*. In other words, it is the ratio between the degrees of rotation of the steering wheel and the degrees the wheel turns consequently. In passenger's cars its value ranges between 12:1 and 20:1 and it depends on the suspension geometry. If it is high, it is necessary to turn more the steering wheel to rotate the wheels, but rotation is easier. The other way around, if it is low, rotation is harder, but the steering wheels should be turned less. Since it is not always easy to find a good trade-off, it is possible to use a variable-ratio steering system. Thanks to its geometry, if the steering wheel is not rotated, steering is less responsive, therefore it is harder to oversteer. When the wheel instead is turned, it becomes more sensitive [7].

When cornering, suspensions are subjected to lateral load in the contact point. This causes the generation of a self-steer. *Compliance steer* is the value of how much self-steer is induced when cornering. It is related to the *camber compliance*. Between the two, when designing a suspension, the choice usually is in favour of compliance steer since it is preferable for safety. This choice penalises the handling and the agility [5].

The same situation is also caused by braking load. It means that also when braking there is a certain amount of self-steer, and it is measured with the so-called *brake steer*. It is related to the traction steer, and, since its aim is to ensure the stability of the car when braking, the priority is to always have an understeer behaviour.

Ackerman steering condition:

Supposing that the vehicle is cornering to the left and so that the front-left wheel is nearer than the front-right wheel to the zero-velocity centre, identified with  $O$ .

By identifying as  $\delta_1$  the steering angle of the front-left wheel and as  $\delta_2$  the steering angle of the front-right wheel, it is possible to find the *Ackerman steering condition*. It highlights the relation between the two steering angles, the track  $t$  and the distance between frontal and rear axis,  $L$  [3]. In detail, it highlights how much the wheels rotate during cornering. These two quantities are obviously different each other since the radius of the curve spotted by the inner wheel is lower than the one spotted by the outer wheel. Therefore, the steering angle of the inner wheel should be higher than the steering angle of the outer wheel. The *Ackerman steer geometry* determines which is the correct steer angle to avoid the tires scrub.

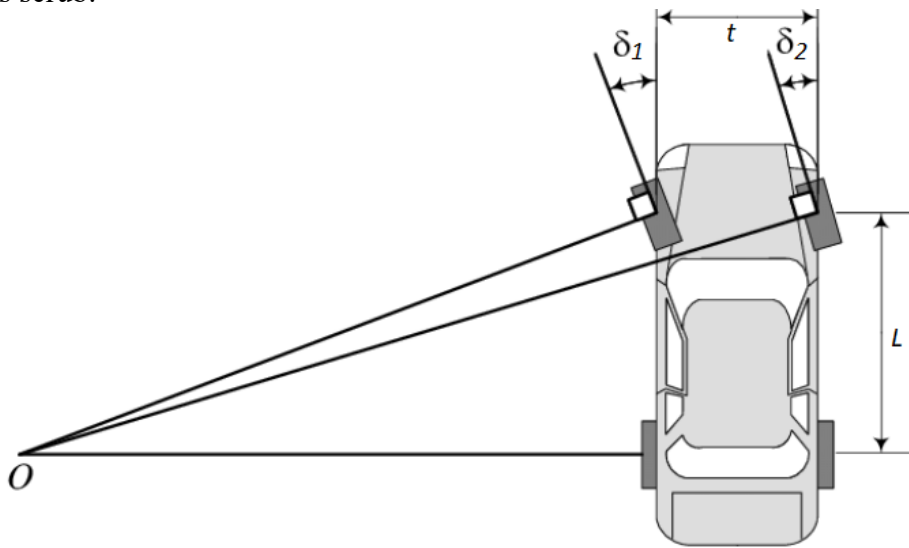


Figure 1.4.6 – Front-wheel steering vehicle and Ackerman condition [8]

As already said, this geometry is studied to avoid that the tires lose adhesion with the ground while cornering. The idea is that the axes of all the four wheels are disposed as they were the radius of circles with the same centre. Since rear wheels are fixed, and so their steering angle is equal to zero, the centre should stay on a line extending from the rear axle, as shown in the picture above [3].

$$\tan \delta_1 = \frac{L}{R - \frac{t}{2}} \quad (1.4.1)$$

$$\tan \delta_2 = \frac{L}{R + \frac{t}{2}} \quad (1.4.2)$$

$$\frac{1}{\tan \delta_2} - \frac{1}{\tan \delta_1} = \frac{t}{L} \quad (1.4.3)$$

Considering that the angles are small, it is possible to approximate, obtaining the following equation, which represents the *Ackerman steering condition*:

$$\frac{1}{\delta_1} - \frac{1}{\delta_2} = \frac{t}{L} \quad (1.4.4)$$

In production cars, Ackerman value is around 60%.

## 1.5 Double-wishbone suspension

For this thesis work, the tested suspension is a *double-wishbone suspension*, shown below.



Figure 1.5.1 – Double-wishbone suspension [1]

It belongs to the category of the independent suspensions. It consists in two wishbone-shaped arms located between the chassis of the car and the steering knuckle. Thanks to this, each wheel can act and react independently one each other. To allow movement in multiple directions, in the two control arms there are ball joints on both the ends. The vertical movement is controlled by means of the shock absorber and of the spring mounted on the suspension. By modifying the lengths between the upper and lower control arms and the relative angles, it is possible to modify the ride and the handling of the car [9].

The upper arm is usually shorter than the lower arm so that, when suspension rises, it induces a negative camber. To face up to acceleration and braking forces, both the arms are equipped with two bushings or ball joints at the chassis. To prevent issues to the anti-dive and anti-squat geometries (used to prevent the vehicle front from compressing and lifting, respectively during braking and acceleration manoeuvres), these joints must not be parallel to the vehicle centre line [10].

The main advantages of this kind of suspensions are:

- The possibility to easily tune them by acting on the joints, to optimize them under a kinematic point of view and to improve the wheel motion.
- The chance to act on some parameters like camber and caster angles.
- The geometry, which requires less space in vertical direction with respect to a standard suspension, thus allowing the lowering of the centre of gravity of the car.

On the other side, the drawbacks are that they are heavier, more complex, and more expensive than some other suspension systems.

However, it is necessary to point out that these components are not the optimal solution for all the cars. They are often used in high performance vehicles and sporty sedans, such as Alfa Romeo Giulia 952, most models of Mercedes Benz, Aston Martin DB7, and in some Formula 1 cars [11].

## 2. Test bench overview

The test bench used for this thesis work is “PoliTO Suspension Test Bench”, which contains a simplified double wishbone suspension, in which some real components are replaced with equivalent dummy elements. Inputs for starting the simulations are imposed manually, by physically moving the mounting position, the wheel orientation to modify the steering angle, the vertical wheel travel and the potentiometers which account for the spring and the damper. Outputs are then acquired by means of potentiometers and inclinometers and then post-processed using a software developed on Matlab.

### 2.1 Hardware overview

Figure 2.1.1 shows the test bench respectively in the frontal, in the upper and in the lateral view.

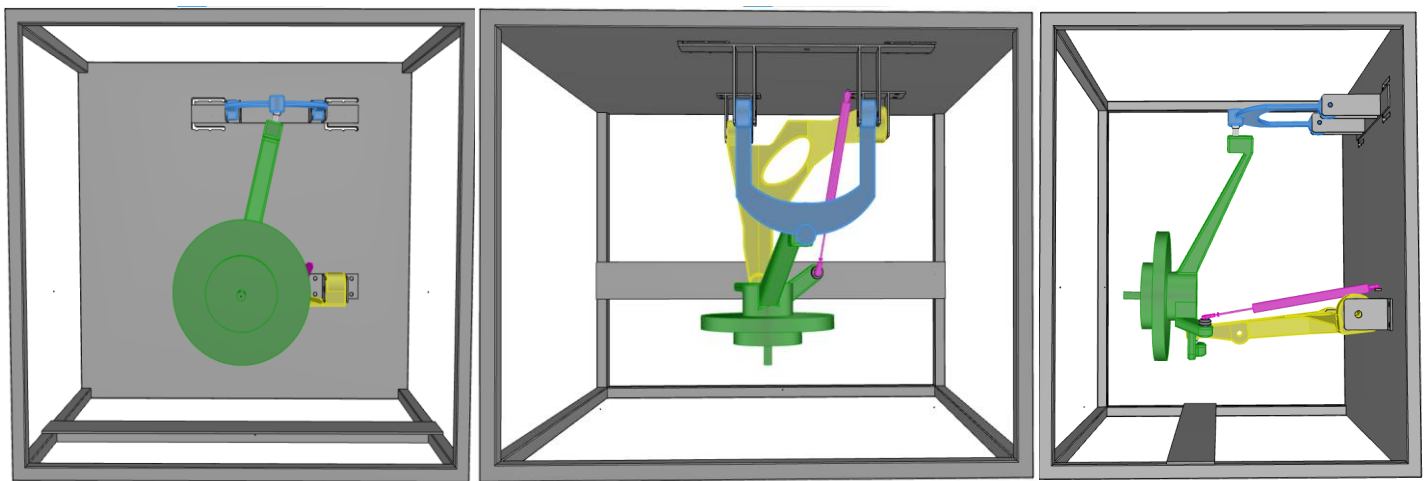


Figure 2.1.1 – Test Bench [1]

In detail, it is possible to spot the upper arm, the blue one, the lower arm, the yellow part, and the wheel connected to the support, highlighted in green.

The measurements are made by means of potentiometers and inclinometers. There are:

- 3 Micro-Epsilon potentiometers for wheel centre position measurements, with an accuracy of  $\pm 0.5$  mm [1].
- 1 Micro-Epsilon potentiometer for spring elongation measurement, with an accuracy of  $\pm 0.5$  mm [1].
- 1 steering potentiometer for steering angle measurements, with an accuracy of  $\pm 0.5$  mm [1].
- 2 SEIKA inclinometers for measuring camber and caster angles; with an accuracy of  $\pm 0.03^\circ$  [1].
- 1 National Instrument Data Acquisition Board [1].

The spring potentiometer is used to simulate the spring compression/extension. This is due to the fact that, since the suspension kinematics is not affected by the elastic element, the spring and the damper have been removed in order to avoid excessive loads on the test bench. The wheel is instead represented by a wooden disk [1].

Before starting the simulations, some preliminary operations are needed. First, it is necessary to remove the plexiglass protective panels; then the threaded feet must be adjusted to level the test bench, so that it is orthogonal to the gravity vector to have reliable results. It is also necessary to connect the test bench to a power supply (24 V DC – 0.5 A) and finally the acquisition system must be connected to a pc through an USB [1].

To best simulate the layout of the suspension and its real working conditions, the steering angle and the mounting position can be modified, as well as the spring potentiometer location. Furthermore, it is possible to add two spacers between the upper control arm and the bench. All these modifications are made by hand. To change the steering angle, it is necessary to loosen the screw present in the steering potentiometer and to turn the wooden disk. Also, for what concerns mounting position the bolt must be unscrewed so that it is possible to move the suspension upper attachment in vertical and in longitudinal direction. The spring potentiometer has, instead, a bar which can be moved left and right, up and down, and in lateral direction, so it is possible to move it in longitudinal, vertical and lateral direction [1].

To simulate the bouncing of the suspension caused by an obstacle, the wheel is moved along the vertical direction. This movement is performed by means of a jack which can rotate clockwise and counter-clockwise by respectively raising and lowering the wheel.

To make experimental and numerical simulations coherent, it is important to know reference system and angle conventions (which in the test bench follows ISO 8855-2011 convention), shown in the following figure:

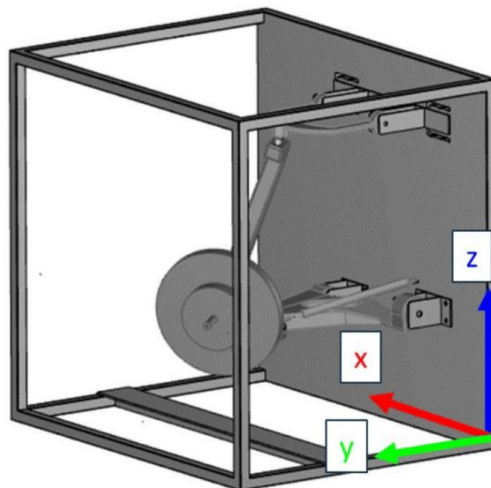


Figure 2.1.2 – Reference system [1]

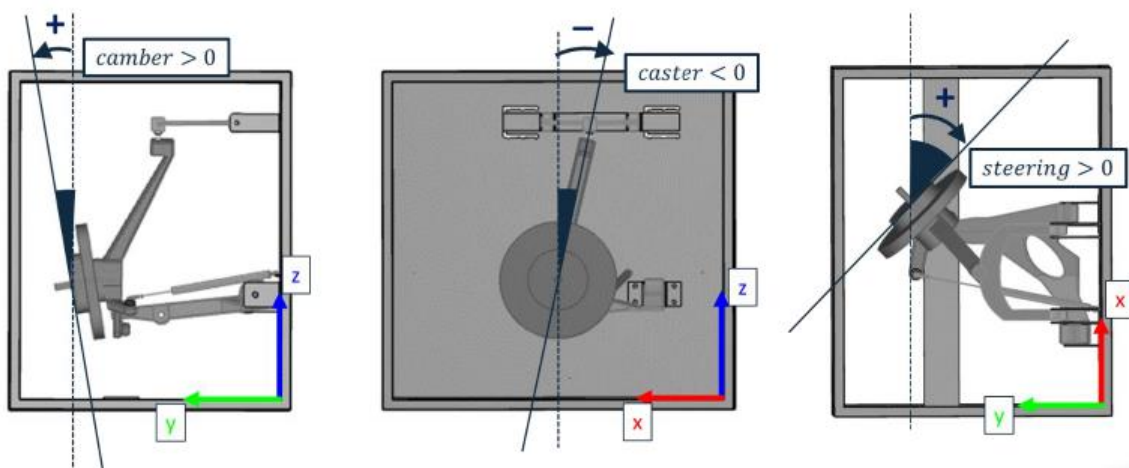


Figure 2.1.3 – Angle conventions [1]

## 2.2 Software overview

The software used, “PoliTO suspension test bench”, runs on a Graphic-User-Interface and the acquisition is made by means of a “National Instruments” acquisition system [1].

It is composed by:

- A “potentiometers measurements” section [1]
- An “inclinometers measurements” section [1]
- “Start”, “Stop” and “Save” buttons, for acquisition management [1]
- A “computed quantities” section [1]
- Time-based / Wheel-based plots [1]

The Data Acquisition occurs with a sample rate set to 20 Hz. The buffer maximum length is fixed to 20, so that the analyses and the plots of the acquired data are done with a rate of 1 s [1].

### 2.2.1 Code analysis

Signal processing occurs by means of a Matlab code structured as follows:

- A first part dedicated to the creation of the icons and the settings of the interface with the user, as well as the creation of panels and buttons for the management of the acquisition by the user. It follows a section of the code necessary for the creation of panels and tables for the 5 potentiometers and for the 2 inclinometers and a part for the creation of the tables for the computed quantities.
- An intermediate part for the data acquisition, the computation of the quantities, and the creation of the plot. Three different structures are created: *channels\_V*, *channels* and *computed*. Each of them is composed by three vectors for the wheel centre position, one vector for the spring, one vector for the steer angle, and two vectors for camber and caster angles. In the first two there is also a vector for the time. The difference between them is that the first one includes the data in terms of voltage [V], the second one in terms of millimetres [mm] and the third in terms of degrees [deg]. The conversion between one unit of measurement and the other is made by means of two functions: “fcn\_posizione\_centro\_ruota” and “fcn\_sterzo”.
- A final part for the creation of the plots, as a result of the acquisition of the data.

### 2.2.2 Data acquisition

Once everything is set up from a hardware point of view, the acquisition of the data can start. To do it, it is necessary to press the *start button* and consequently, the values measured by potentiometers are acquired by the software and organized in vectors. Acquisition continues until *stop button* is pressed. It is therefore possible both to post-process these data or to immediately have graphs representing the trend of the output parameters, both with respect to time and to the wheel travel along z direction.

### 3. Test bench analysis

#### 3.1 Test plan

As already mentioned, the tests were carried out by varying a series of parameters, choosing those deemed most relevant. In particular, the results obtained with different steering angles, mounting position and spring position were analysed.

To best develop the work, the first step was so to organize a test plan.

To do that it was established a way to immediately identify the parameters set for the tests, creating a kind of “acronyms”.

For example, the following abbreviation allows to immediately understand that the steering angle is set to zero, the mounting position is in the “E” position, the spring potentiometer position in frontal, vertical and longitudinal direction is zero, and that there are no spacers.

“SA0\_MPE\_SPf0\_SPv0\_SPI0\_DNO”

Once this was established, it was decided to modify one parameter at a time, to be able to better keep track of it, except for the steering angle which was modified for each test.

For all the tests, what was highlighted are:

- Wheel centre in longitudinal direction
- Wheel centre in lateral direction
- Camber angle
- Caster angle
- Spring position
- Steering angle

For each of them, is obtained the behaviour both with respect to time and with respect to the vertical wheel travel, but only the latter is shown in this thesis.

As regards the duration of the test, it was chosen to make an excursion along the vertical direction, equal to about 130 mm uphill and as many downhill. This decision was led by the fact that, going beyond these limits, the test bench did not respond in the correct way.

The first test was done starting from the position that was identified as the “zero reference position”, that means that steering angle, and spring potentiometers were set to zero. The mounting position was the central one, identified by the “E” and there were no spacers.

### 3.2 Test analysis

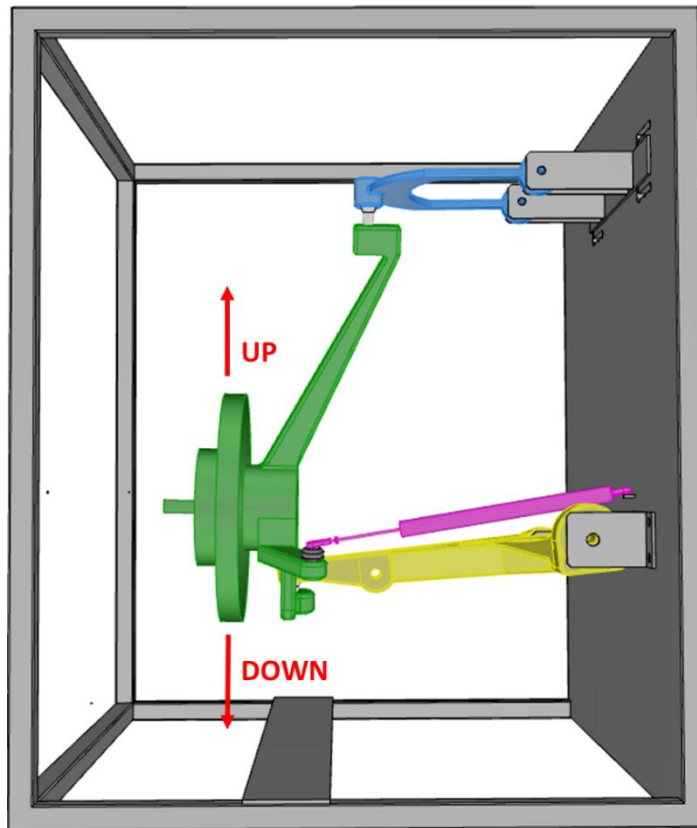


Figure 3.2.1 – Wheel movement convection

From now on, the wheel going upward (compressive stroke of the spring) will be described as “up”; whereas, the wheel going downward (extensive stroke of the spring) will be described as “down”. As can be seen from the following figure, a hysteretic behaviour of the suspension tested on the bench can be spot. Anyway, since MSC/Adams Car does not consider such behaviour, both the forward and reverse displacement of the wheel centre will be approximated to their average, thus allowing a simpler comparison between the simulated and the experimental data.

Before starting the analysis, to be sure that the tests are reliable, it was investigated about what was the correct way to set the test bench. The major doubt was if to keep loosen or not the screw in correspondence of the steering potentiometer. To this purpose, the behaviour of the steering angle was analysed in MSC/Adams, performing two different tests.

Both the tests were made with a vertical excursion of 200 mm and a parallel wheel travel motion. The starting and consequently the ending points are the only difference.

*First test:* vertical wheel centre from -100 mm to +100 mm

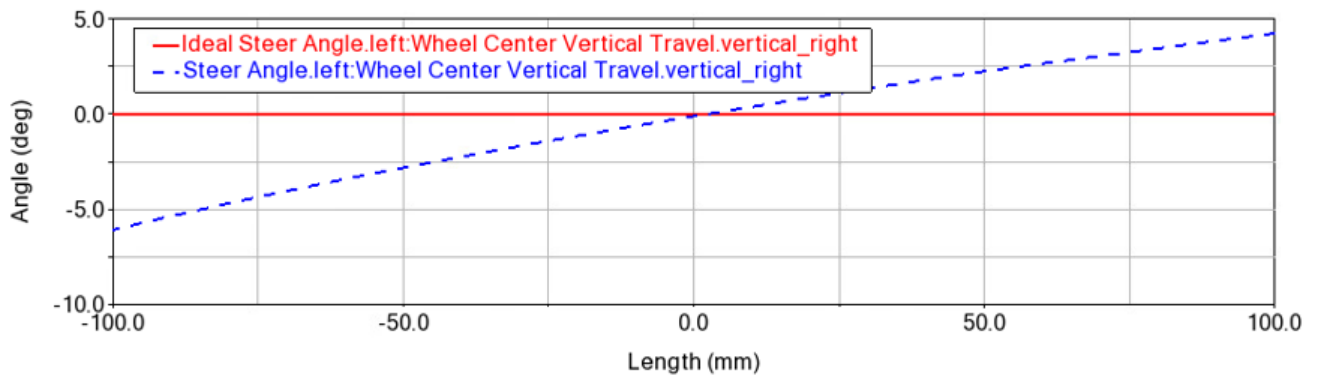


*Figure 3.2.2 - First test: steering angle behaviour*

*Second test:* vertical wheel centre from 0 mm to +200 mm

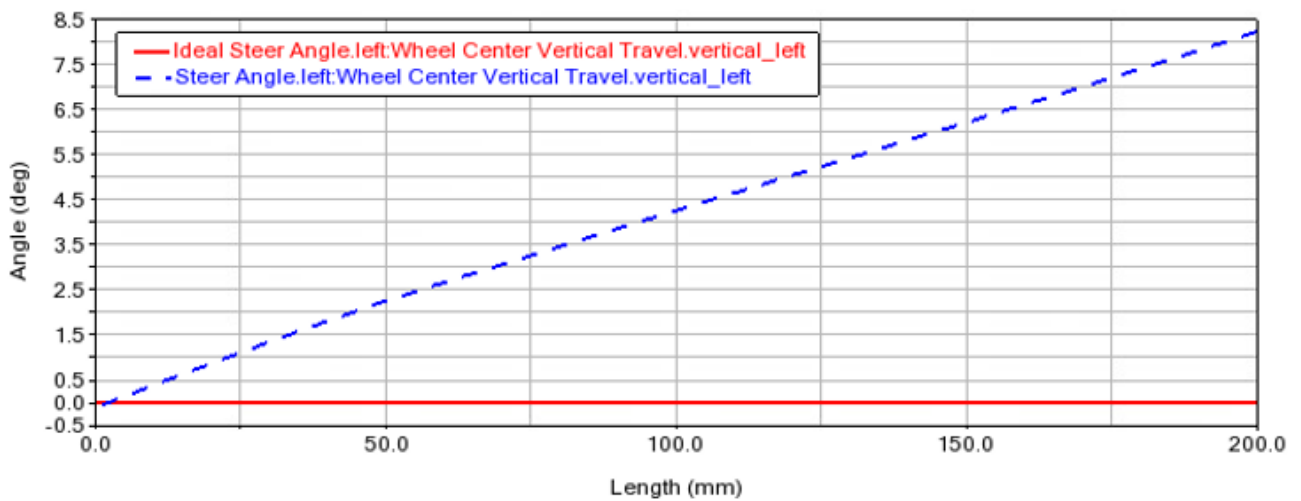


*Figure 3.2.3 - Second test: steering angle behaviour*

Both the graphs show that ideally the steering angle remains constant during all the test, but the real one changes of about 10°.

To conclude this analysis, it was also verified that the centre of mass of the internal tie rod was completely coincident with the centre of mass of the external one, in all the directions and for the entire duration of the test.

First test: vertical wheel centre from -100 mm to +100 mm

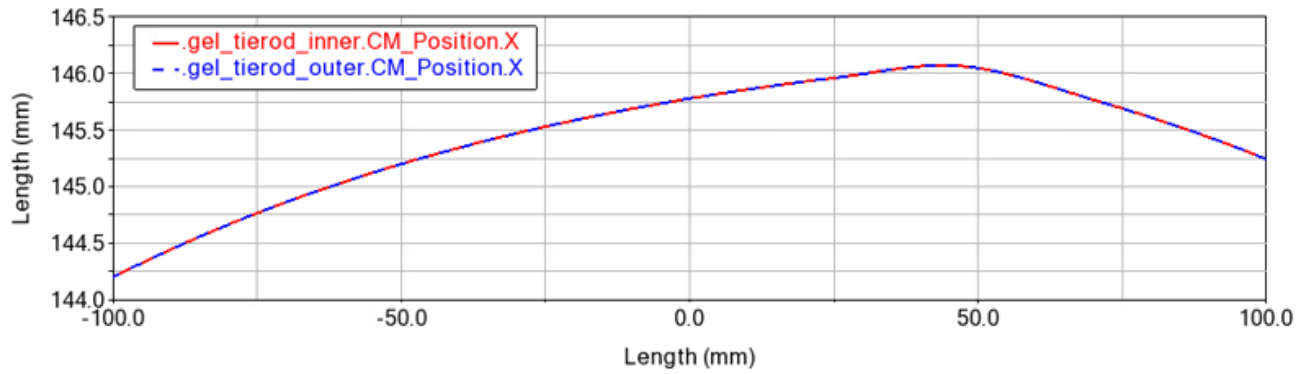


Figure 3.2.4 – First test: x CM position

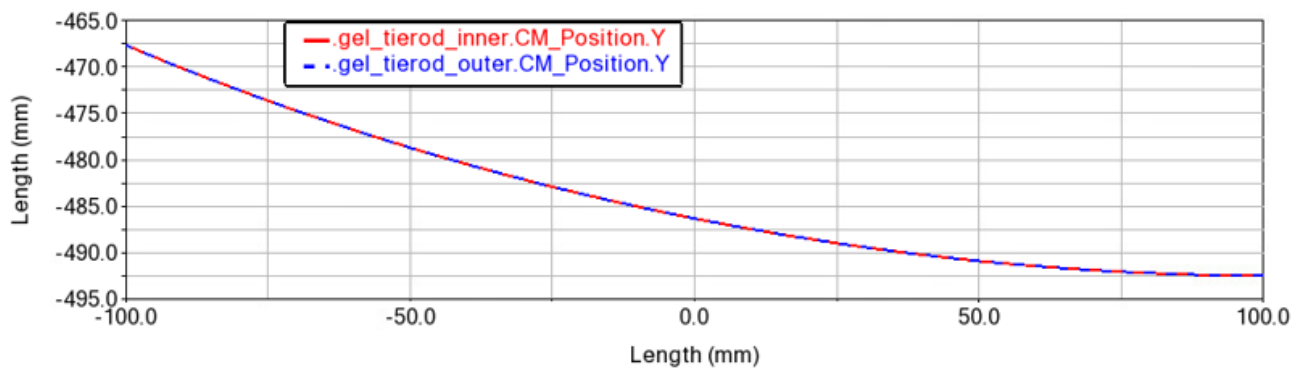


Figure 3.2.5 – First test: y CM position

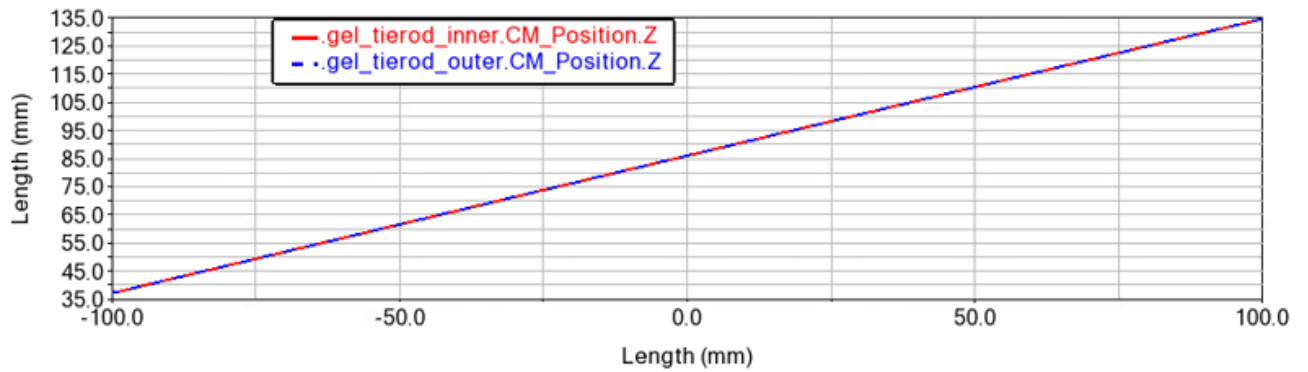


Figure 3.2.6 – First test: z CM position

Second test: vertical wheel centre from 0 mm to +200 mm

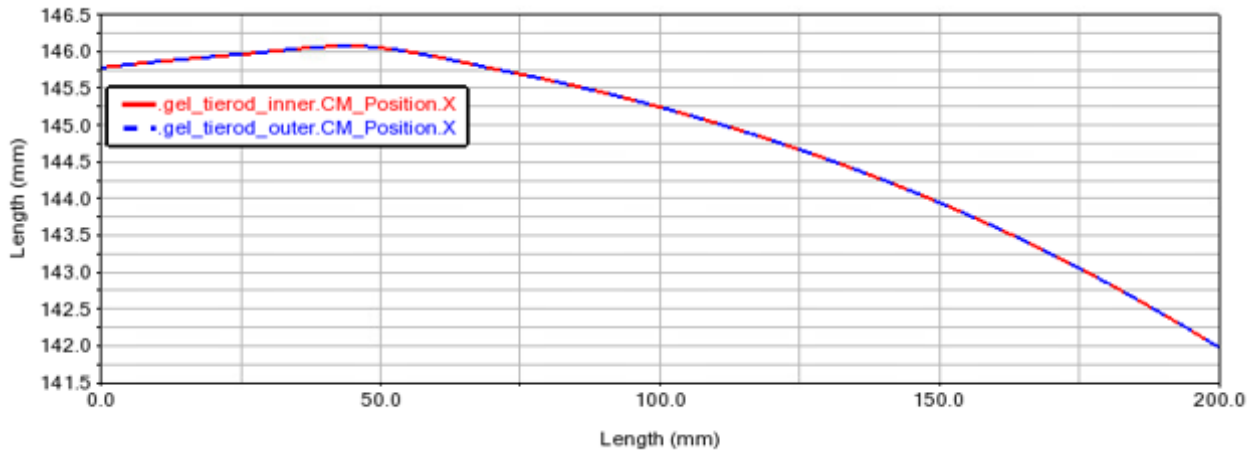


Figure 3.2.7 – Second test: x CM position

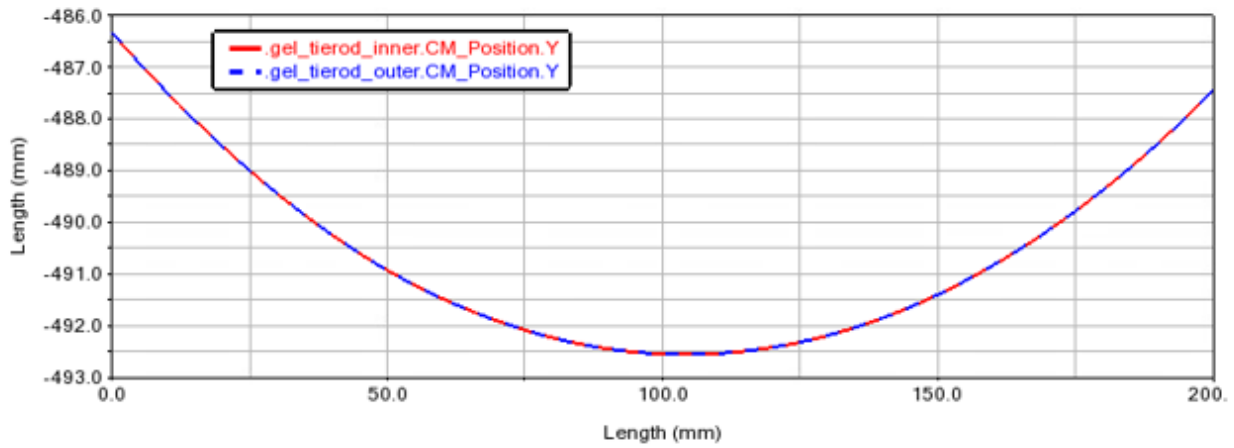


Figure 3.2.8 – Second test: y CM position

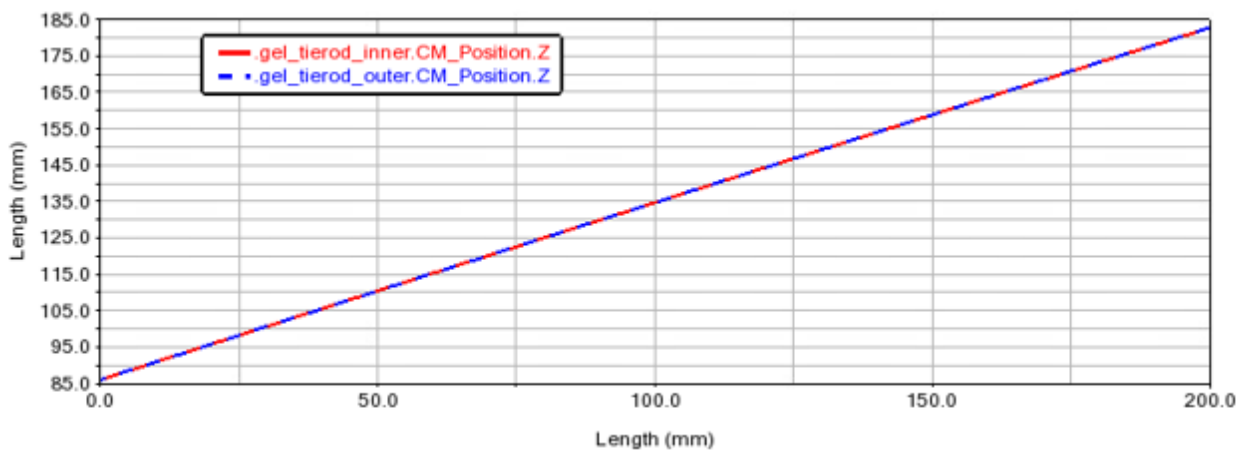


Figure 3.2.9 – Second test: z CM position

These graphs confirm that there is no relative motion between the two centres of mass, so that ideally there is no steering angle variation. The conclusion is so that the screw must not be kept loose during the test. This also ensures their repeatability.

### 3.2.1 First tests: proofs at different steering angles – parameters in reference condition

#### *Results as a function of the time*

As already anticipated, it is possible to have results both with respect to time and to vertical wheel displacement. Anyway, since vertical wheel displacement with respect to time is not a repeatable operation, being made by hand, time-dependent tests will not be reported apart from the following chart. The latest underlines the behaviour of the vertical wheel centre and how its displacement is related to the time.

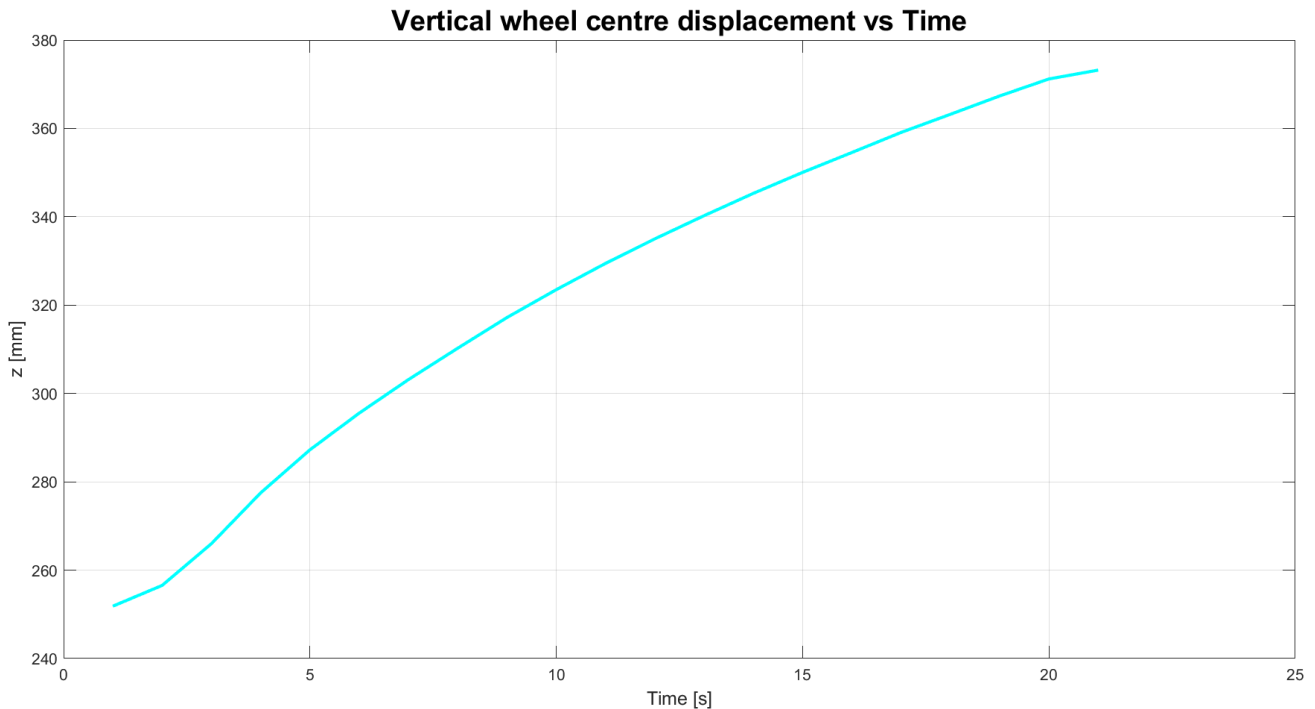


*Figure 3.3.1.1.1 – Wheel centre displacement in vertical direction vs Time*

This graph shows how the wheel centre moves along vertical direction during the time. Obviously, it depends on the test performed. In this case the suspension was only moved up. The slope of the curve and its shape strongly depends on how much constant is the jack rotational speed.

Furthermore, also the starting and ending point depends on time.

To overcome the problem of the unreliability of the behaviour in respect to time two solutions are possible:

- To automatize the bouncing of the suspensions, which is a theme dealt at the end of the thesis.
- To analyse the curves only in function of the vertical wheel centre, which is the solution adopted in this thesis work.

From now on, all the graphs are shown only in dependence of the movement of the wheel centre in vertical direction.

*Results as a function of the vertical wheel centre*

Parameters:

- Mounting position = E
- Spring position in vertical, frontal, and longitudinal direction = zero reference position
- Spacers = NO
- Variable vertical excursion

Longitudinal wheel centre:

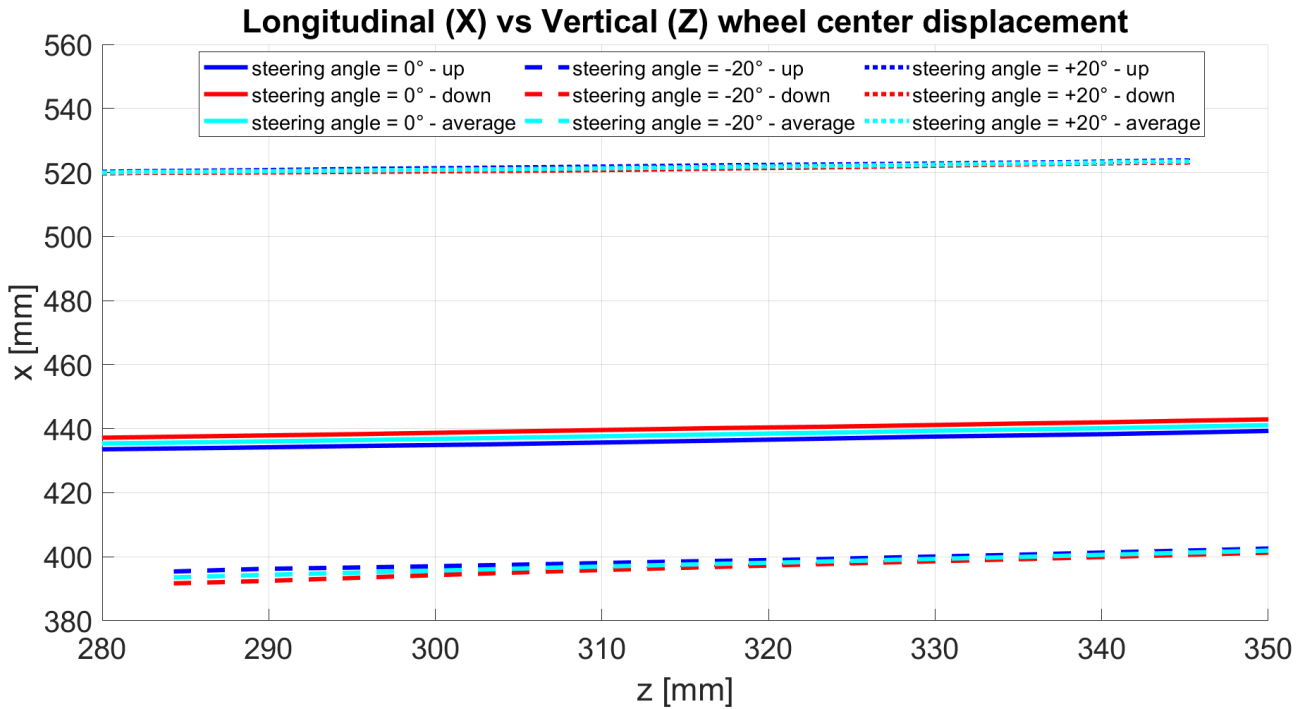


*Figure 3.2.1.1 – Wheel centre displacement in x direction*

This graph shows how the wheel centre moves in x direction during bouncing. The tests have been made with three different steering angles and for each of them what is analysed is: the behaviour when lifting the suspension, the behaviour when lowering it, and then the average between the two cases.

What is possible to note is that:

- By setting a certain steering angle at the beginning of the test, also the starting position of the wheel centre in longitudinal direction changes.
- How the wheel centre behaves in longitudinal direction is, instead, independent from the set steering angle. In fact, all the curves increase with a comparable slope.
- The quantity under analysis does not suffer any relevant hysteresis. Its behaviour is the same both during the lifting and the lowering of the suspension. It means that its trend is perfectly reversible.

Lateral wheel centre:

### Lateral (Y) vs Vertical (Z) wheel center displacement

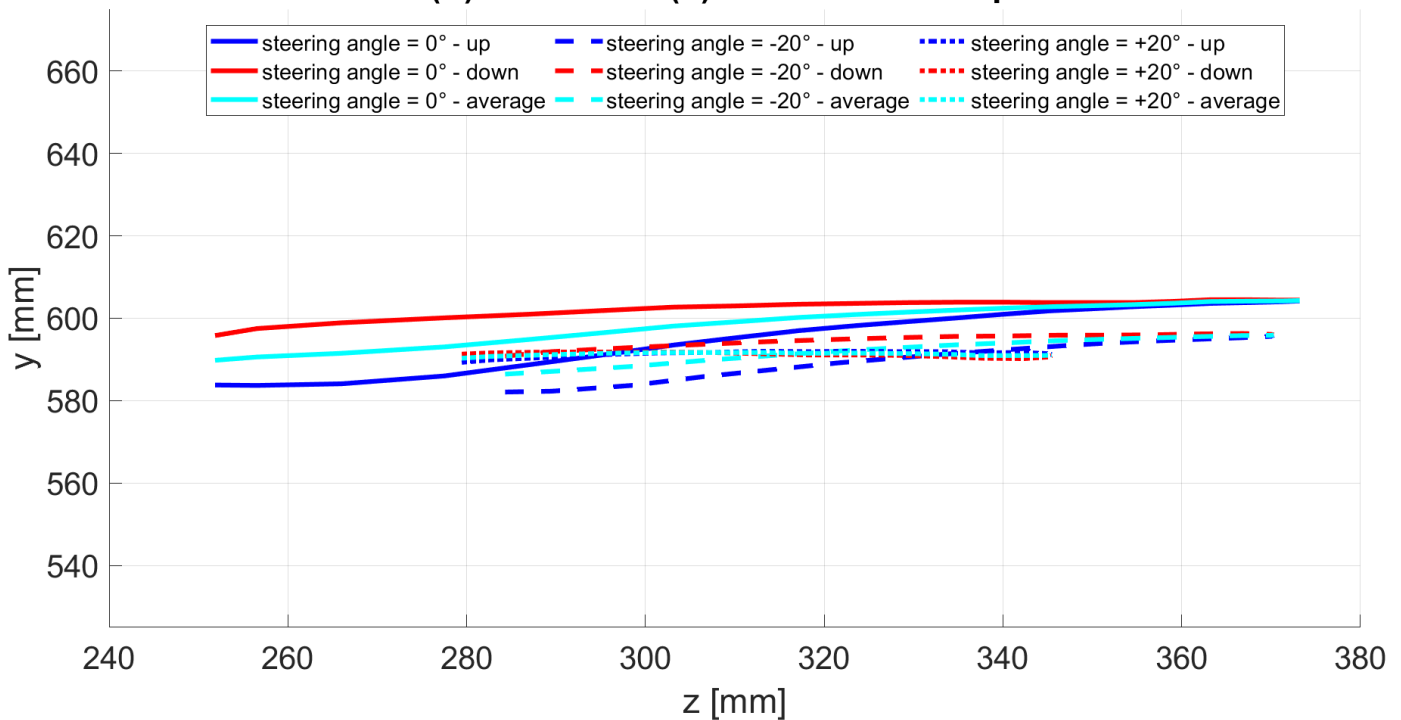


Figure 3.2.1.2 – Wheel centre displacement in  $y$  direction

This graph shows how the wheel centre moves in  $y$  direction during bouncing. Also, in these tests what changes is the steering angle. Again, they are analysed: the behaviour when lifting the suspension, the behaviour when lowering it, and then the average between the two cases.

What is possible to note is that:

- The wheel centre position in lateral direction is not affected by the set steering angle. In fact, regardless of its value, the starting position is always almost the same.
- The trend is not perfectly coherent between the three tests, since the case “steering angle =  $+20^\circ$ ” shows a flat curve, differently from the other two, whose trend is growing with a comparable slope.
- All the three curves have a relevant hysteresis at the beginning of the test which tends to decrease at the end.

Camber angle:

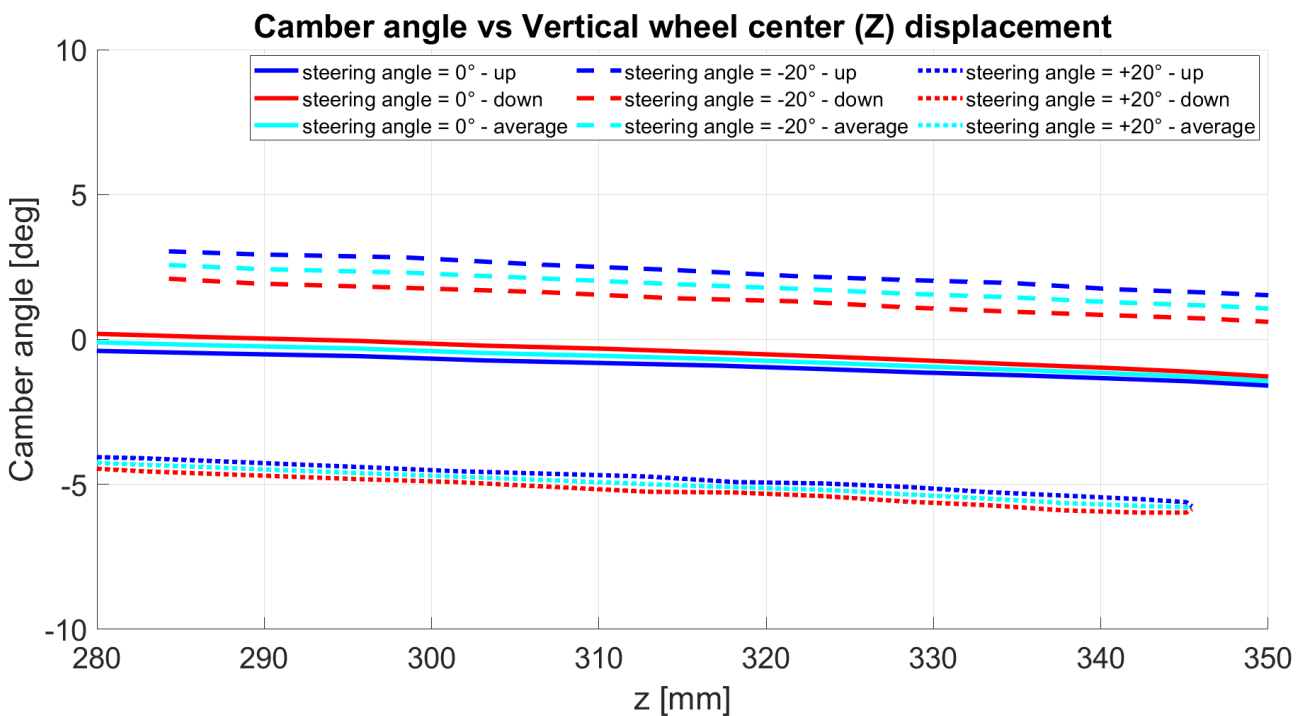


Figure 3.2.1.3 – Camber angle

As already said, the camber angle is the angle between the vertical axis of the wheel and the vertical axis of the vehicle. It must not be excessive since it can lead to an increase of tire wear and a consequent worsening of the handling.

The graph shows the camber angle behaviour for three different steering angles.

What is relevant is that:

- To different steering angles correspond different camber angles.
- The behaviour is not influenced by the steering angle since it has a decreasing trend in all the three cases.
- During the compression camber angle decreases while during extension it increases. It means that the analysed suspension has a good *camber recovery*. This is an important aspect since, thanks to that, the contact patch between the tire and the ground is optimized during rolling.

Caster angle:

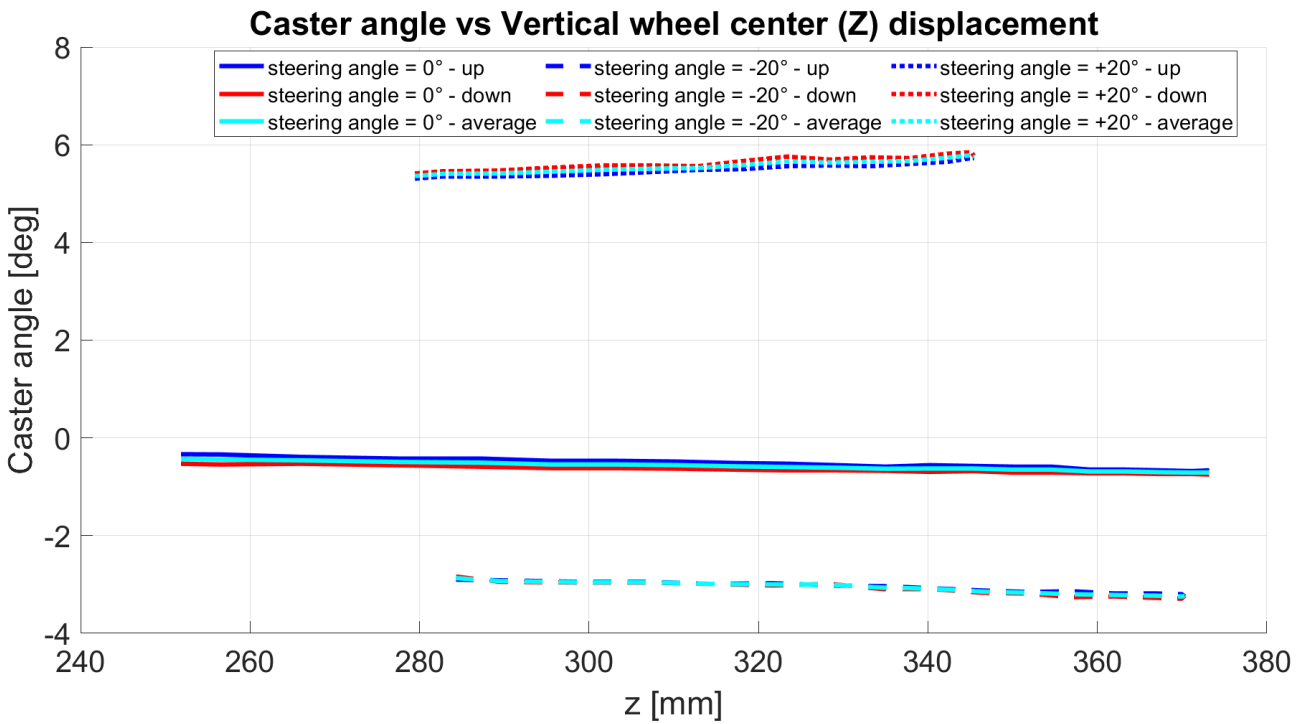


Figure 3.2.1.4 – Caster angle

Caster angle is the displacement of the steering axis from the vertical one in a steered wheel, from a lateral point of view. This angle also influences the camber angle, together with the kingpin. It must be small, otherwise the steering becomes heavier and less responsive. On the other hand, a bigger caster angle improves camber gain when cornering.

Considerations about the graph:

- As expected, for a steering angle equal to zero, also the caster angle is null. Positive steering angle gives a positive caster angle and negative one gives negative caster angle.
- All the three curves show a behaviour almost constant; it means that the variation of the caster angle during bouncing is negligible.
- The most relevant result is that it has no hysteresis, the behaviour during lifting is almost coincident to the one during lowering.

Spring motion ratio (spring to wheel displacement ratio):

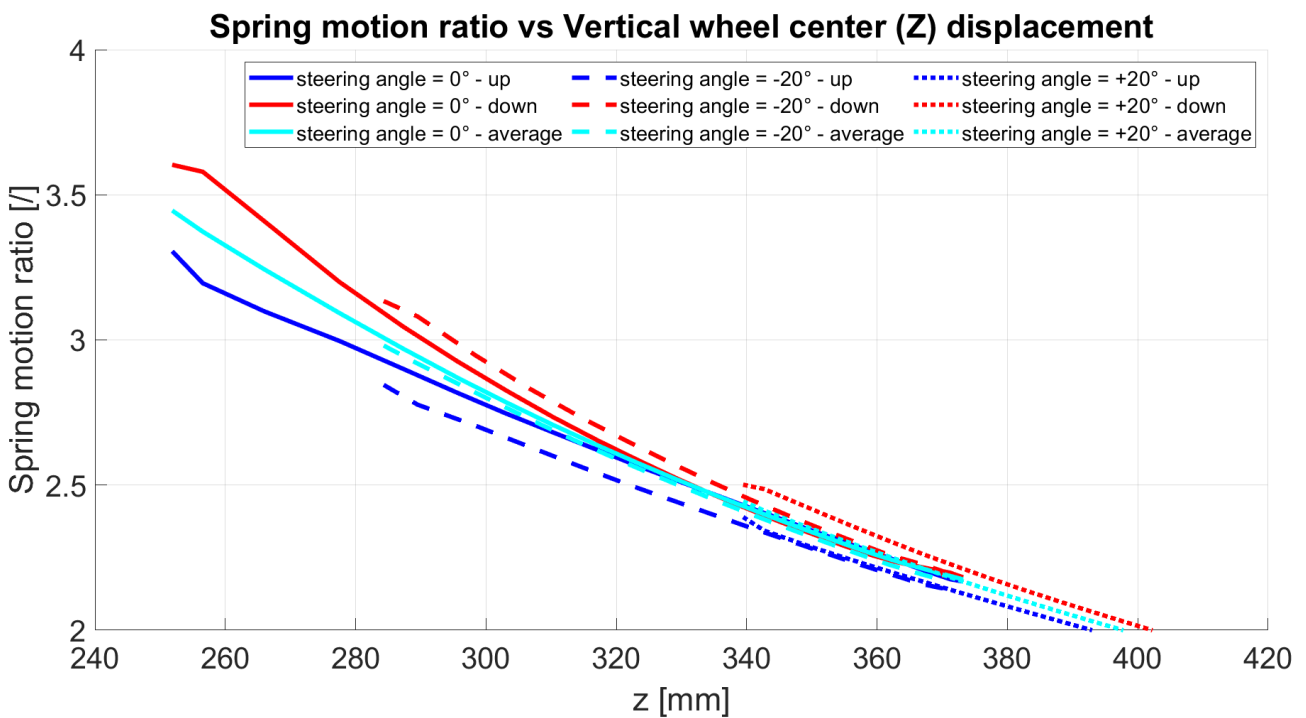


Figure 3.2.1.5 – Spring motion ratio

For what concerns the spring, what is computed is the *installation ratio*. It is the ratio between spring and damper displacement with respect to the wheel centre displacement. Usually, the spring and the damper movements are lower than the one of the wheel centre.

By means of this quantity it is possible to understand how much the spring and the damper deflect because of the wheel displacement.

Analysing the installation ratio for three different steering angles, what comes out is that:

- Spring motion ratio does not depend on the steering angle.
- All the three tests show the same trend: spring motion ratio decreases by lifting the suspension. It means that, the more the suspension is raised up, the lower is the relative spring deflection.
- This quantity suffers for hysteresis, particularly for low z values.

Steering angle:

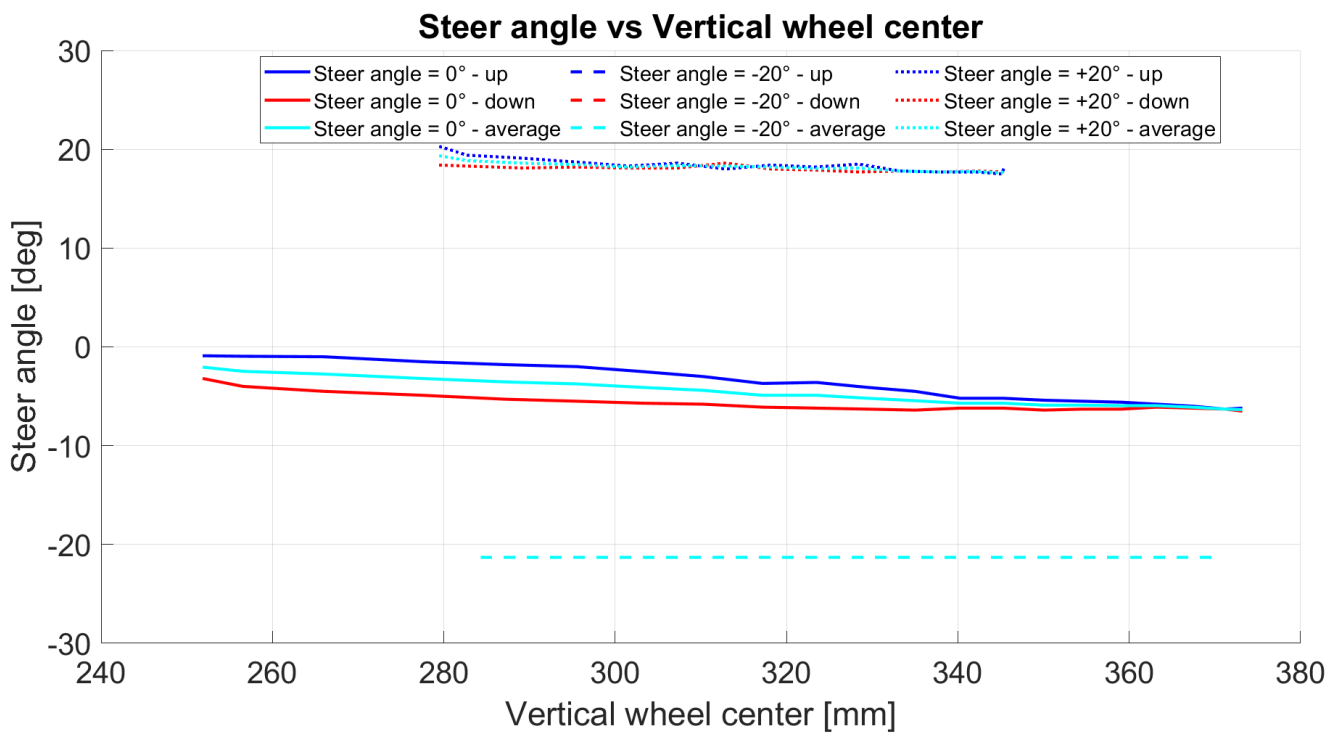


Figure 3.2.1.6 – Steer angle

As it possible to see from the graph above, once the steering angle is set, it remains constant during the bouncing movement. There are some little variations and some oscillations since it is a real model and not an ideal one.

### 3.2.2 Second tests: proofs at different spring potentiometer positions in vertical direction

Parameters:

- Mounting position = E
- Spring position in frontal and longitudinal direction = zero reference position
- Spring position in vertical direction  $\cong 750$  mm and  $\cong 900$  mm
- Spacers = NO
- Vertical excursion: 110 mm

For all the following tests, since the influence of steering angle variation has already been analysed, it was kept constant at zero degrees.

The consideration about the graphs that are shown below is always the same, and it is that for all the quantities, the changes in the position of the spring potentiometer in vertical direction does not affect their behaviour. In fact, the curves are almost all overlapped and there are no differences in the trend. What changes is, obviously, only the spring motion ratio, which takes higher values when the potentiometer is in the upper position and lower values when it is in the lower position. The curve obtained with the potentiometer in the zero-reference position stays between the other two. Except for that, there is not any other difference, in fact the trend is always the same and the offset between the three curves is constant for the entire duration of the test.

For this reason, in the other subsequent tests carried out, this parameter was taken unvaried and not considered anymore.

Longitudinal wheel centre:

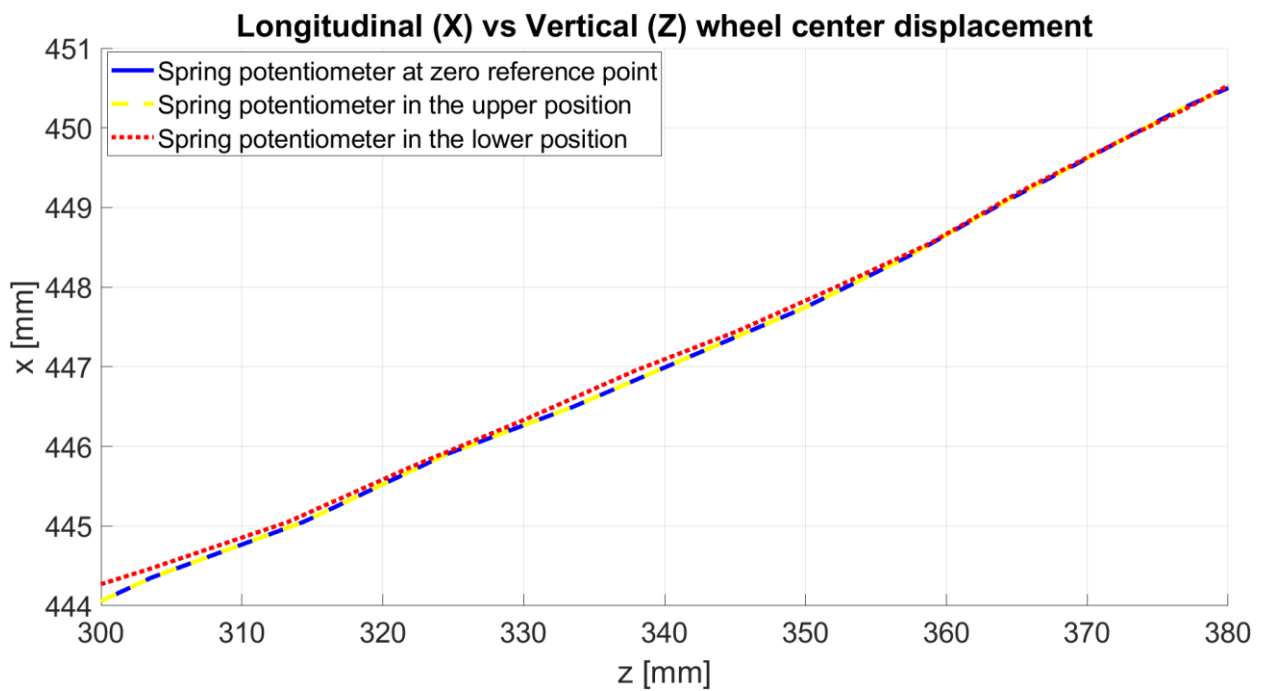


Figure 3.2.2.1 – Wheel centre displacement in x direction

Lateral wheel centre:

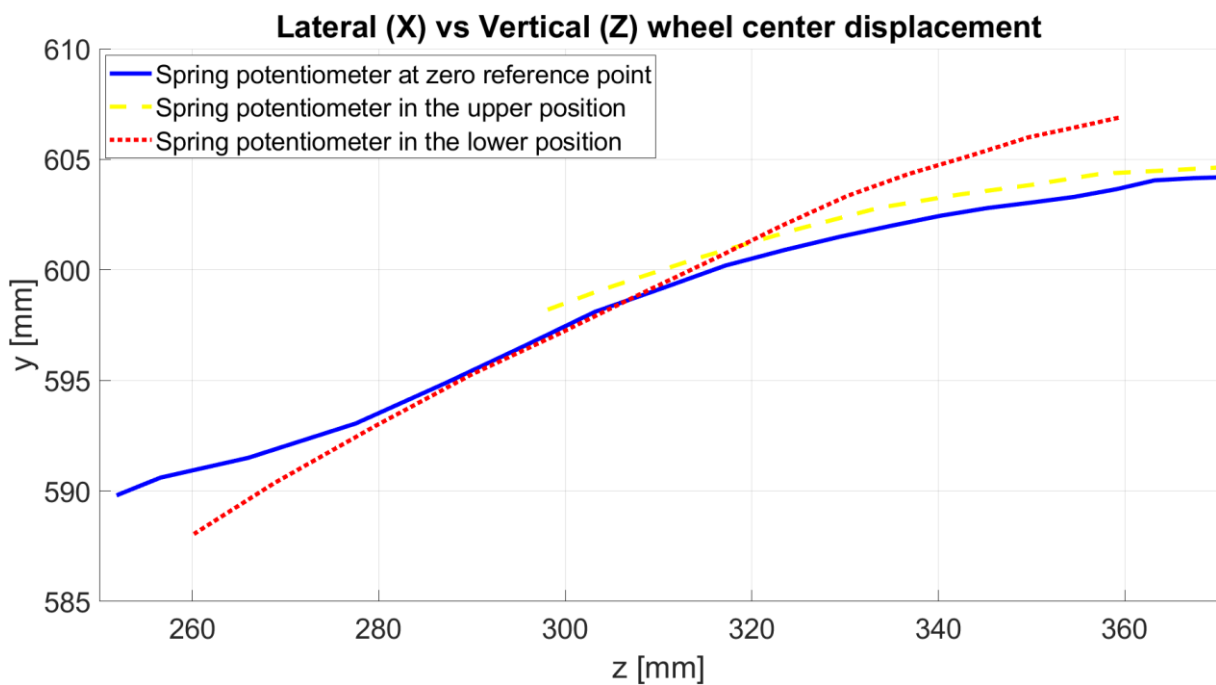


Figure 3.2.2.2 – Wheel centre displacement in y direction

Camber angle:

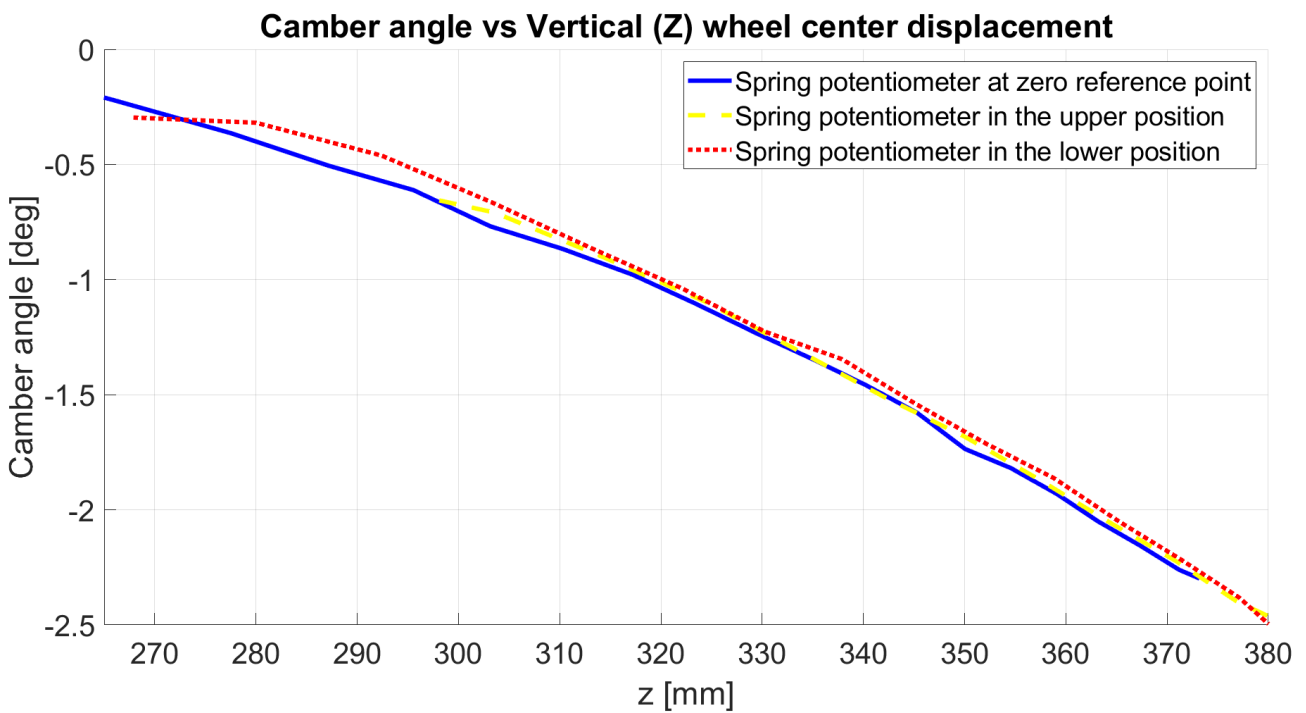


Figure 3.2.2.3 – Camber angle

Caster angle:

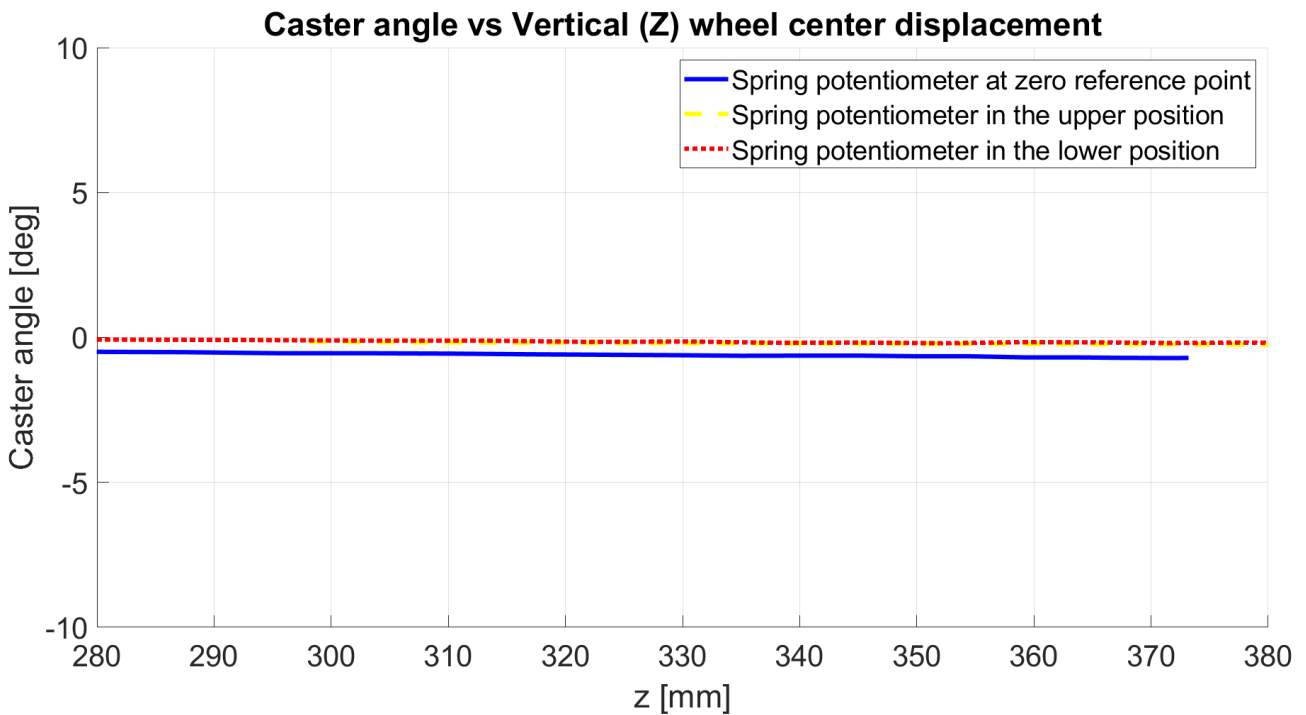


Figure 3.2.2.4 – Caster angle

Spring motion ratio (spring to wheel displacement ratio):

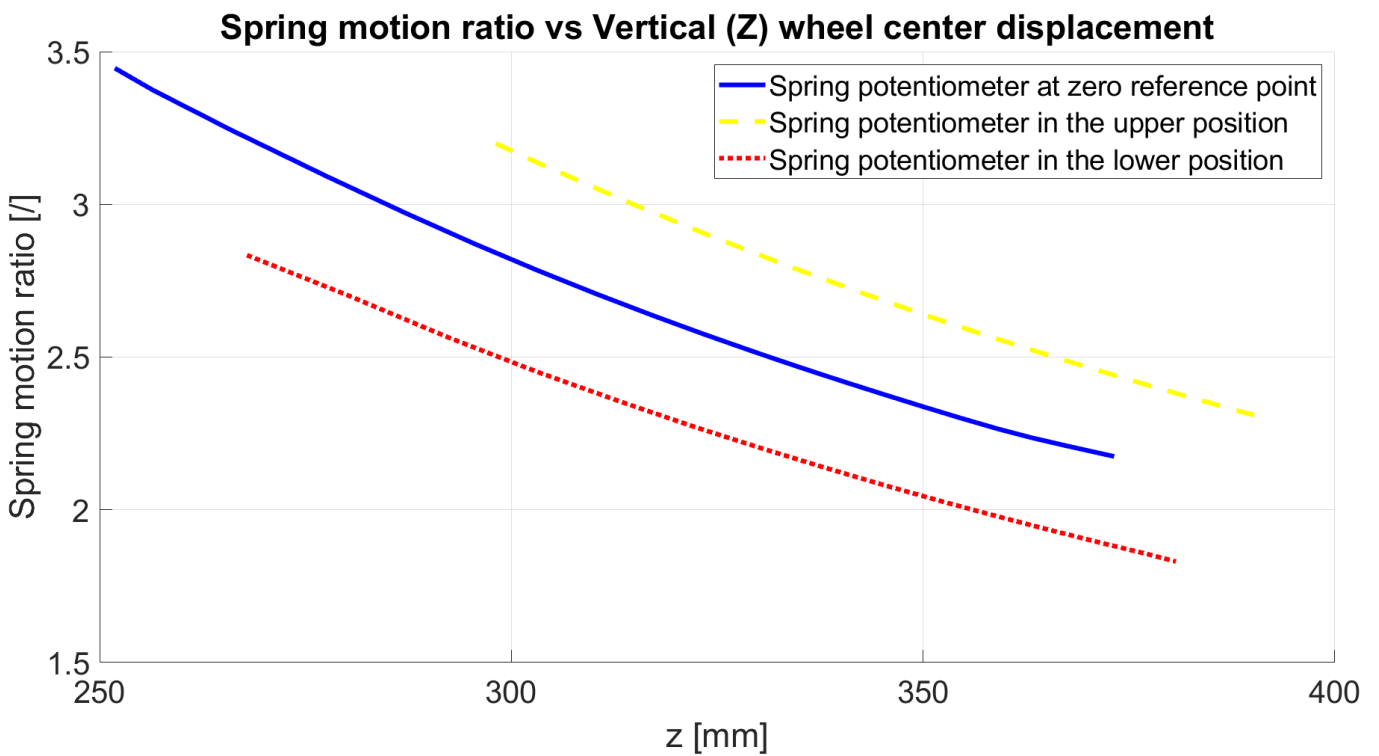


Figure 3.2.2.5 – Spring motion ratio

Steering angle:

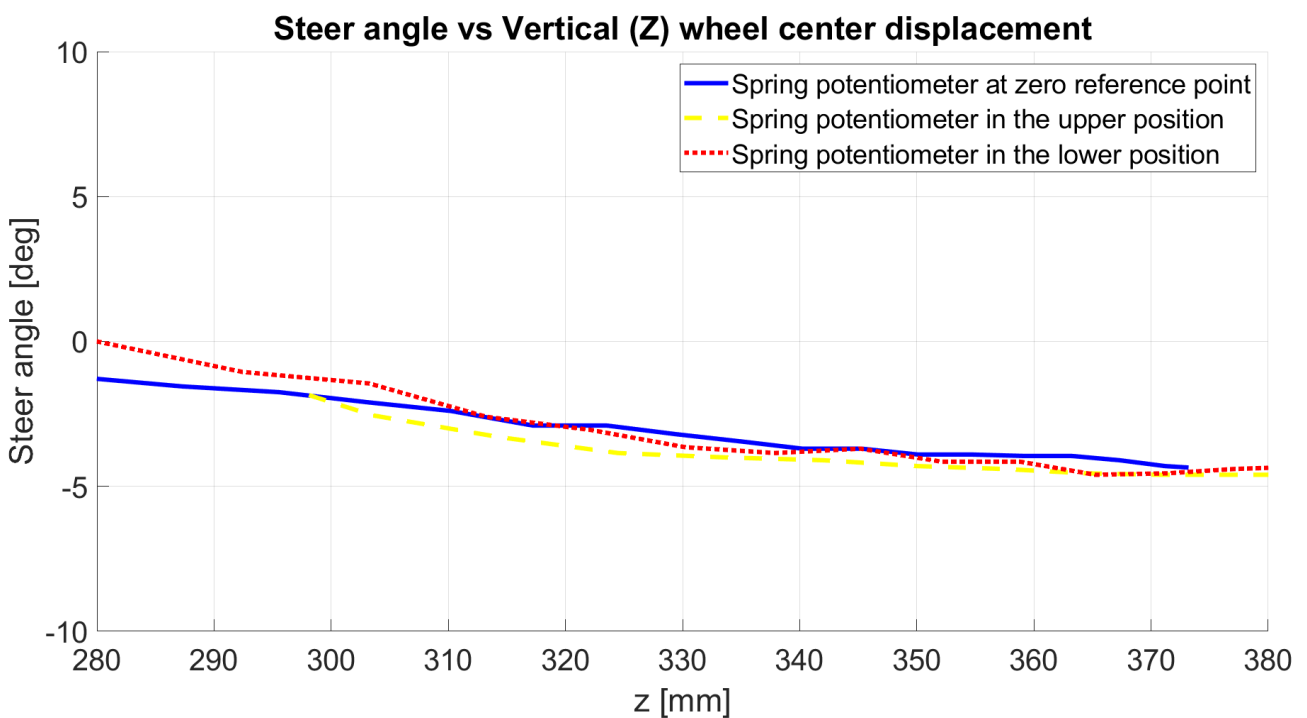


Figure 3.2.2.6 – Steer angle

### 3.2.3 Third test: proofs at different spring potentiometer positions in longitudinal direction

Parameters:

- Mounting position = E
- Spring position in frontal and vertical direction = zero reference position
- Spring moved to right and left in longitudinal direction.
- Spacers = NO
- Vertical excursion: 110 mm

As in the previous case, also for the following proofs the steering angle has been kept unchanged at  $0^\circ$ , since it is known yet how it influences the behaviour of the quantities.

The purpose of this test is complementary to the previous one: it wants to prove that, by changing the position of the spring potentiometer along x coordinate, no changes arise on the behaviour of the wheel centre in longitudinal and lateral direction, neither in the camber, caster, and steer angles.

Longitudinal wheel centre:

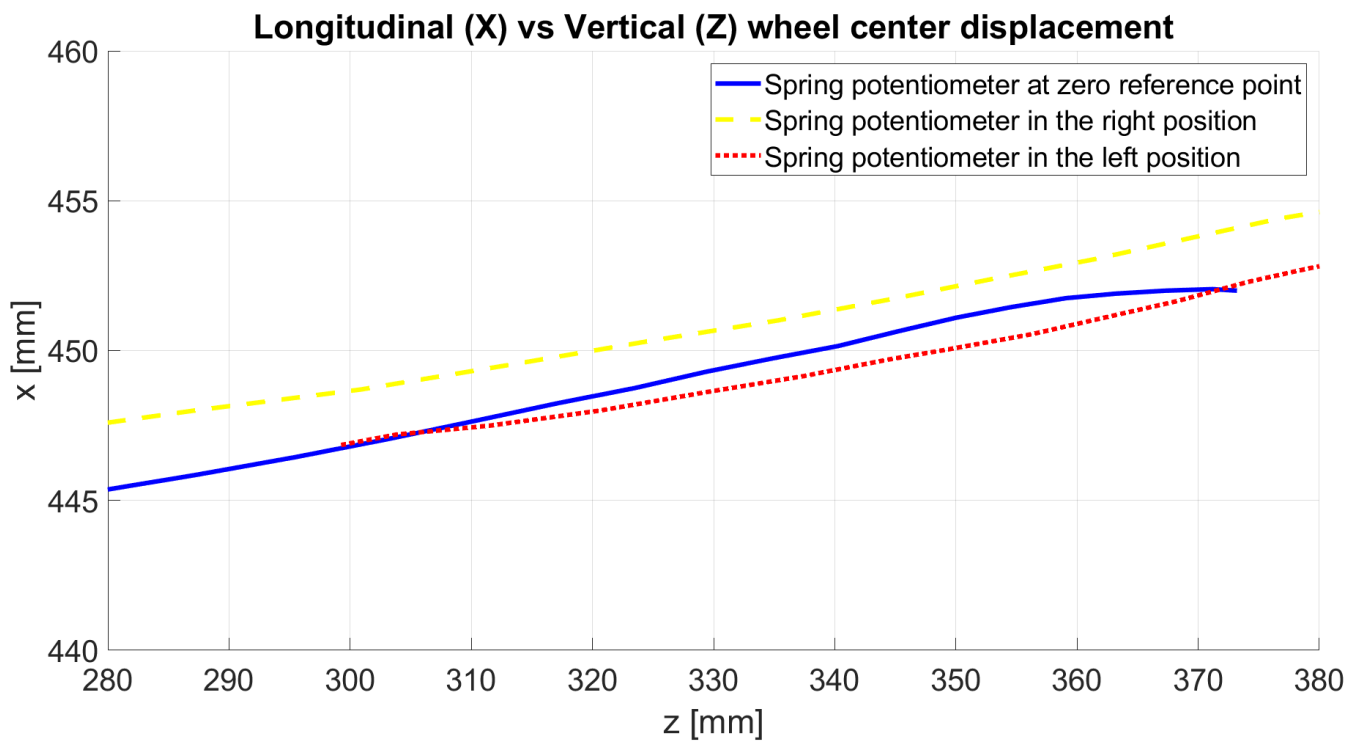


Figure 3.2.3.1 – Wheel centre displacement in  $x$  direction

Lateral wheel centre:

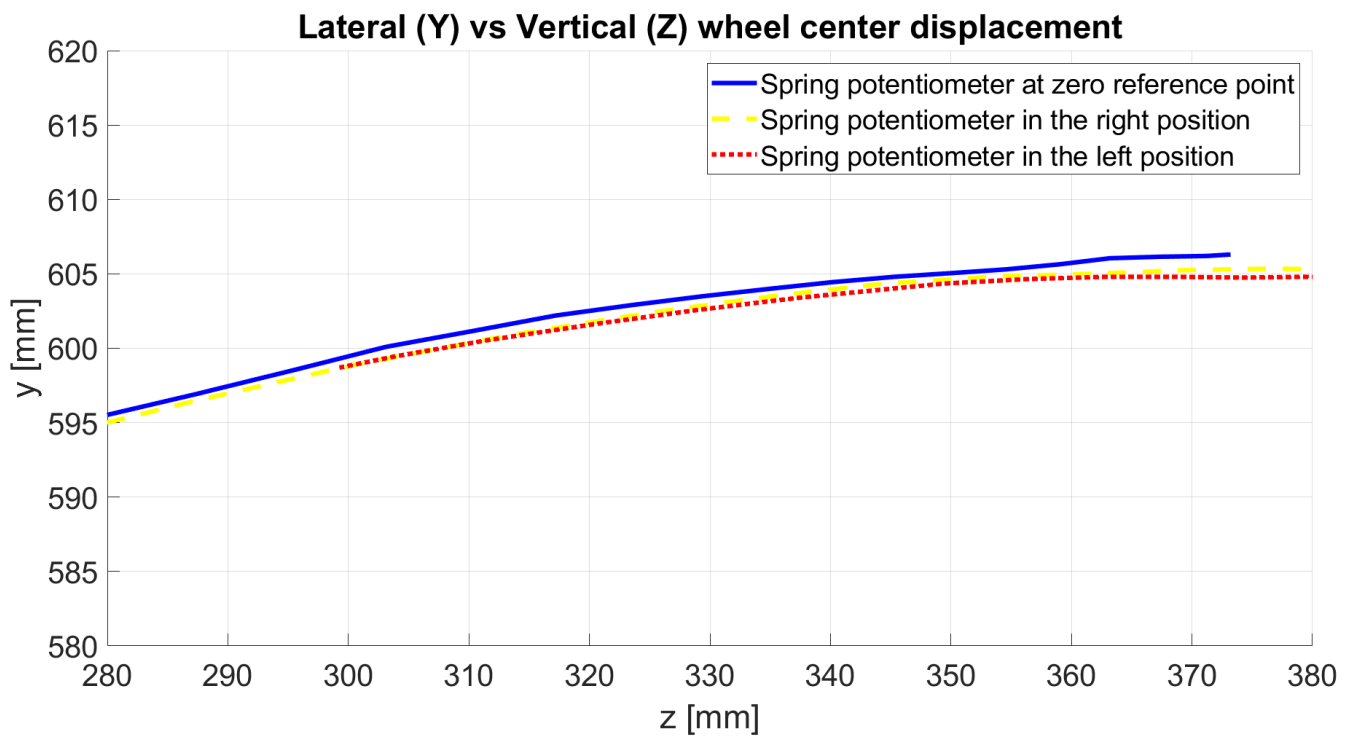


Figure 3.2.3.2 – Wheel centre displacement in  $y$  direction

Camber angle:

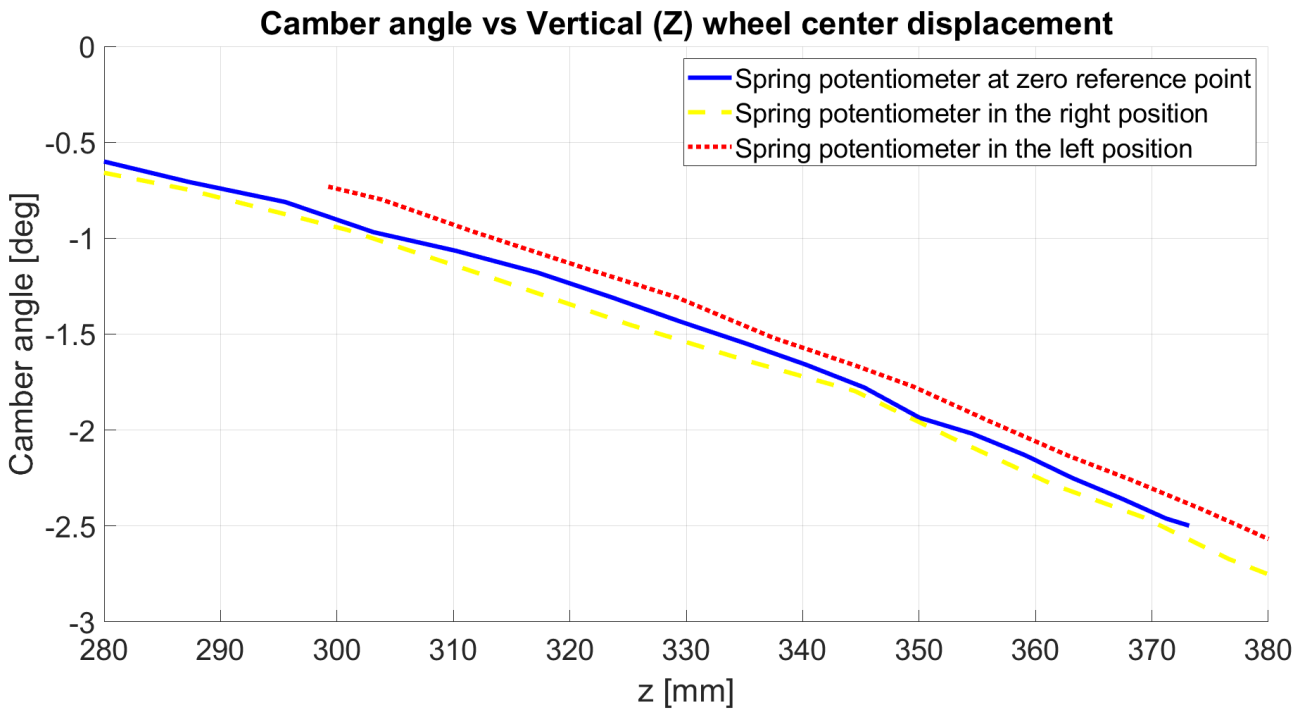


Figure 3.2.3.3 – Camber angle

Caster angle:

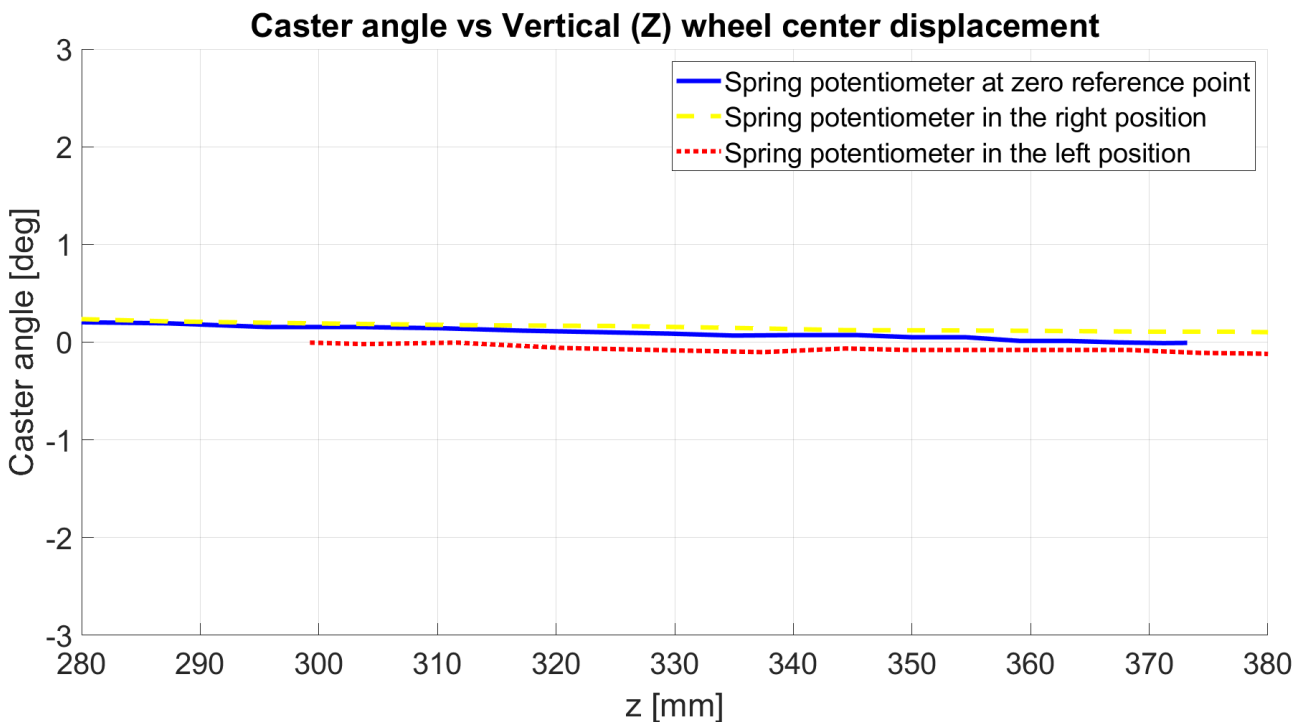


Figure 3.2.3.4 – Caster angle

Spring motion ratio (spring to wheel displacement ratio):

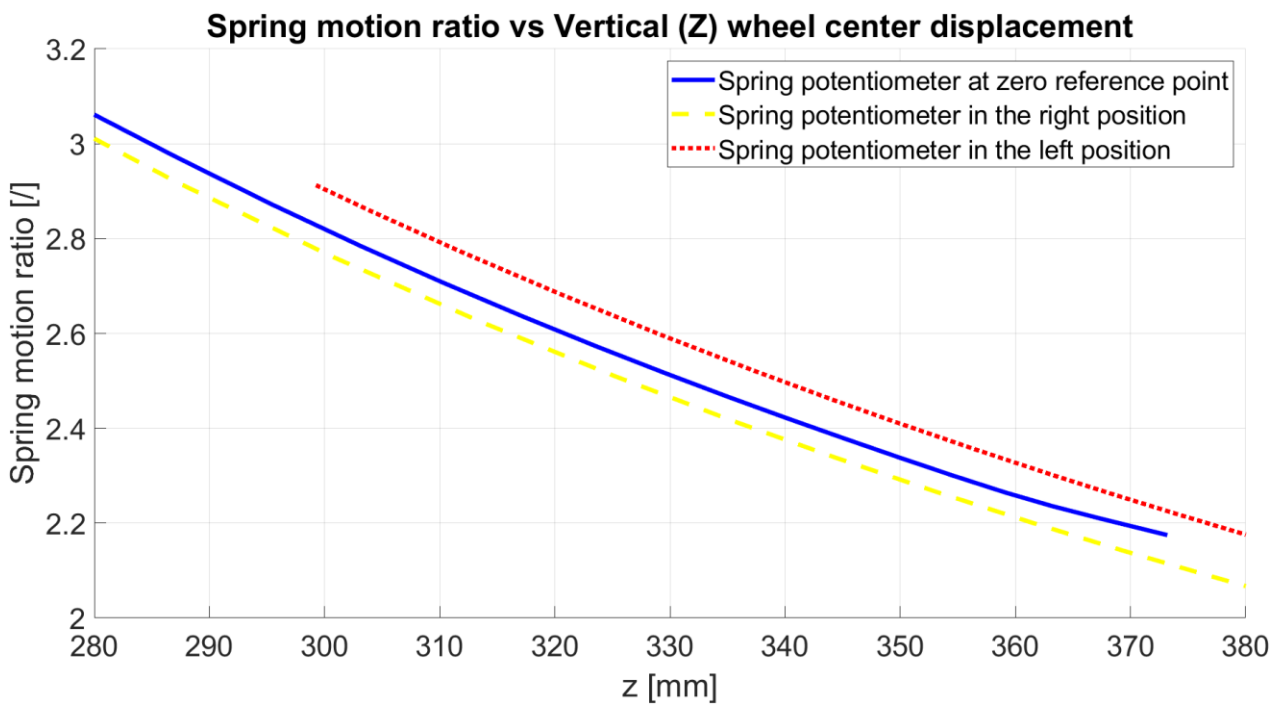


Figure 3.2.3.5 – Spring motion ratio

Steering angle:

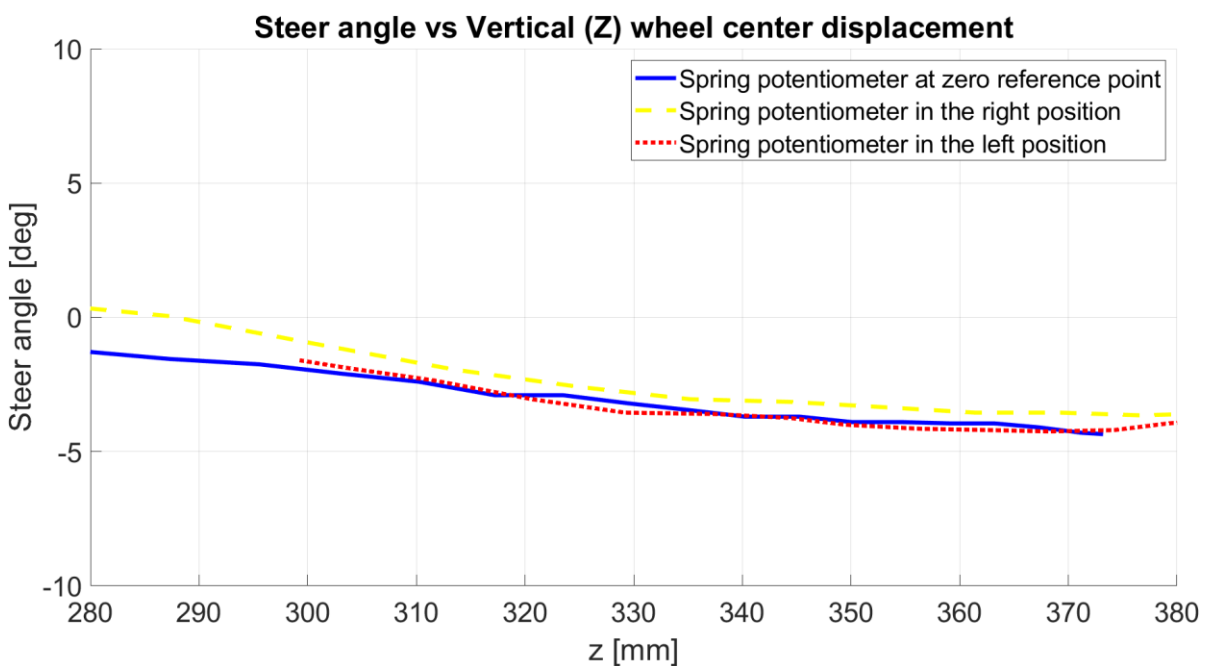


Figure 3.2.3.6 – Steer angle

Basing on this, for all the following proofs, the spring potentiometer position was not changed anymore.

### 3.2.4 Fourth test: proofs at different mounting position

Parameters:

- Mounting position = A, C, E, G, I
- Spring position in frontal, longitudinal and vertical direction = zero reference position
- Spacers = NO
- Vertical excursion: 130 mm

The following graphs will show the behaviour or:

- Wheel centre position in x direction
- Wheel centre position in y direction
- Camber angle
- Caster angle
- Steer angle

The spring motion ratio was not anymore modified neither considered since it is yet analysed what is its influence on these quantities.

The parameter which varies between these tests is the mounting position. In detail, 5 mounting positions were analysed:

- The central mounting position, E
- The North-Est position, C
- The Sud-Est position, I
- The North-West position, A
- The Sud-West position, G

The variation of this parameter leads to a difference in the coordinates of the upper control arm, and so in the geometry of the suspension. In particular, from one position to another, the difference is  $\pm 4$  mm in x direction and  $\pm 4$  mm in z direction. Coordinates in y direction are unchanged.

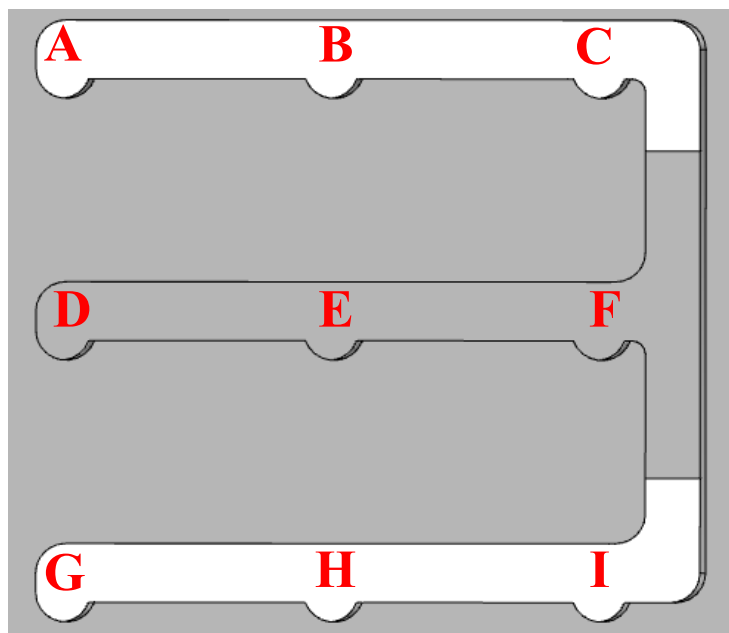


Figure 3.2.4.1 – Mounting position scheme

All the tests were performed with the tie rod screw completely close and more than one bouncing to see the repeatability of the test.

The curves related to the test bench simulations were then drawn up, obtaining for each of them a trend curve. This operation was done to have clearer plot, to make the comparison with MSC/Adams Car simulations clearer and more intuitive.

Trend lines were obtained on Excel, by approximating the curves with a second-degree polynomial interpolation. These polynomials were expressed as a function of the vertical wheel centre displacement. They are all listed in the tables below the graphs.

For each trend curve, it was also computed  $R^2$  value, which is also reported in the table. It is an index about the reliability of the approximation, so that it is possible to demonstrate the correctness of the trend lines: the more its value is near to one, the higher is the affordability.

It was chosen a second-degree polynomial since if it would be chosen a first-degree one, the trend would not be enough coherent anymore. In fact,  $R^2$  value would be lowered. This consequence is particularly drastic for quantities which behaviour is not linear.

Wheel travel in longitudinal direction

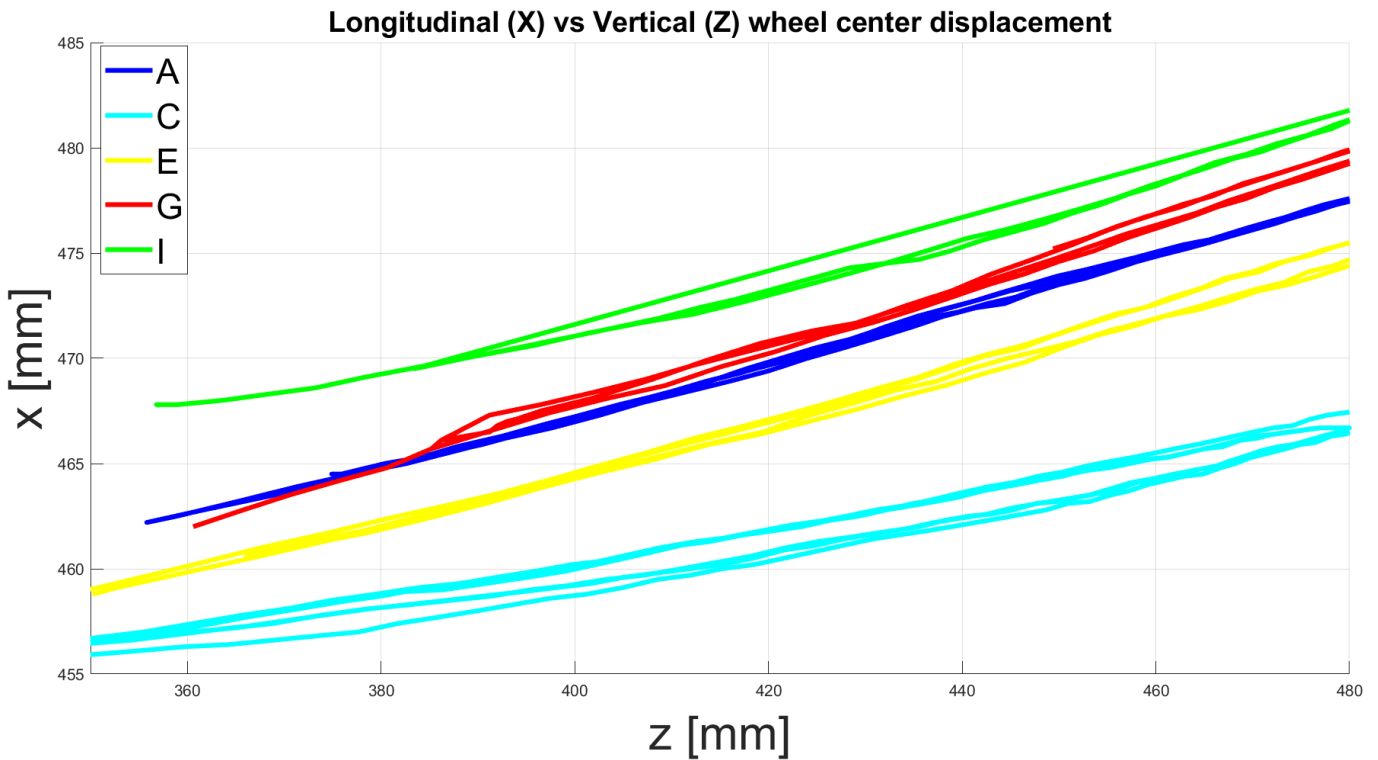


Figure 3.2.4.2 – Wheel travel in longitudinal direction – Test bench

Comments on the graph above:

- The variation of the mounting position does not influence a lot the trend of the curves. For all the five different positions, in fact, x value increases by increasing the wheel centre in vertical direction, even if the slope is not perfectly the same.
- All the tests show a great repeatability.
- The disposition and the starting points are not as expected, since, starting from the yellow curve, which is the one related to the central mounting position, the expectation was to find:
  - “C” and “I” curves above the “E” one, since with these two mounting positions, the upper control arm is moved to the right.
  - “G” and “A” curves below the “E” one, since with these two mounting positions, the upper control arm is, instead, moved to the left.

Wheel travel in longitudinal direction: trend curves

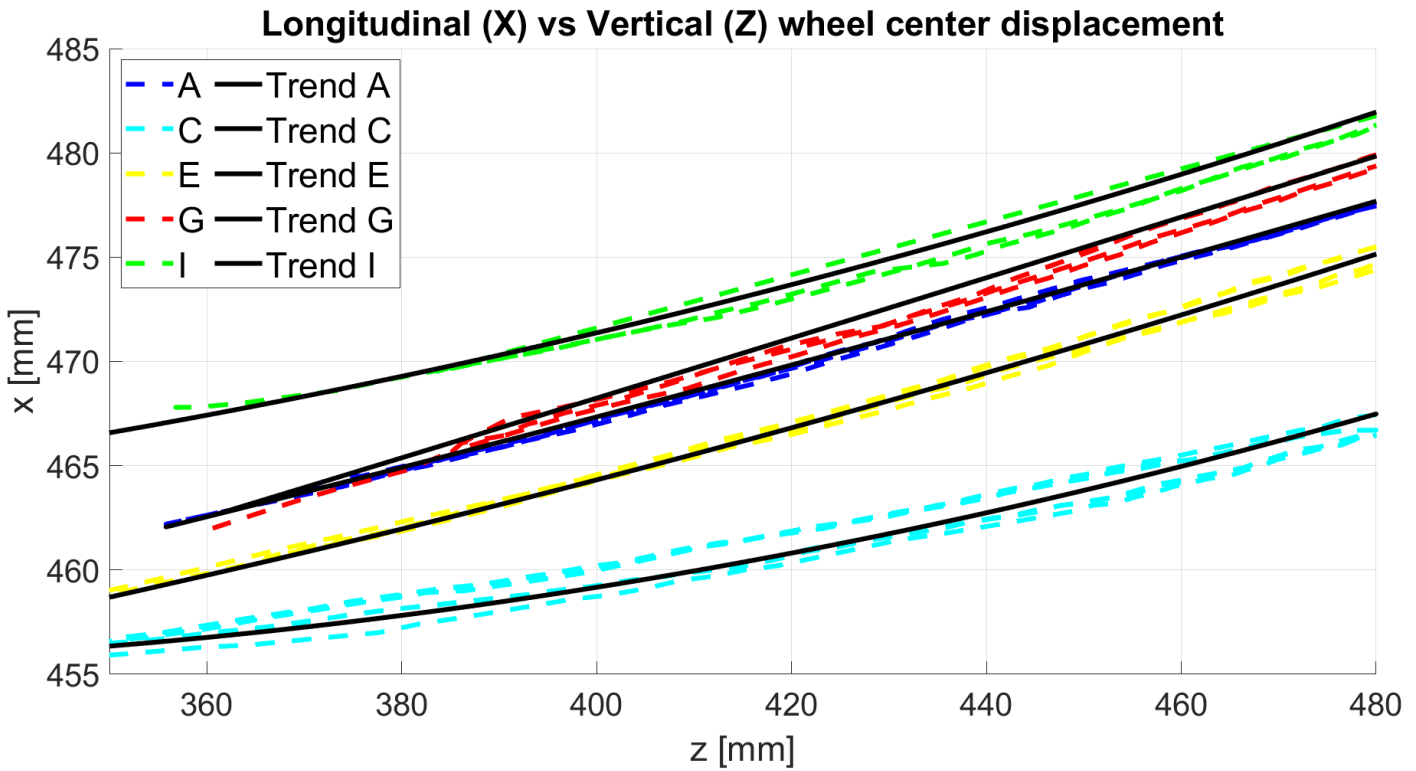


Figure 3.2.4.3 – Wheel travel in longitudinal direction – Trend curves

LONGITUDINAL WHEEL TRAVEL		
	Equation	$R^2$
<b>A</b>	$0.00008 \cdot Z^2 + 0.0589 \cdot Z + 430.98$	0.9991
<b>C</b>	$0.000365 \cdot Z^2 - 0.2173 \cdot Z + 487.69$	0.9792
<b>E</b>	$0.000175 \cdot Z^2 - 0.0187 \cdot Z + 443.8$	0.9971
<b>G</b>	$0.00002 \cdot Z^2 + 0.1275 \cdot Z + 414.04$	0.9946
<b>I</b>	$0.00028 \cdot Z^2 - 0.1141 \cdot Z + 472.21$	0.9857

Table 3.2.4.1 – Trend curve equations

The graph shows that trend lines are perfectly overlapped with the original curves. Furthermore,  $R^2$  values are very close to one. The one related to the “I” curve is lower than the others because of a little bit of hysteresis.

*Wheel travel in lateral direction*

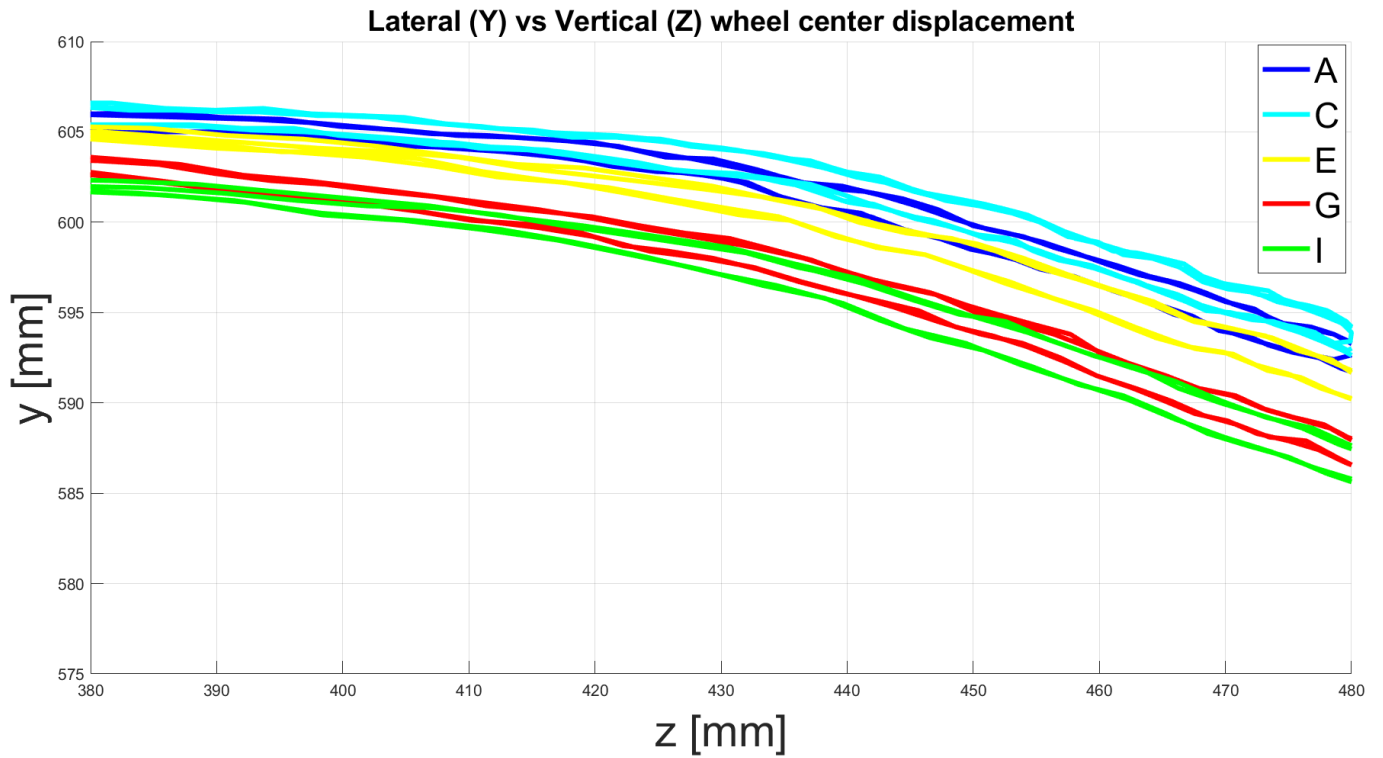


*Figure 3.2.4.4 – Wheel travel in lateral direction – Test bench*

In this case, the scenery is exactly what was expected: all the curves are almost overlapped. There is no influence of the mounting position in the wheel travel in lateral direction. This was predictable, since all the different mounting positions have the same y coordinate. The curves confirm the repeatability of the tests, since hysteresis is very small.

Wheel travel in longitudinal direction: trend curves

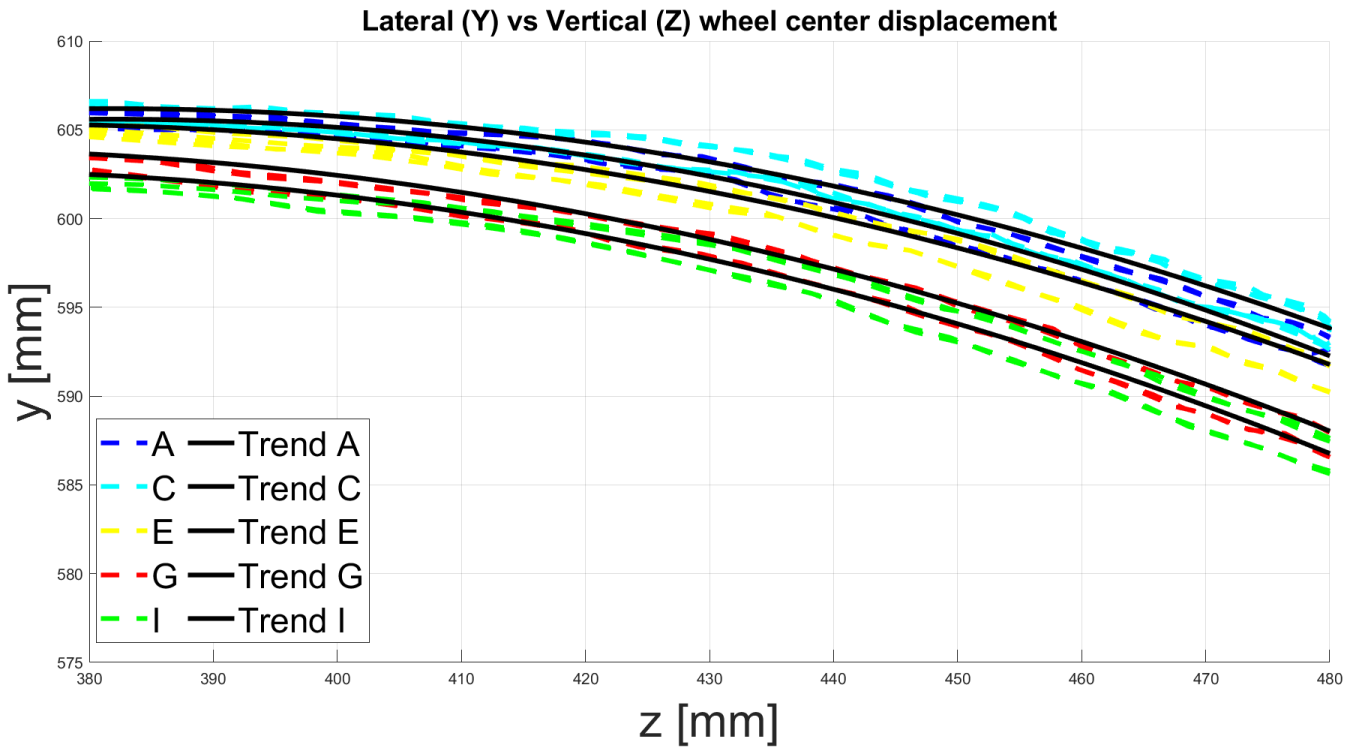


Figure 3.2.4.5 – Wheel travel in lateral direction – Trend curves

LATERAL WHEEL TRAVEL		
	Equation	$R^2$
<b>A</b>	$-0.00138 \cdot Z^2 + 1.0535 \cdot Z + 404.54$	0.9815
<b>C</b>	$-0.001275 \cdot Z^2 + 0.9728 \cdot Z + 420.64$	0.9777
<b>E</b>	$-0.0012 \cdot Z^2 + 0.897 \cdot Z + 437.7$	0.9922
<b>G</b>	$-0.0012 \cdot Z^2 + 0.8759 \cdot Z + 444.08$	0.9936
<b>I</b>	$-0.001233 \cdot Z^2 + 0.9032 \cdot Z + 437.32$	0.9908

Table 3.2.4.2 – Trend curve equations

As in the previous case, trend curves are perfectly above the real ones and equation reliability is very high.

## Camber angle

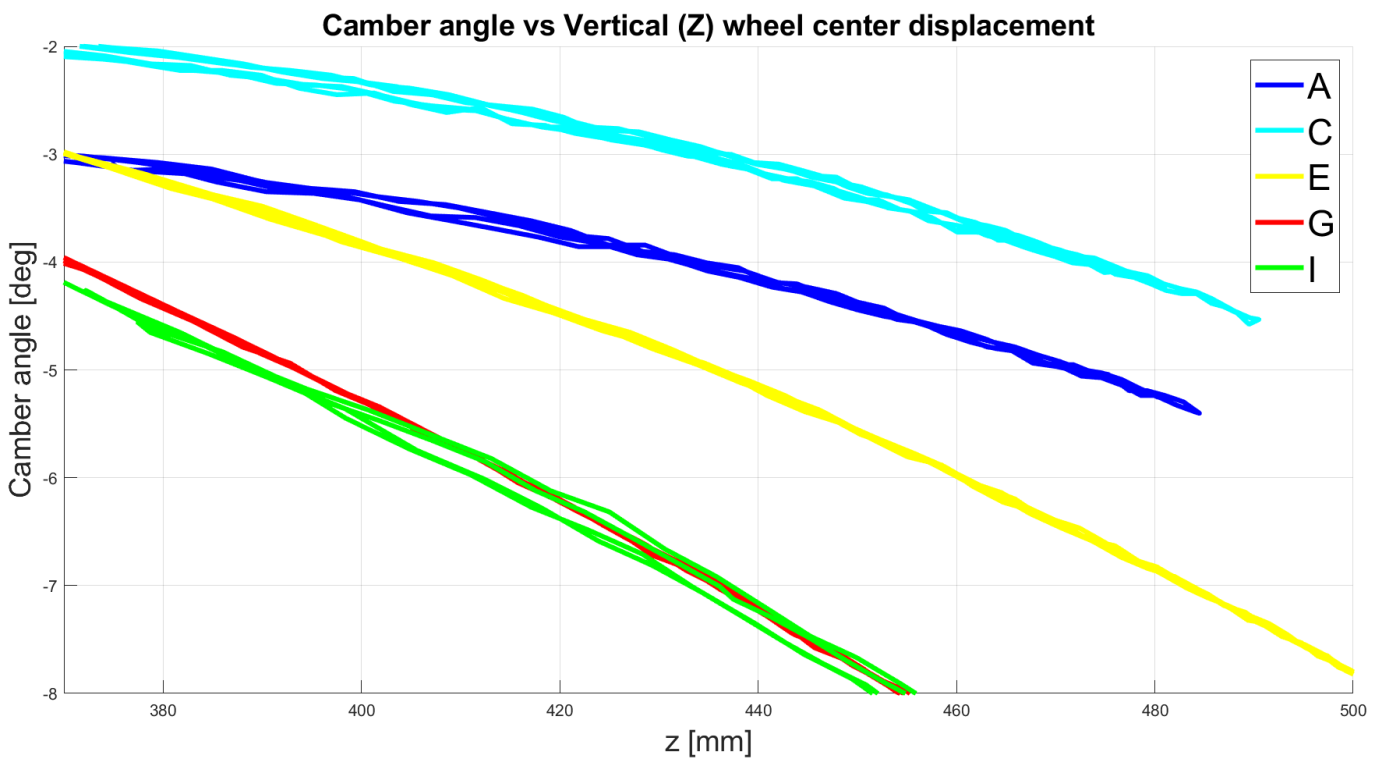


Figure 3.2.4.6 – Camber angle – Test bench

Comments on the graph above:

- The variation of the mounting position leads to differences also in the camber angle. In detail, A and C mounting positions, which are the ones in the upper part of the scheme, produce a lower camber angle. The opposite considerations apply for the “G” and “I” positions. They are in the lower part of the scheme, and they lead to a higher (more negative) camber angle.
- The central mounting position leads to intermediate camber angle values with respect to the extreme cases.
- For what concerns the slope, it is possible to spot three different behaviours:
  - “C” and “A” curves have a lower slope, which means that in these two positions, camber angle is not subjected to relevant variation during bouncing.
  - “G” and “I” curves have a big slope, so there is an increase of camber angle because of the bouncing of the suspension.
  - “E” curve has an intermediate behaviour. Camber angle changes but not too much.

As already said, it is better if camber angle is not too high, since higher values lead to an increase of wear. Consequently, the handling would be worsening.

Camber angle: trend curves

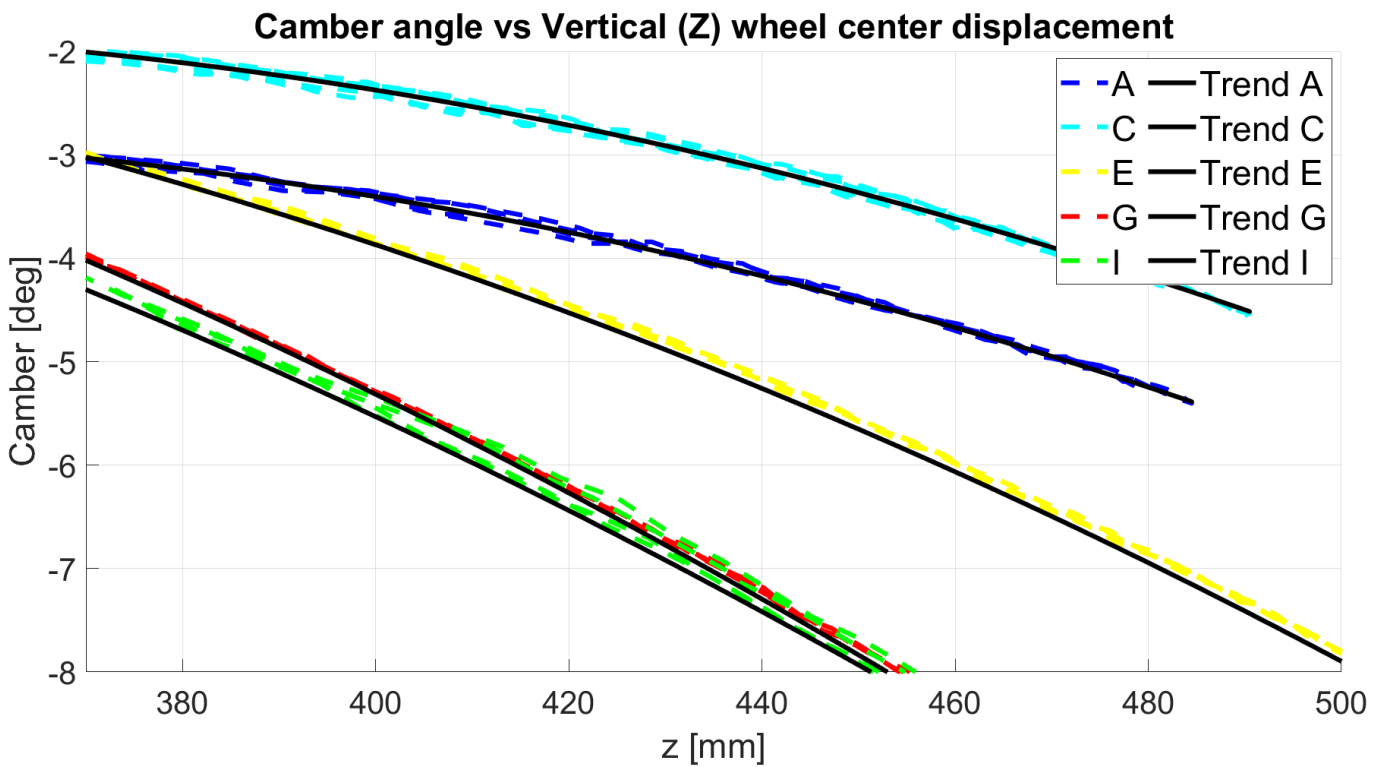


Figure 3.2.4.7 – Camber angle - Trend curves

CAMBER ANGLE		
	Equation	$R^2$
<b>A</b>	$-0.0000965 \cdot Z^2 + 0.0619 \cdot Z - 12.725$	0.9977
<b>C</b>	$-0.0000945 \cdot Z^2 + 0.0605 \cdot Z - 11.455$	0.9969
<b>E</b>	$-0.0000923 \cdot Z^2 + 0.0428 \cdot Z - 6.2216$	0.9998
<b>G</b>	$-0.00009 \cdot Z^2 + 0.0261 \cdot Z - 1.355$	0.9999
<b>I</b>	$-0.000088 \cdot Z^2 + 0.0268 \cdot Z - 2.1717$	0.9998

Table 3.2.4.3 – Trend curve equations

Trend curves obtained for camber angle are extremely precise.

## Caster angle

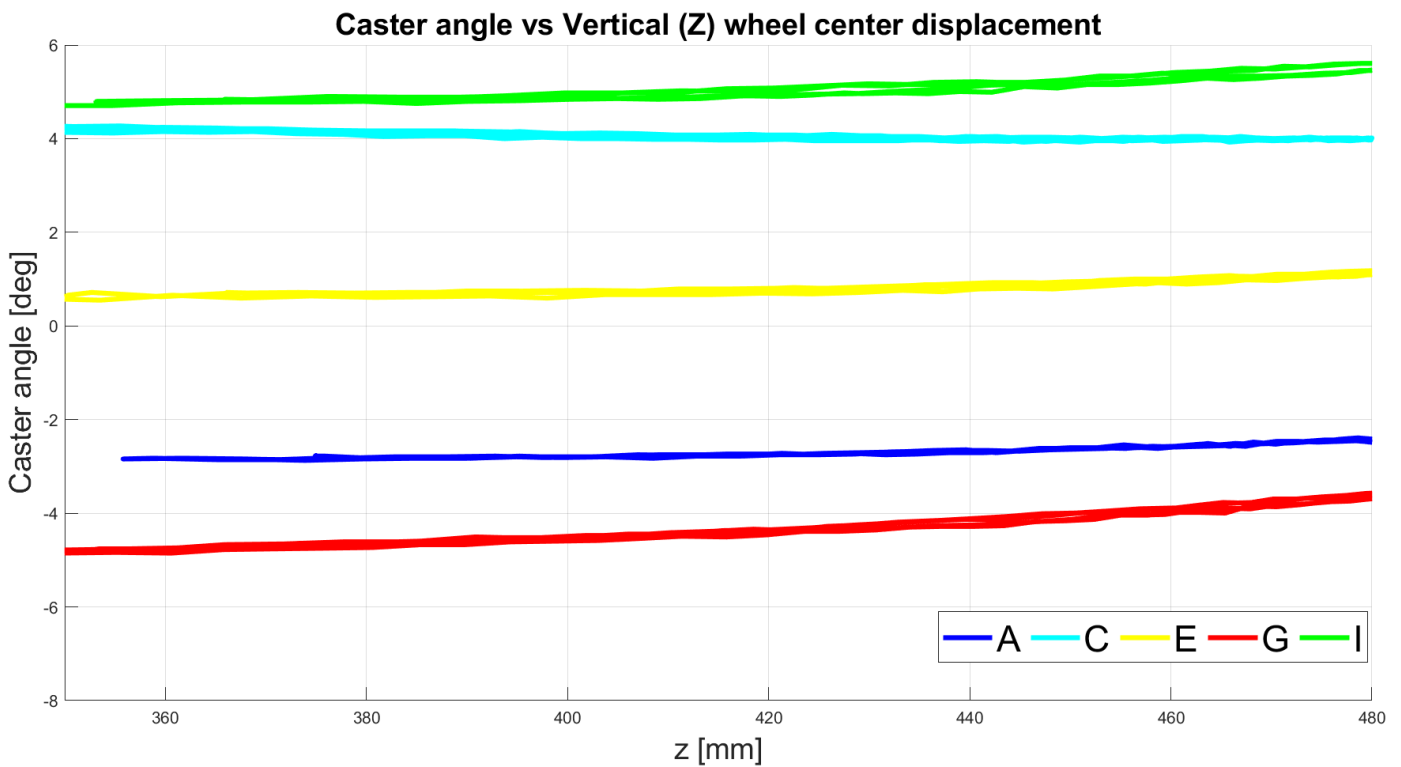


*Figure 3.2.4.8 – Caster angle – Test bench*

For what concerns the caster angle, the extreme positions “A”, “G”, “C” and “I”, show the same behaviour but in a mirrored way.

All the five positions have the same trend, that is an almost constant caster angle during the entire test. What is different is only the starting value: the two positions that lead to have the upper control arm nearer to the origin produce a negative caster angle. On the other hand, the two positions which move the upper control arm further away from the origin, lead to a positive camber angle.

Caster angle: trend curves

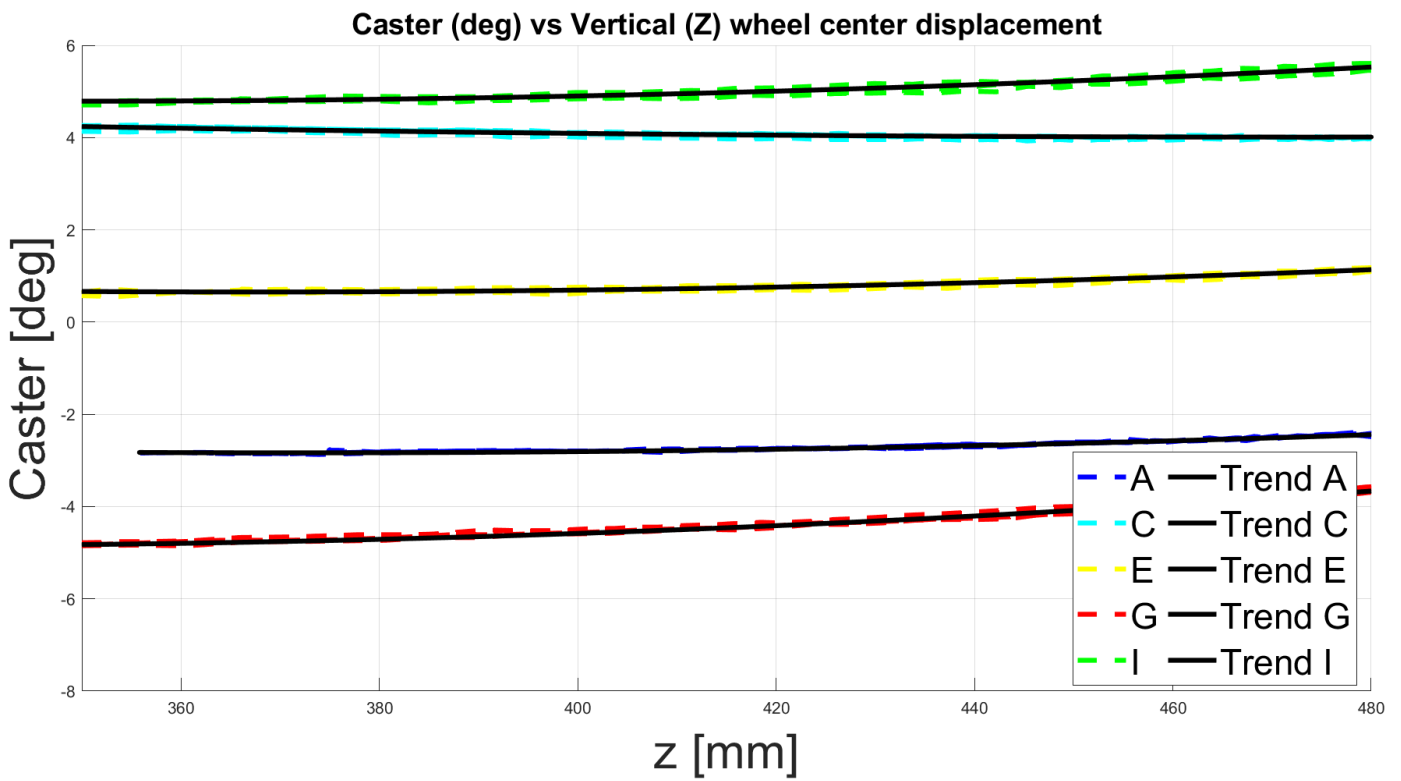


Figure 3.2.4.9 – Caster angle - Trend curves

CASTER ANGLE		
	Equation	$R^2$
<b>A</b>	$0.0000335 \cdot Z^2 - 0.0249 \cdot Z + 1.7918$	0.9747
<b>C</b>	$0.000015 \cdot Z^2 - 0.0142 \cdot Z + 7.3707$	0.9738
<b>E</b>	$0.000038 \cdot Z^2 - 0.0279 \cdot Z + 5.7732$	0.9697
<b>G</b>	$0.000051 \cdot Z^2 - 0.0334 \cdot Z + 0.6177$	0.9889
<b>I</b>	$0.000043 \cdot Z^2 - 0.03 \cdot Z + 10.021$	0.9723

Table 3.2.4.4 – Trend curve equations

Caster angle trend lines show a good correspondence with the experimental curves.  $R^2$  term is not as higher as the previous ones only because of some oscillations present in the curves which, however, does not compromise the reliability.

## Steer angle

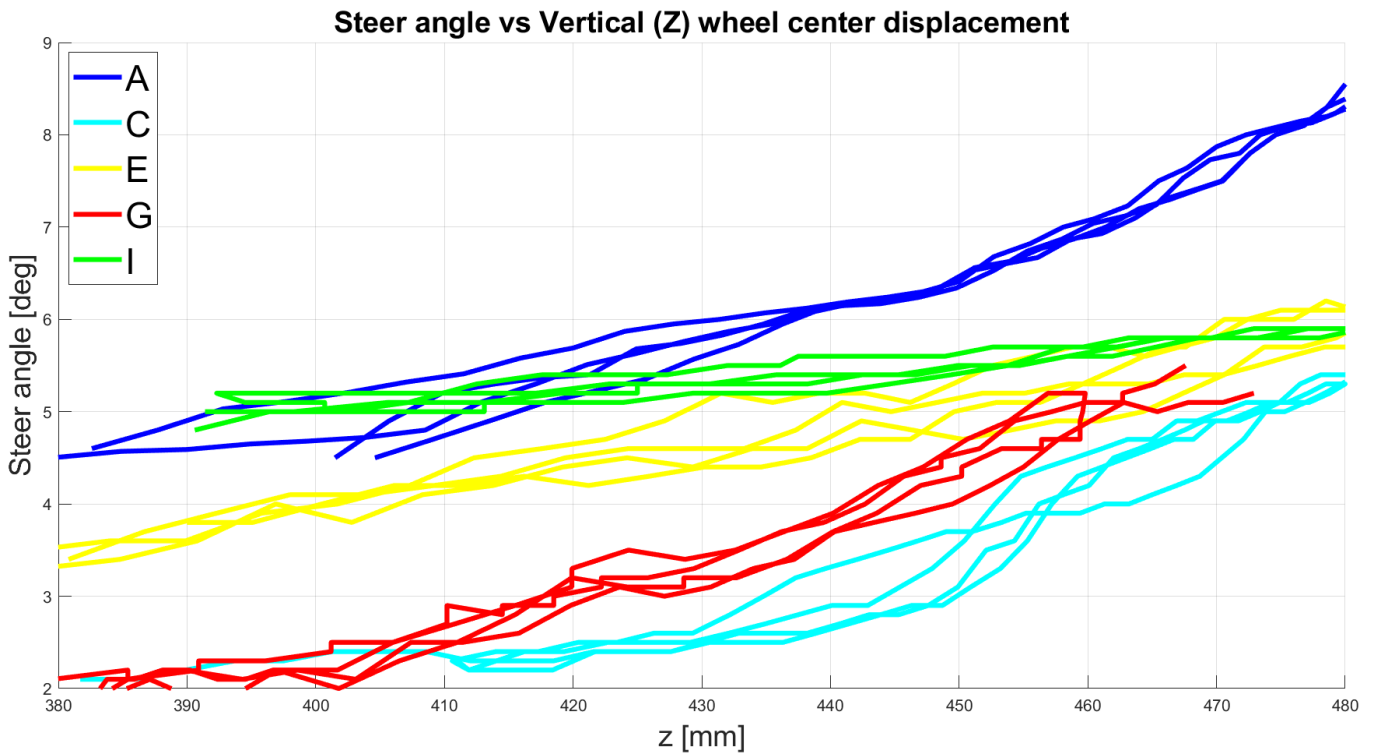


Figure 3.2.4.10 – Steer angle – Test bench

The steering angle acquisition is the most complex. It is not directly done by a potentiometer which acquires the angle, but it is the result of geometrical calculations. The latter are computed inside the function “fcn\_sterzo”, which is included in the Matlab code.

Moreover, it is not linear, but it presents a lot of oscillations because of the screw instability, which leads to have a certain relative motion between the inner and the outer parts of the tie rod. This faulty behaviour is particularly evident for too low and too high z values. For this reason, the tests have been performed only for wheel vertical displacement ranging from 380 mm and 480 mm.

Steer angle: trend curves

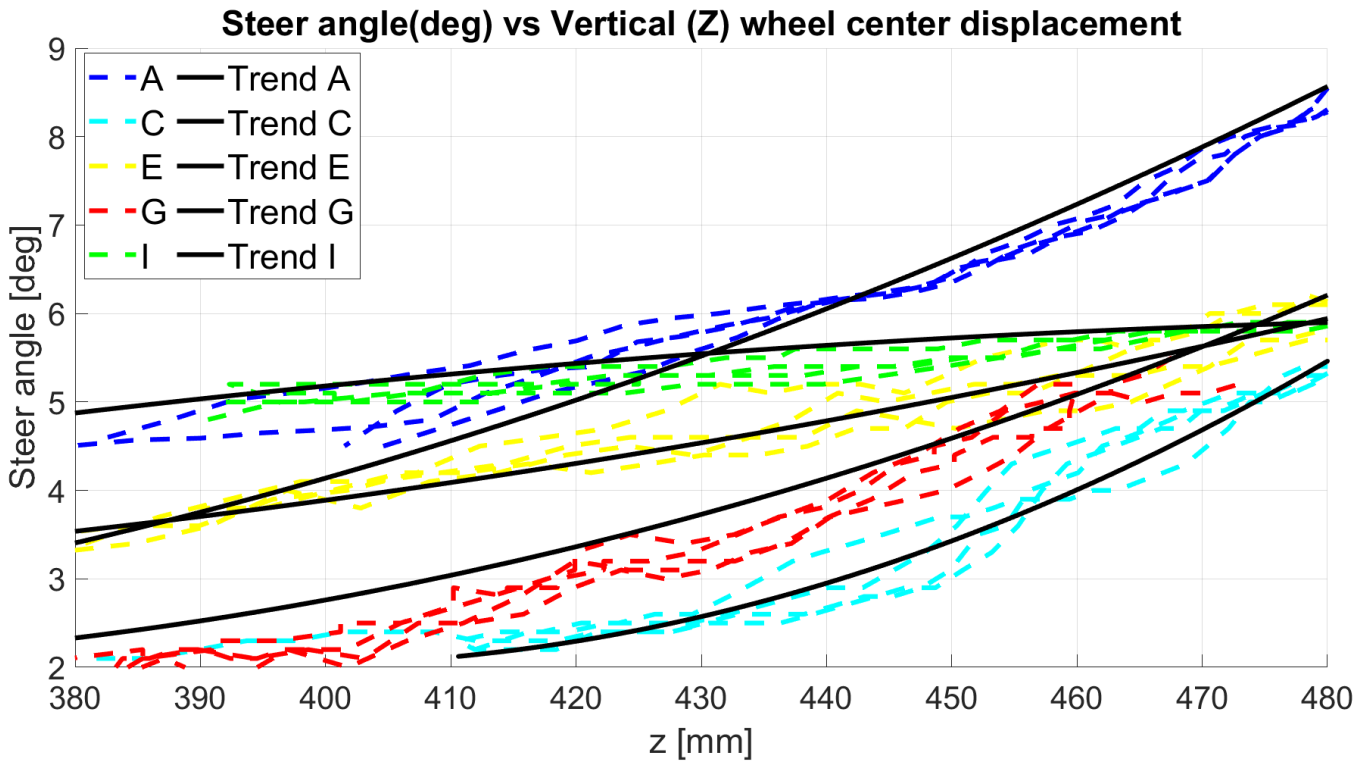


Figure 3.2.4.11 – Steer angle - Trend curves

STEER ANGLE		
	Equation	$R^2$
<b>A</b>	$0.000187 \cdot Z^2 - 0.1092 \cdot Z + 12.898$	0.9436
<b>C</b>	$0.000499 \cdot Z^2 - 0.3963 \cdot Z + 75.716$	0.954
<b>E</b>	$0.000081 \cdot Z^2 - 0.0456 \cdot Z + 4.1683$	0.9528
<b>G</b>	$0.000216 \cdot Z^2 - 0.147 \cdot Z + 22$	0.8814
<b>I</b>	$-0.000063 \cdot Z^2 + 0.0644 \cdot Z - 15.499$	0.8585

Table 3.2.4.5 – Trend curve equations

For the reasons listed above, plot is not precise. Trend lines are not perfectly overlapped because of the irregular behaviour of the steering angle, and so  $R^2$  in some cases assumes low values.

## 4. MSC/Adams car

MSC/Adams is a software used in multibody dynamics field to investigate the behaviour of bodies. It solves the equations kinematics and dynamics are based on. It is one of the most used software since thanks to it, it is possible to analyse the dynamics of parts in movement. Moreover, it is possible to know also forces and loads distribution, basing on the resolution of non-linear equation. Its advantage is that, on doing it, it is faster and more precise than a FEA (finite element analysis). This is due to the fact that, regards the computation of loads and forces, MSC/Adams simulations give a more precise assessment about how do they vary on a wide range of movement and operational environments. It is also possible to add several parameters: velocities, masses, forces, and initial conditions. It also includes elements such as springs, contact between bodies, frictions and everything useful for replicating the reality.

The idea for this thesis is to replicate the test bench thanks to the multibody approach, being possible to virtual simulate the real conditions. Simulations are done both over the time and in relation to the vertical wheel centre displacement and as output it is possible to have animations, plots of all the parameters and numerical data.

The section “MSC/Adam’s car” is dedicated both to complete vehicle and vehicle subsystem analysis. For the construction of a model, the starting point is the “*template*” section, in which the typology of the system is defined and the construction of the system from a geometric point of view begins.

Once it is completed, in the “*subsystem*” environment the parameters of interest are modified according to the requests. As a last step there is the “*assembly*” section, which involves the match of several subsystems previously set up to create a complete suspension system.

Once the model is ready, simulations can be run. The software allows to choose between several types of simulations, so that it is possible to replicate almost all the real road conditions and the consequent vehicle motions. According to the obtained results it is possible to easily change the parameters until the optimal response is obtained. This kind of analysis, once the built models become reliable, permits to have an economic and time saving, enabling an early system-level validation.

## 4.1 Assembly system set-up

As already anticipated, the aim in this thesis work is to investigate the behaviour of a left double-wishbone suspension in terms of characteristics angles, such as camber angle, caster angle and steering angle, as response to a vertical deviation. To do that, as a first step, a double wishbone subsystem and a steering subsystem are chosen as starting points. In this case, the “TR FRONT SUSPENSION” and the “TR STEERING” subsystems are the initial models. The following step consists of the modification of both the subsystems to create geometries as much similar as possible to the ones of the real double-wishbone suspension, to make numerical results comparable with the experimental ones. This point predicts the need to know faithfully the dimensions of the different parts of the suspension in the test bench and therefore a double measure is made: the first one is done taking measures by hand on the test bench and the second one by means of the 3D CAD, released together with the bench.

These measures are taken by referring to an intermediate position of the suspension, it means with all the parameters set in the reference position and the wheel centre at 325 mm in z direction, which is the position at which the 3D model is defined.

The results obtained from the 3D CAD are reported in the table below, as a sequence of positional coordinates relative to the origin. The measurements taken manually, instead, are not further reported as they completely coincide with those of the CAD, as expected (except for some measurement errors of a few mm).

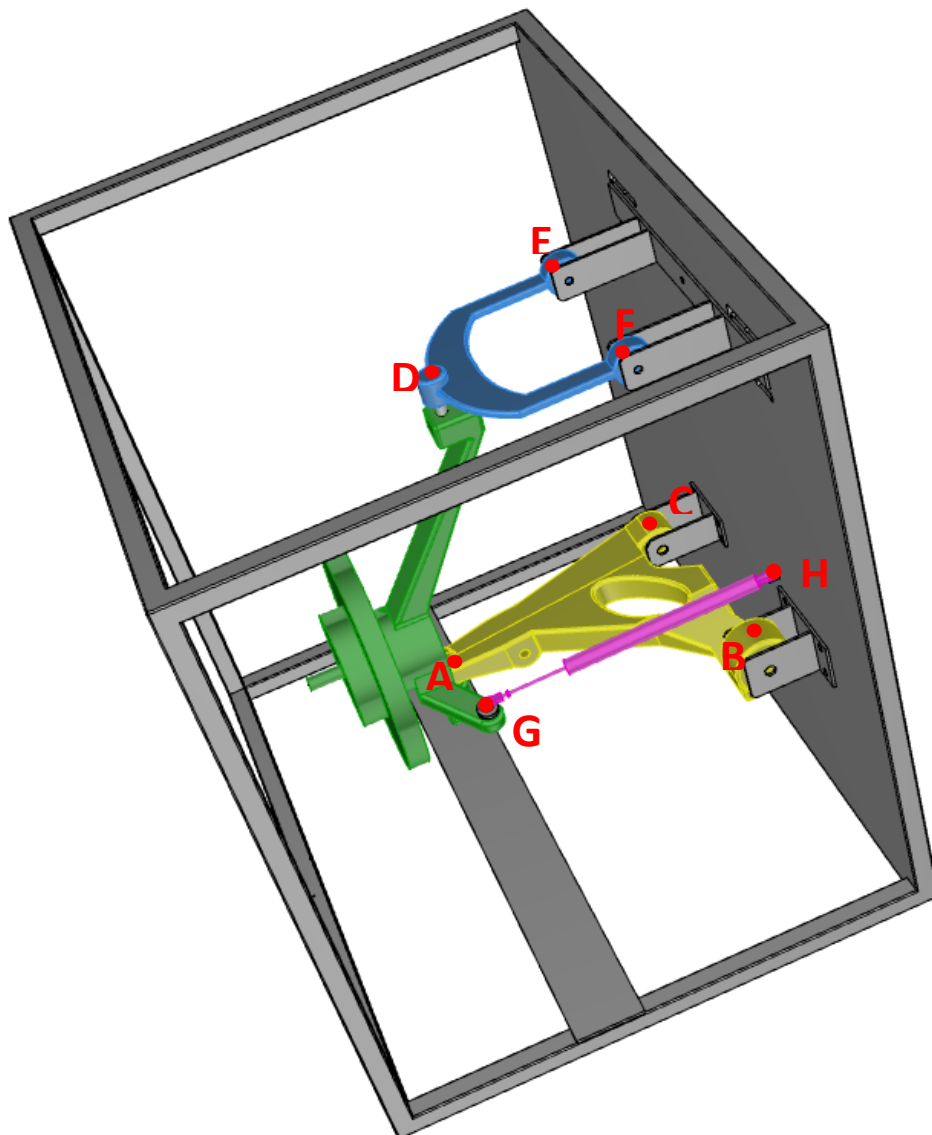


Figure 4.1.1 - Landmarks

<b>POINT</b>	<b>X</b>	<b>Y</b>	<b>Z</b>
<b>A</b>	516	457.4	267.83
<b>B</b>	227	0	325.4
<b>C</b>	573	0	325.4
<b>D</b>	408	349	785
<b>E</b>	530	0	785
<b>F</b>	285.5	0	785
<b>G</b>	369.27	425.303	286.53
<b>H</b>	302	0	390.8
<b>STRUT MOUNT</b>	460	320	270
<b>WC</b>	481.75	526.25	325.4

*Table 4.1.1 – Test bench reference coordinates – Mounting position E*

These measures are referred to the suspension in mounting position “E”, which is the central one. By varying it, also the coordinates relative to the upper control arm changes.

Here below are listed the coordinates of the three points subjected to variation:

<b>POINT</b>	<b>X</b>	<b>Y</b>	<b>Z</b>
<b>D</b>	448	349	825
<b>E</b>	570	0	825
<b>F</b>	325.5	0	825

*Table 4.1.2 – Test bench reference coordinates – Mounting position C*

<b>POINT</b>	<b>X</b>	<b>Y</b>	<b>Z</b>
<b>D</b>	368	349	825
<b>E</b>	490	0	825
<b>F</b>	245.5	0	825

*Table 4.1.3 – Test bench reference coordinates – Mounting position A*

<b>POINT</b>	<b>X</b>	<b>Y</b>	<b>Z</b>
<b>D</b>	368	349	745
<b>E</b>	490	0	745
<b>F</b>	245.5	0	745

*Table 4.1.4 – Test bench reference coordinates – Mounting position G*

<b>POINT</b>	<b>X</b>	<b>Y</b>	<b>Z</b>
<b>D</b>	448	349	745
<b>E</b>	570	0	745
<b>F</b>	325.5	0	745

*Table 4.1.5 – Test bench reference coordinates – Mounting position I*

Once these measurements are taken, the suspension is perfectly known under a geometric point of view. All these measures are then reported in the previously built MSC/Adams Car suspension subsystem. This is done by modifying the placement in space of the hard points which identify the different elements.

MSC/Adam's suspension assembly has some components which are not physically present on the test bench, since they are substituted by potentiometers. Because of that, these components coordinates were chosen with criteria, by reproducing a situation as much similar as possible to a real suspension geometry.

To be clearer, a detailed description of the suspension subsystem is done:

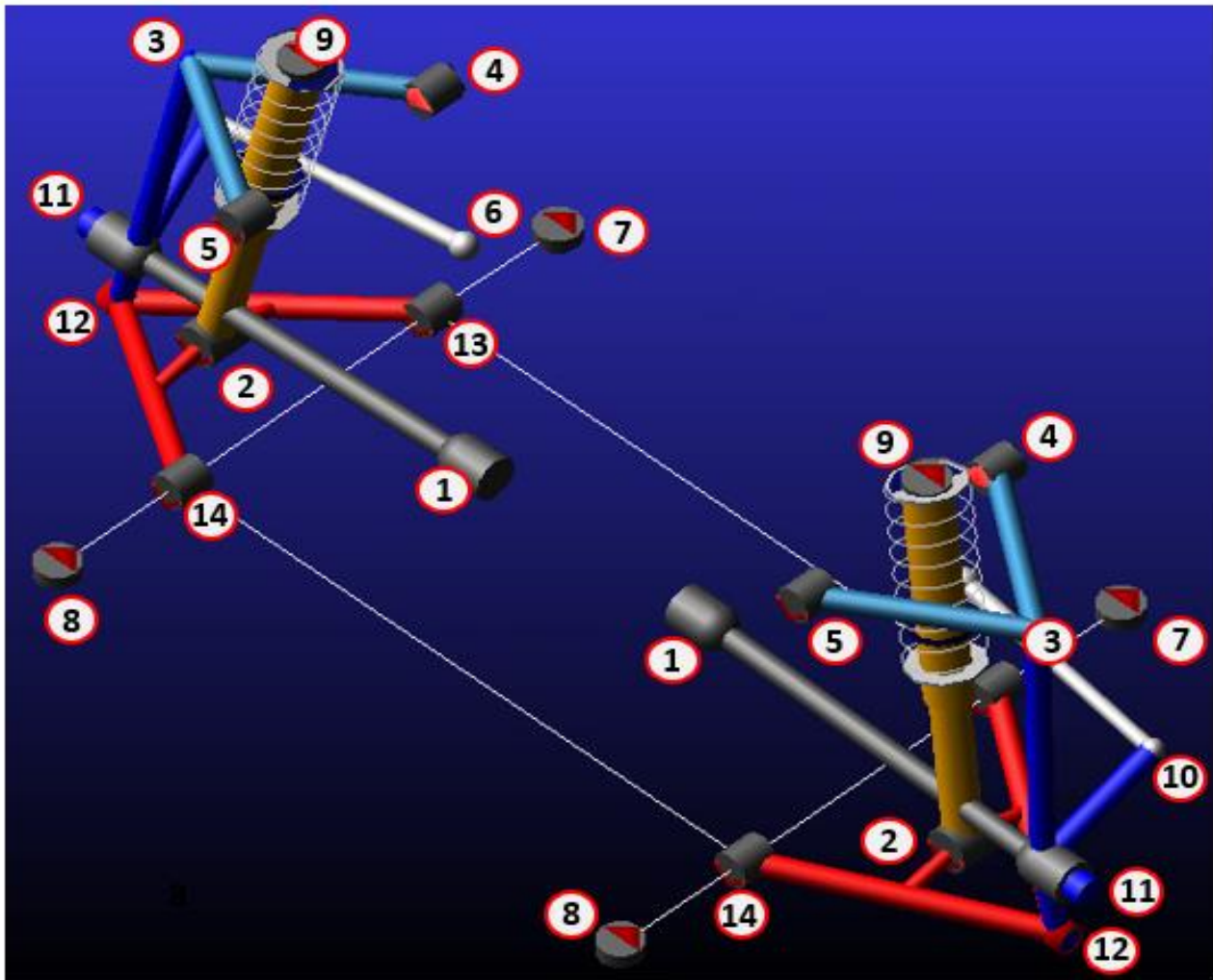
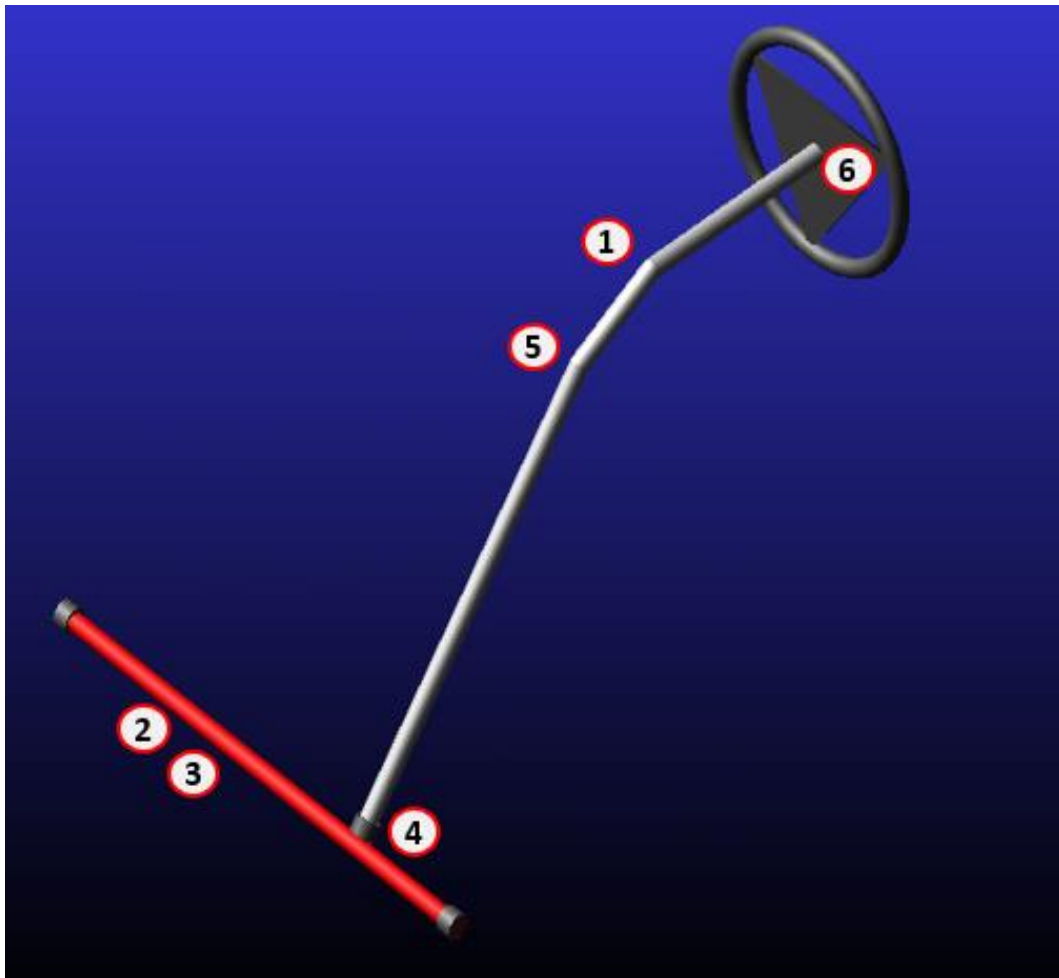


Figure 4.1.2 – Suspension hardpoints

- |                            |                             |
|----------------------------|-----------------------------|
| 1. Drive shaft             | 8. Subframe front           |
| 2. Lower structure mount   | 9. Top mount                |
| 3. Upper control arm outer | 10. Tierod outer            |
| 4. Upper control arm rear  | 11. Wheel centre            |
| 5. Upper control arm front | 12. Lower control arm outer |
| 6. Tierod inner            | 13. Lower control arm rear  |
| 7. Subframe rear           | 14. Lower control arm front |

The following picture shows the steering subsystem used for the assembly construction, which is the “TR\_steering”:



*Figure 4.1.3 – Steering subsystem*

It is composed by:

- 1- Intermediate shaft reward
- 2- Rack house mount
- 3- Tie rod inner
- 4- Pinion pivot
- 5- Intermediate shaft forward
- 6- Steering wheel centre

The tie rod is not visible since it is internal to the rack house mount but its coordinates are the same to the ones reported in the suspension subsystem.

After completing the creation of the two subsystems, they are integrated together to create the assembly system being analysed, shown in the picture below, which also includes the wheel.

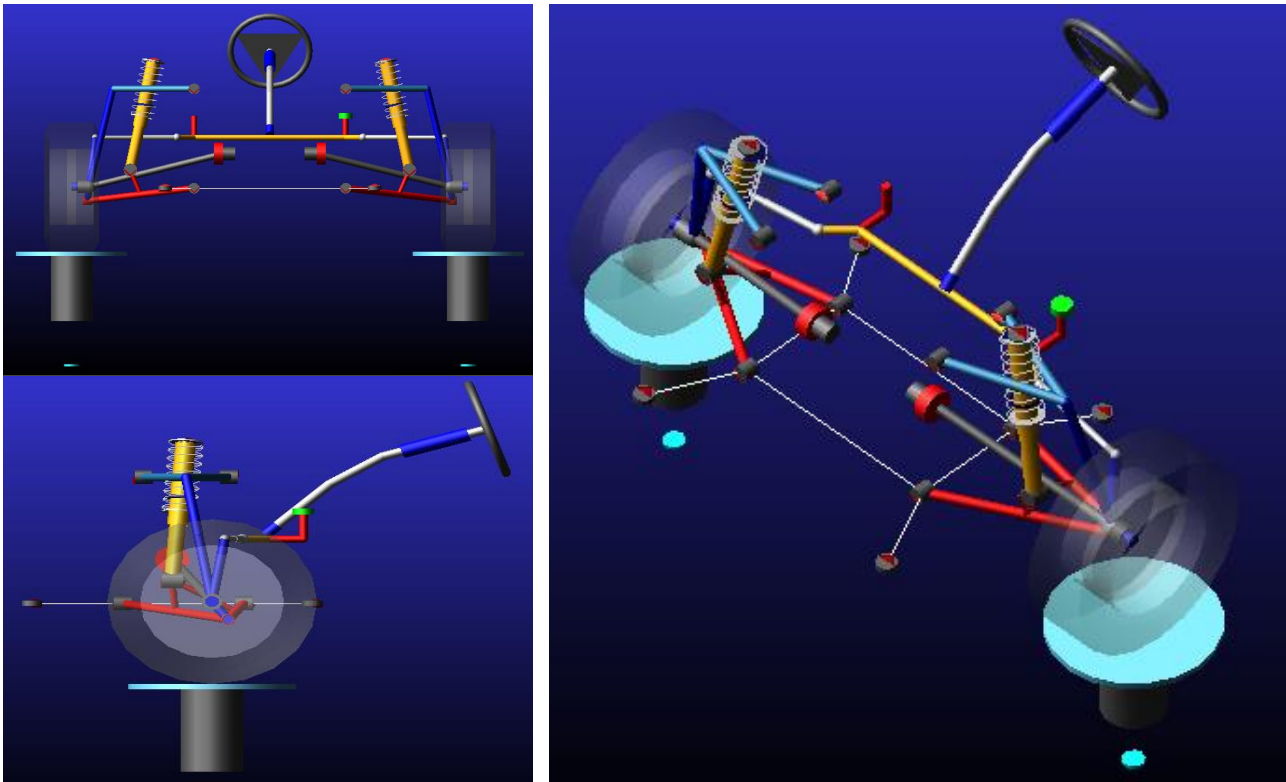


*Figure 4.1.4 – MSC/Adams Car assembly: ISO, front, and lateral view [14]*

For the construction of this assembly, the linking points are equipped with ideal bushings, so that there is no stiffness torque. It could be done since what is being carried out is a kinematic test and so dynamic quantities are not relevant.

What is important to highlight is that, the creation of this model is not done by simply reporting the coordinates from the test bench to the software, since, by doing this, the model leads to some problems during the starting of the simulation.

The following procedure is described here below:

- Starting from the initial suspension model, to keep unvaried wheel centre coordinates in x and y direction.
- To choose a coordinate for the wheel centre in z direction which was coherent with the model
- To define all the other hardpoint coordinates, by accurately reporting the real distances between the different parts as a function of the distance from the wheel centre coordinates.

All the coordinates are reported to the left side suspension, since in the test bench it is present a left wheel suspension system.

The comparison between Test Bench suspension coordinates and MSC/Adams Car model coordinates are shown below, referred to the central mounting position E:

Test Bench coordinates			
POINT	X	Y	Z
A	-516	-457.4	267.83
B	-227	0	325.4
C	-573	0	325.4
D	-408	-349	785
E	-530	0	785
F	-285.5	0	785
G	-369.27	-425.303	286.53
H	-302	0	390.8
STRUT MOUNT	-460	-320	270
WC	-481.75	-526.25	325.4

Table 4.1.6 – Test bench coordinates

MSC/Adams Car coordinates			
POINT	X	Y	Z
A	-34.25	-731.15	15.155
B	254.75	-273.75	72.725
C	-91.25	-273.75	72.725
D	73.75	-622.75	532.325
E	-48.25	-273.75	532.325
F	196.25	-273.75	532.325
G	112.48	-699.05	33.855
H	179.75	-273.75	138.125
STRUT MOUNT	21.75	-593.75	17.325
WC	0	-800	72.725

Table 4.1.7 – MSC/Adams Car coordinates

As already said, MSC/Adams Car reference system is different from the one set in the Test Bench. In detail, x and y axes are in the opposite way. For this reason, all the coordinates of the bench suspension are changed in sign.

The table above shows the coordinates after this operation, therefore with the coordinates in the opposite direction in respect to the real situation.

The offset between Test Bench and MSC/Adams Car coordinates, related to the wheel centre, is:

- In x direction = - 481.75 mm
- In y direction = 273.75 mm
- In z direction = 252.7 mm

Obviously, to maintain the coherence between the real and the virtual suspensions, the same offset is reported in all the other points. These offset are then taken in consideration during the post processing of the data, in order to make simulation results comparable.

Here below are listed the differences in MSC/Adams Car model between the different mounting positions, exclusively relative to the upper control arm:

POINT	X	Y	Z
D	33.75	-622.75	572.325
E	-88.25	-273.75	572.325
F	156.25	-273.75	572.325

Mounting position C

POINT	X	Y	Z
D	113.75	-622.75	492.325
E	-8.25	-273.75	492.325
F	236.25	-273.75	492.325

Mounting position G

POINT	X	Y	Z
D	113.75	-622.75	572.325
E	-8.25	-273.75	572.325
F	236.25	-273.75	572.325

Mounting position A

POINT	X	Y	Z
D	929.75	-622.75	492.325
E	1051.75	-273.75	492.325
F	807.25	-273.75	492.325

Mounting position I

## 4.2 Simulation parameters

In each simulation it is possible to change all the specifications here below:

- Actuation type: it is possible to choose between “contact patch” and “wheel centre”.
- Tire unloaded radius: it is different from the tire loaded radius since tire is a deformable body, whose deformation is not negligible. It is equal to the ratio between the *zero velocity centre* of the system and the *angular speed* [3].
- Tire stiffness: it depends on the vertical load, on the air pressure, on the camber, on the rim size, on the speed and on the wear. It also changes according to the lateral forces (through the slip angle) and longitudinal forces (through the slip ratio) [3].
- Wheel mass: it is part of the unsprung mass, together with the tires, the differential and the brakes [3].
- Sprung mass: it includes the chassis, the motor, the interior, the body and all the passengers [3].
- CG height: the centre of mass can be defined as a unique point at which a vehicle behaves as all its mass is concentrated there, therefore, by applying a force on it, the car starts moving without rotating. It is very important for what concerns vehicle handling, because it influences the balance and the steering. The load transfer depends on its height, therefore it is relevant when cornering. The lower it is, the higher the performance advantages are [12].
- Wheelbase: it is the distance between the front and the rear axle. It has effect on the weight distribution and, because of that, balance and steering depend on it [13].
- Drive ratio: this parameter leads to understand how the movement transfers between gears.
- Brake ratio: it is the ratio between the braking force against the wheels and the vehicle weight.
- Camber angle: as already anticipated, it is the angle between the plane on which the wheel rolls and the vertical axis of the vehicle. It can be positive, neutral, or negative and its aim is to improve the adherence.
- Toe angle: it is the angle between each wheel and the longitudinal axis of the vehicle. It can be positive, nil or negative and it is used to improve braking stability.

Furthermore, different types of simulations are available: parallel wheel travel, opposite wheel travel, single wheel travel, full vehicle [...].

In this thesis, it is always used parallel wheel travel, since it is the one that enable the suspension to perform the same motion performed also in the test bench. The opposite wheel travel is not used since it takes also into account the eventual presence of a roll bar, which, instead, is not considered on the test bench suspension.

### 4.3 Simulation set-up

Once the model is ready and parameters are set, it is important to be sure that the initial conditions are the same as those set in the test bench.

In detail, the lower and the upper points reached by the wheel centre during the simulation correspond to the ones reached by the wheel centre in the test bench.

During the post processing of the data, the offset reported in MSC/Adam's Car model are taken into account by reporting them in the results of all the performed simulations. They are:

- $X_{MSC/Adams} = X_{TestBench} + 482$
- $Y_{MSC/Adams} = Y_{TestBench} - 274$
- $Z_{MSC/Adams} = Z_{TestBench} - 253$

Moreover, because of different sign conventions, it is necessary to modify the results for the longitudinal and the lateral wheel centre displacement and the ones for the camber angle, which are in the opposite direction in respect to the one of the test bench.

All the tests are done by simulating a “parallel wheel travel”, by following the procedure illustrated below:

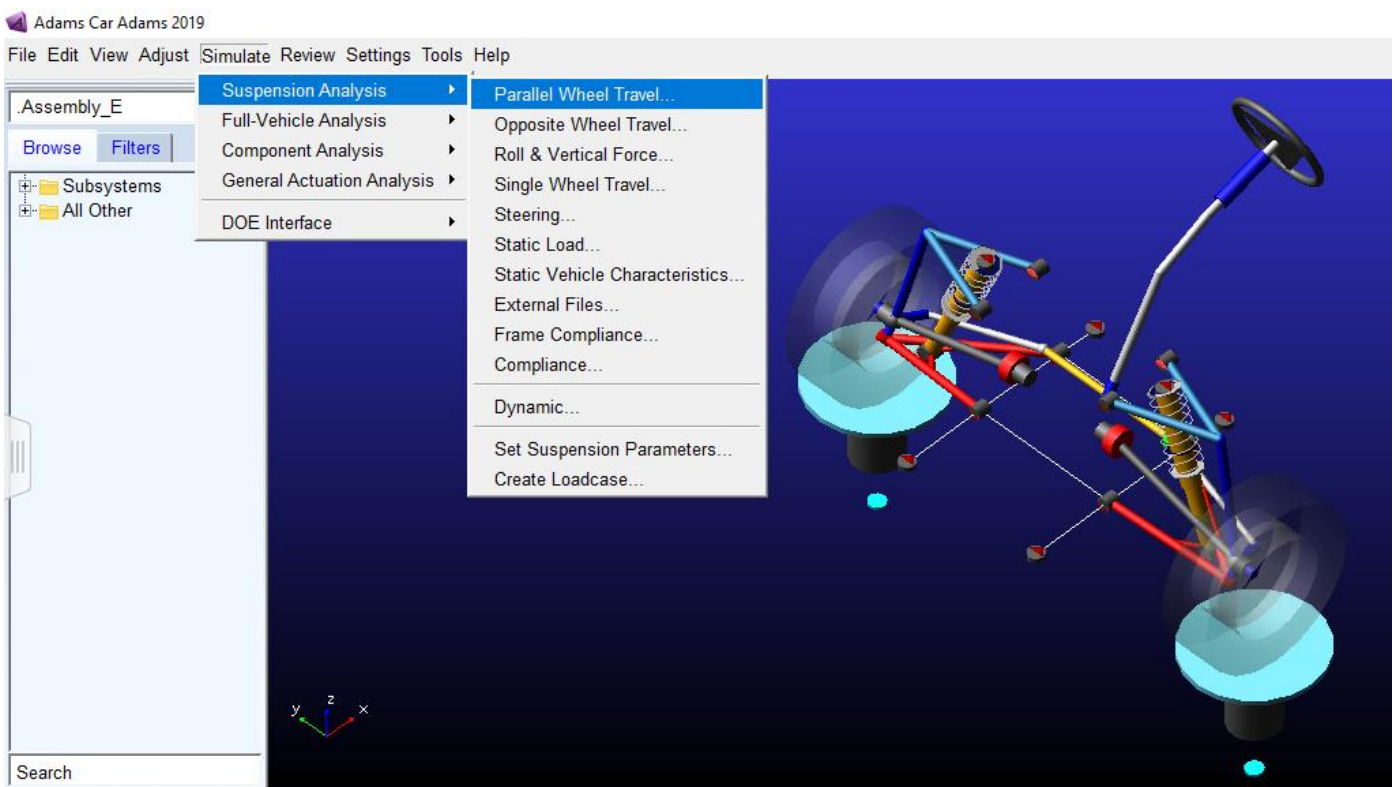


Figure 4.3.1 – MSC/Adams Car screenshot [14]

Once the simulation type is selected, it is necessary to complete the field with the required informations:

- Suspension assembly: it must indicate the assembly to which perform the simulation. In the case shown in the following screenshot, it is launched a simulation for the assembly relative to the suspension in “E” mounting position.
- Output prefix: this field requires the insertion of the name with which the test will be saved.
- Number of Steps: it is chosen a total of 50 steps, that is enough for this simulation, since this is a kinematic analysis.
- Mode of simulation: it is left the default choice, “interactive”.
- Travel relative to: “Wheel Centre” choice provides that the imposed limits are relative to the wheel centre displacement.
- Bump travel: it requires the lower point reached by the wheel centre.
- Rebound travel: it requires the higher point reached by the wheel centre.

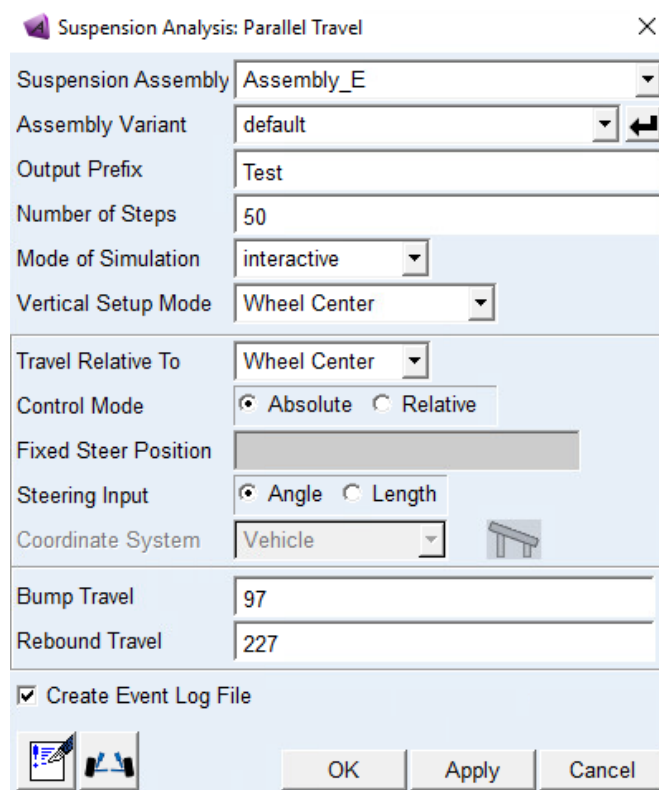


Figure 4.3.2 – MSC/Adams Car simulation screenshot [14]

For all the tests, it is imposed a total vertical excursion of around 130 mm. In detail, by considering that in the test bench the lower and the upper limits are respectively 350 mm and 480 mm, and, by considering the offset in z coordinate, the limits in MSC/Adams Car are 97 and 227 mm.

Once the simulation is completed and the loading of the results is done, clicking on “Review”, it is possible to open the “Post processing window”. MSC/Adams Post Processor gives different alternatives:

- Animation
- Plotting
- Report
- Plot3D
- 4D Plotting
- VideoFile
- PlotCurve3D

In this case, the selected solution is “Plotting”.

The interface is the one shown below:

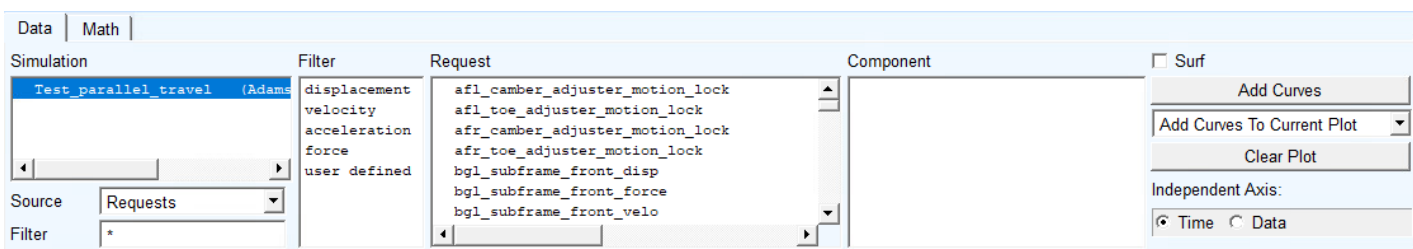


Figure 4.3.2 – MSC/Adams Car Post Processor Window [14]

- In “simulation” field are available all the performed simulations
- By selecting the voice “Data”, which is below the voice “Independent Axis”, it is possible to select the variable the plotted quantities are related to. The following screenshot will open, and, after selecting “user defined” and “testrig” it is sufficient to choose the quantity of interest.

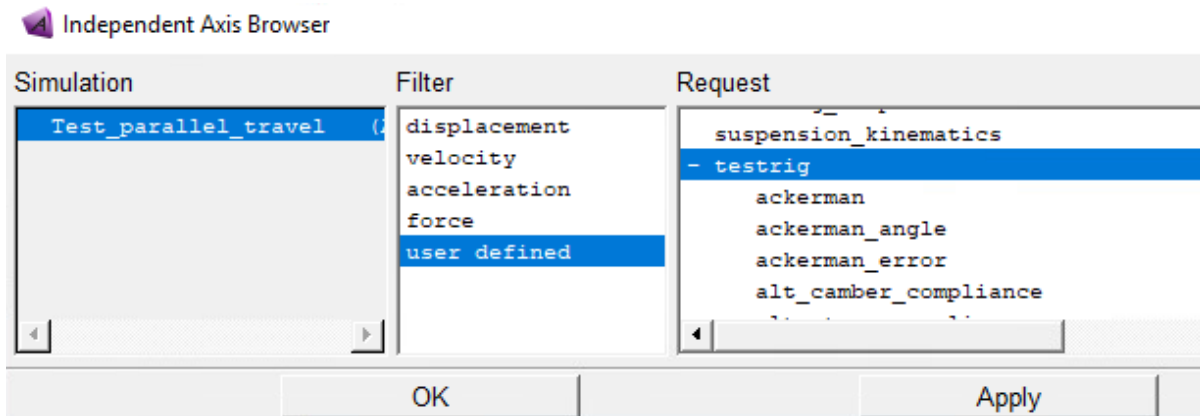


Figure 4.3.3 – MSC/Adams Car screenshot [14]

- The following step is to choose, from “Request” field, all the quantities the user is interested on.

The result is a plot like the one represented here below:

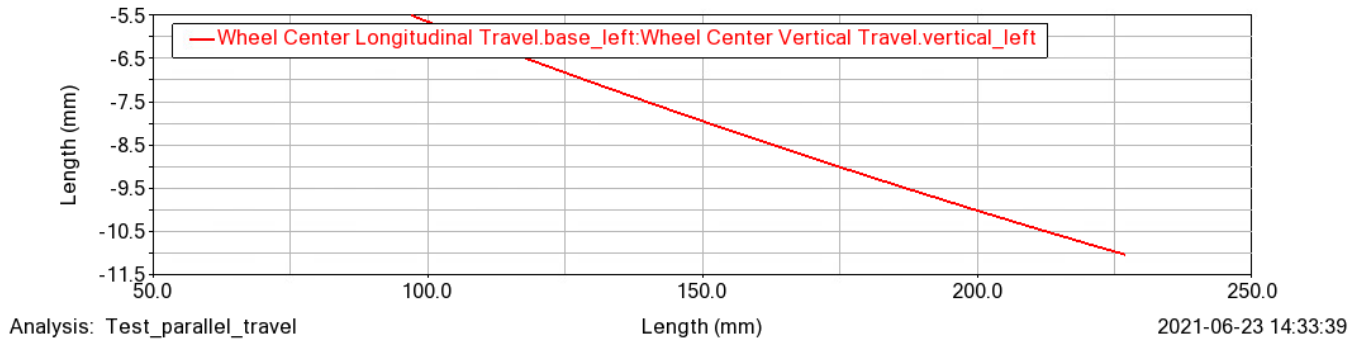


Figure 4.3.4 – MSC/Adams Car plot [14]

The data saving process occurs by clicking on “Export” and by selecting the voice of own interest.

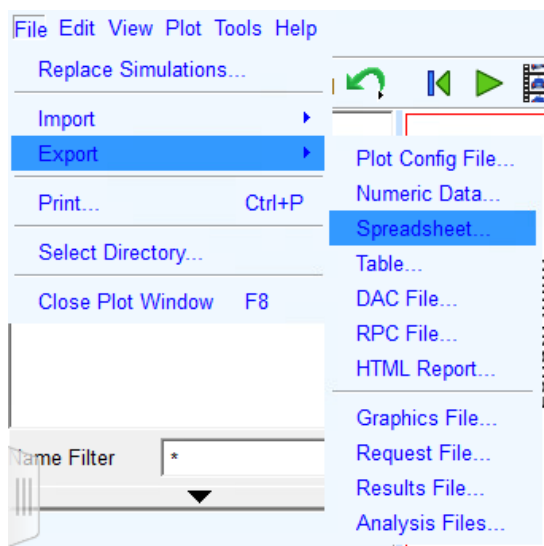


Figure 4.3.5 – MSC/Adams Car saving process [14]

In this case it is selected “Table” and “spreadsheet” format:

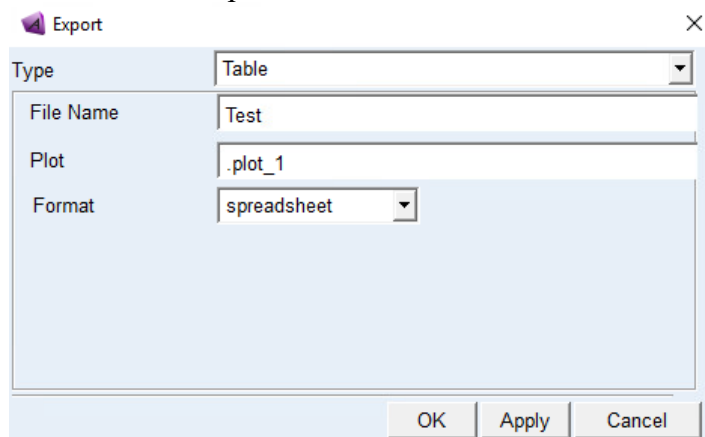


Figure 4.3.6 – MSC/Adams Car saving process [14]

By following this procedure, it is obtained a “TAB file” with all the data which are later postprocessed on Matlab making them comparable with the ones obtained experimentally.

## 4.4 Original vs modified suspension behaviour

The purpose of this chapter is to demonstrate in a short way the correctness of the model after modification, verifying that it doesn't behave abnormally. To do that, it follows a comparison of all the analysed quantities behaviour in the original suspension and in the modified one. As already said, the starting template is "TR\_FRONT\_SUSPENSION", which assembled with the steering subsystem gives, upstream of any modification, the model showed below:

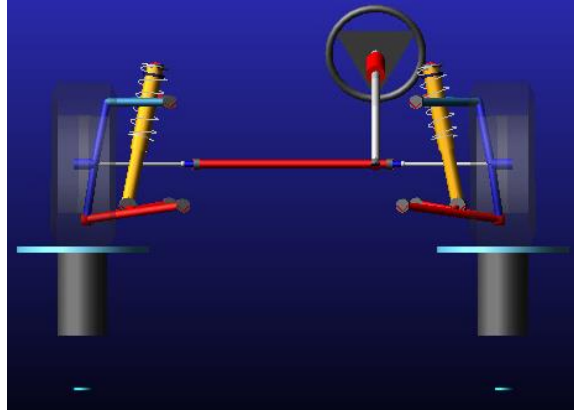


Figure 4.4.1 – Original assembly

To highlight the differences, here are reported two tables with the coordinates of all the hardpoints of both the original and the modified suspensions.

		X	Y	Z
<b>Original suspension</b>	<b>Drive shaft</b>	0	-200	225
	<b>LCA front</b>	-200	-450	150
	<b>LCA outer</b>	0	-750	100
	<b>LCA rear</b>	200	-450	155
	<b>Lower strut mount</b>	0	-600	150
	<b>Subframe front</b>	-400	-450	150
	<b>Subframe rear</b>	400	-450	150
	<b>Tie rod inner</b>	200	-400	200
	<b>Tie rod outer</b>	150	-750	300
	<b>Top mount</b>	40	-500	650
	<b>UCA front</b>	-100	-450	525
	<b>UCA outer</b>	40	-675	525
	<b>UCA rear</b>	200	-450	525
	<b>Wheel centre</b>	0	-800	200

		X	Y	Z
<b>Modified suspension</b>	<b>Drive shaft</b>	0	-200	225
	<b>LCA front</b>	-91.25	-273.75	72.725
	<b>LCA outer</b>	-34.25	-731.15	15.155
	<b>LCA rear</b>	245.75	-273.75	72.725
	<b>Lower strut mount</b>	21.75	-593.75	17.325
	<b>Subframe front</b>	-400	-273.75	65.4
	<b>Subframe rear</b>	400	-273.75	65.4
	<b>Tie rod inner</b>	179.75	-273.75	138.25
	<b>Tie rod outer</b>	112.48	-699.053	33.855
	<b>Top mount</b>	40	-380	530
	<b>UCA front</b>	-88.25	-273.75	492.325
	<b>UCA outer</b>	33.75	-622.75	492.362
	<b>UCA rear</b>	156.25	-273.75	492.325
	<b>Wheel centre</b>	0	-800	72.725

Table 4.4.1 – Original and modified suspension's coordinates

<b>Original</b>	<b>Tierod inner</b>	0	-400	300
	<b>Int. Shaft forward</b>	0	-200	860
	<b>Int. Shaft reward</b>	0	-200	930
	<b>Steering WC</b>	1167	-200	900

<b>Modified</b>	<b>Tierod inner</b>	179.75	-273.75	138.25
	<b>Int. Shaft forward</b>	400	0	500
	<b>Int. Shaft reward</b>	600	0	500
	<b>Steering WC</b>	900	0	700

Table 4.4.2 – Original and modified steering system coordinates

In these simulations, no offsets are added since the comparison is MSC/Adams-MSC/Adams and not with simulations performed on the test bench. The only difference considered is the one in wheel centre z coordinate, since the upper and the lower limits during bouncing are computed in respect to it.

*Wheel travel in longitudinal direction*

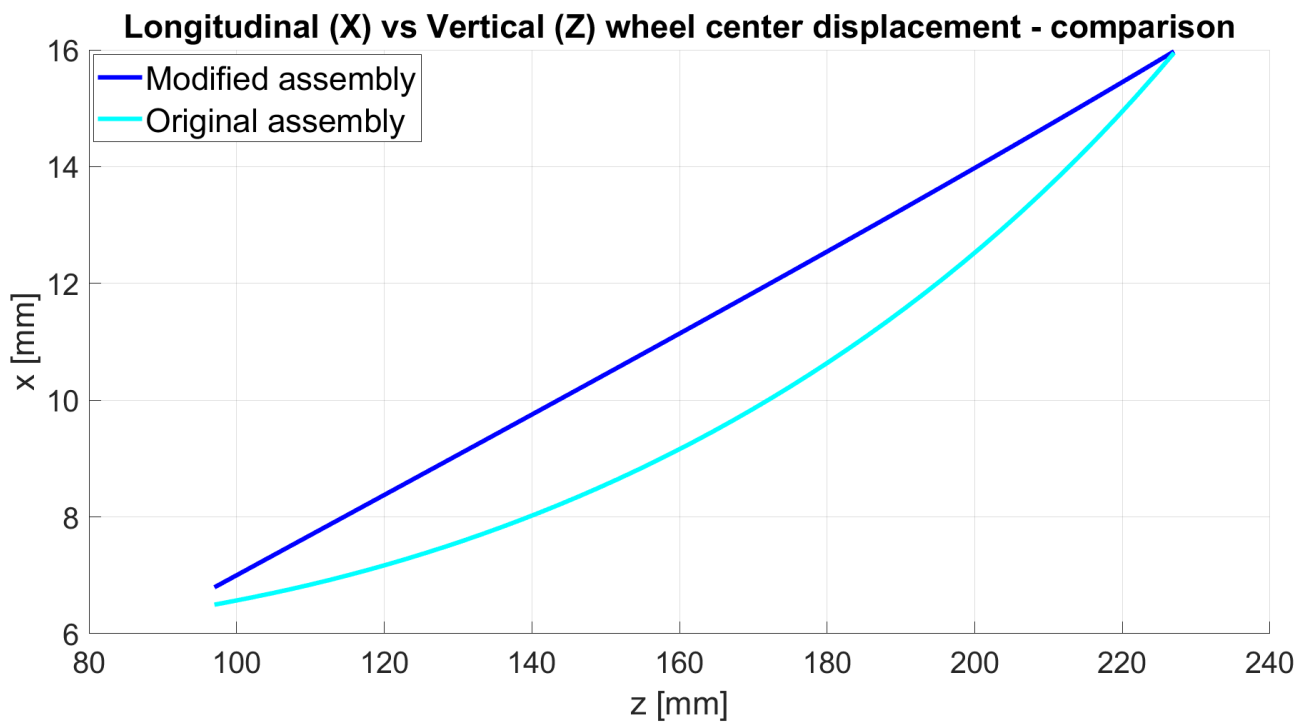


*Figure 4.4.2 – Modified VS original assembly: longitudinal wheel travel*

About the graph above, what it gives away is that:

- Starting and ending points are coincident, it means that both the suspensions, given a certain excursion in  $z$  direction, are subjected to the same displacement in longitudinal direction.
- The trend is slightly different in the two cases, since the modified suspension has a linear behaviour, differently from the original one.
- The curve related to the original suspension is not coincident with the one obtained on the test bench. The modified suspension, instead, reflects what was obtained experimentally.

*Wheel travel in longitudinal direction*

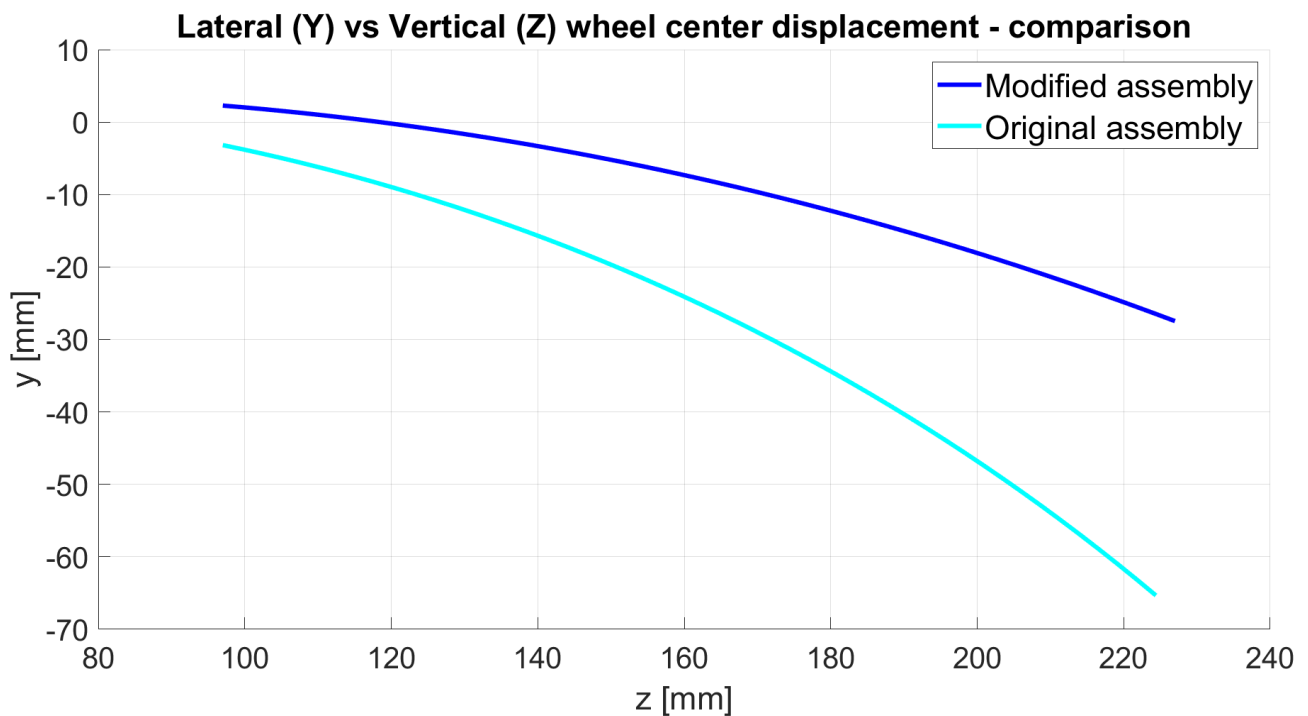


*Figure 4.4.3 – Modified VS original assembly: lateral wheel travel*

In lateral direction what emerges is that:

- The starting point in the two cases has a difference of about 5 mm. This offset grows up by moving on z direction, by arriving at the end of the bouncing, to 38 mm of difference. This means that, for the same excursion along z, the wheel centre of the original suspension is subjected to a displacement in y direction higher than the one of the modified suspension. In detail, in the latter, wheel centre position variation is equal to 20 mm, while the original suspension moves for 60 mm.
- Both the curves are subjected to a higher displacement in respect to the displacement obtained experimentally. However, in the simulation with the modified assembly, there are only 5 mm of difference, since, in test bench, the wheel centre moves of only 15 mm.
- The trend is for both the curves parabolic, as it happens in the test bench.

## Camber angle

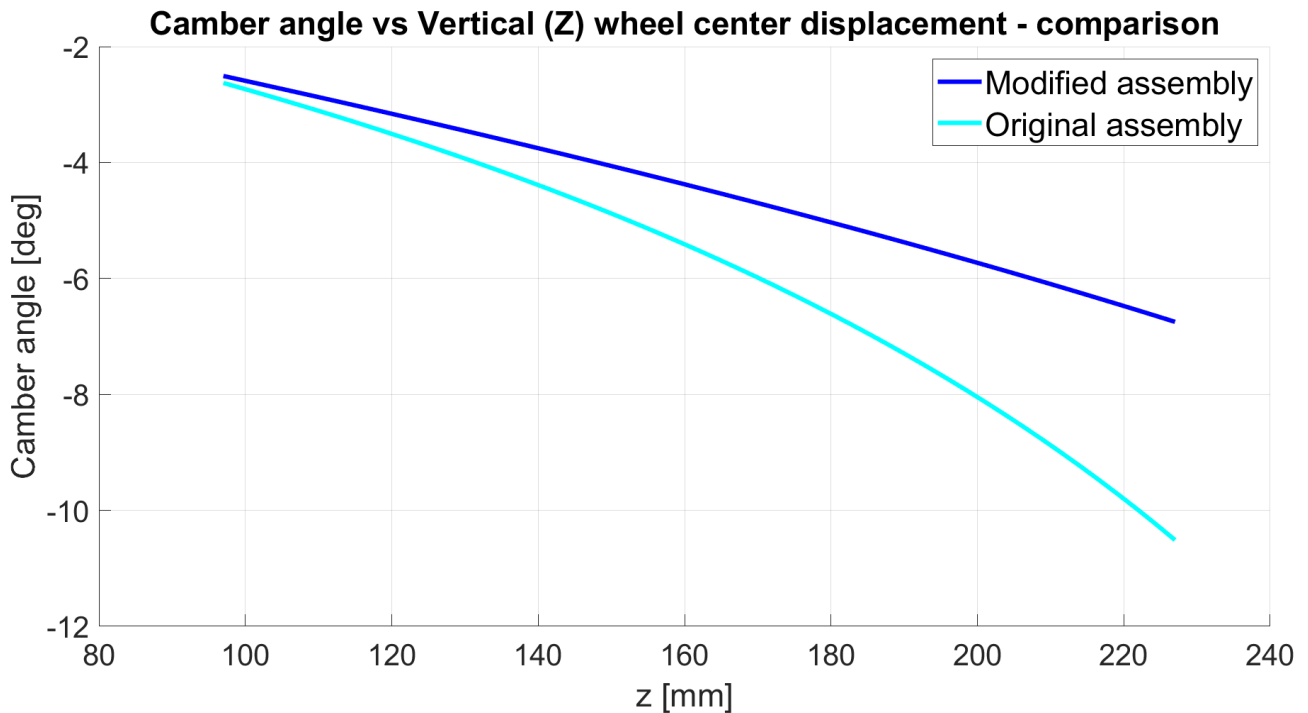


Figure 4.4.4 – Modified VS original assembly: camber angle

About the camber angle, considerations are like the previous ones:

- Starting point between the two curves is the same.
- In the upper limit of the simulation, the camber angle value is different.
- The original suspension's wheel centre variation is a little bit higher than the one of the modified one, equals respectively to 8 and 5.5 degrees. It is due to the difference on the geometry of the upper control arm.
- The trend of the two curves is not coincident since the modified suspension follows a linear behaviour and the original suspension does not.
- In terms of angle variation, the modified suspension shows a better correlation with the experimental results, which show a variation of 5 degrees.

This angle is particularly affected by the geometry of the suspension and especially of the steering wheel. The difference in the construction of the two models leads to this difference in camber behaviour.

Caster angle

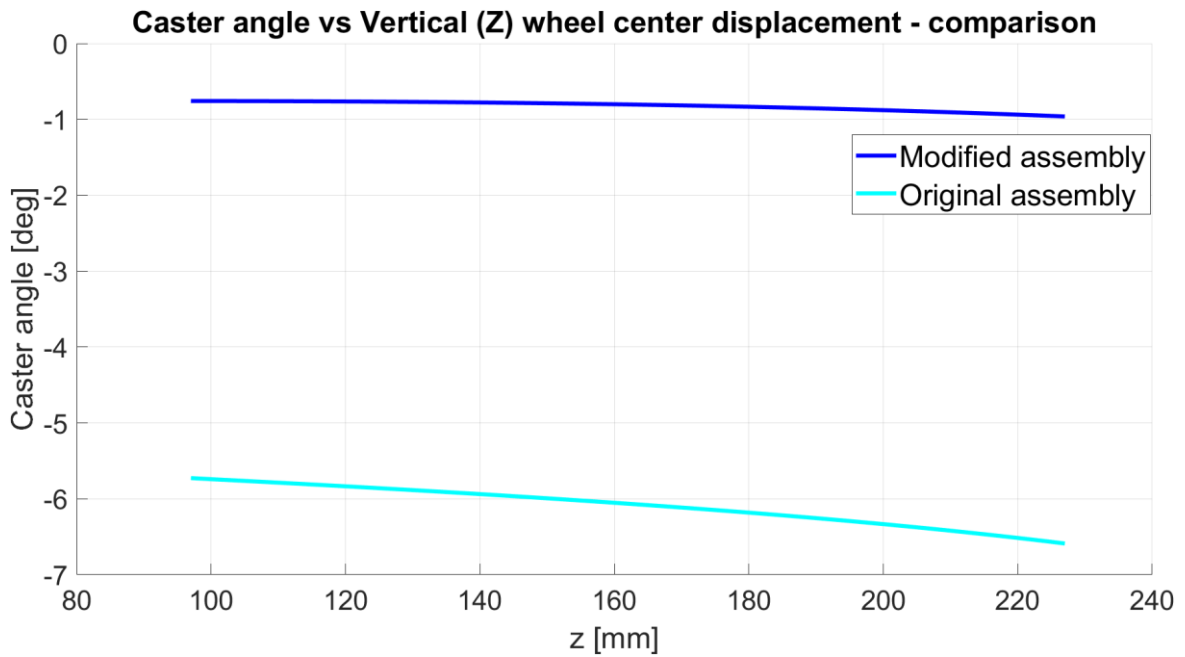


Figure 4.4.5 – Modified VS original assembly: caster angle

For a better analysis of the caster angle, below are reported the two curves in separate graphs, so that it is possible to see them in detail.

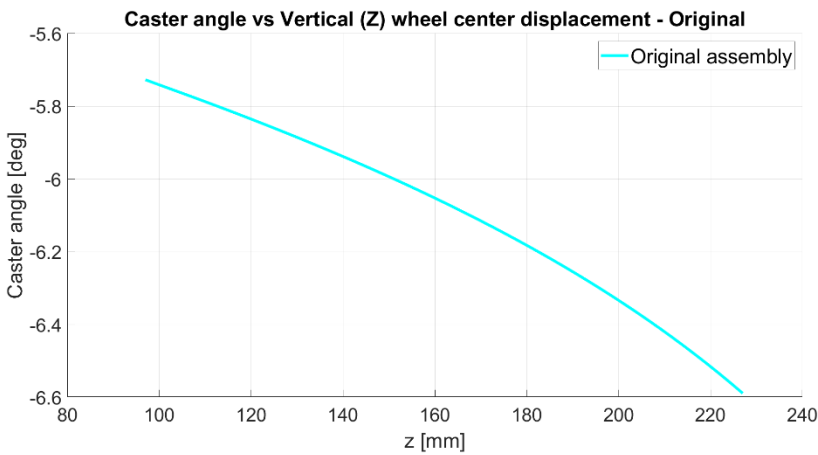


Figure 4.4.6 – Original assembly: caster angle

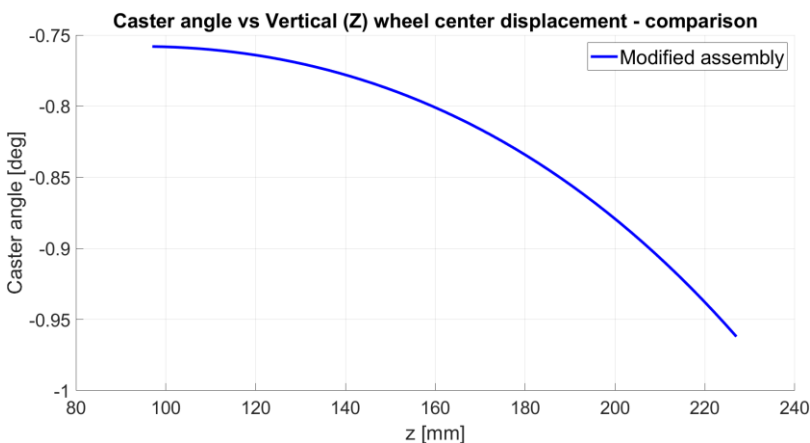


Figure 4.4.7 – Modified assembly: caster angle

- The higher difference between the two is the starting value. The original suspension has a certain caster angle value since the beginning. This is due only to the fact that the inclination of the steering axis in respect to the vertical axis is different in the two models.

- The variation is in both cases very small. It is equal to about 0.8 mm in the original suspension and to 0.3 mm in the modified one. The situation is the same also in the test bench.

Steer angle

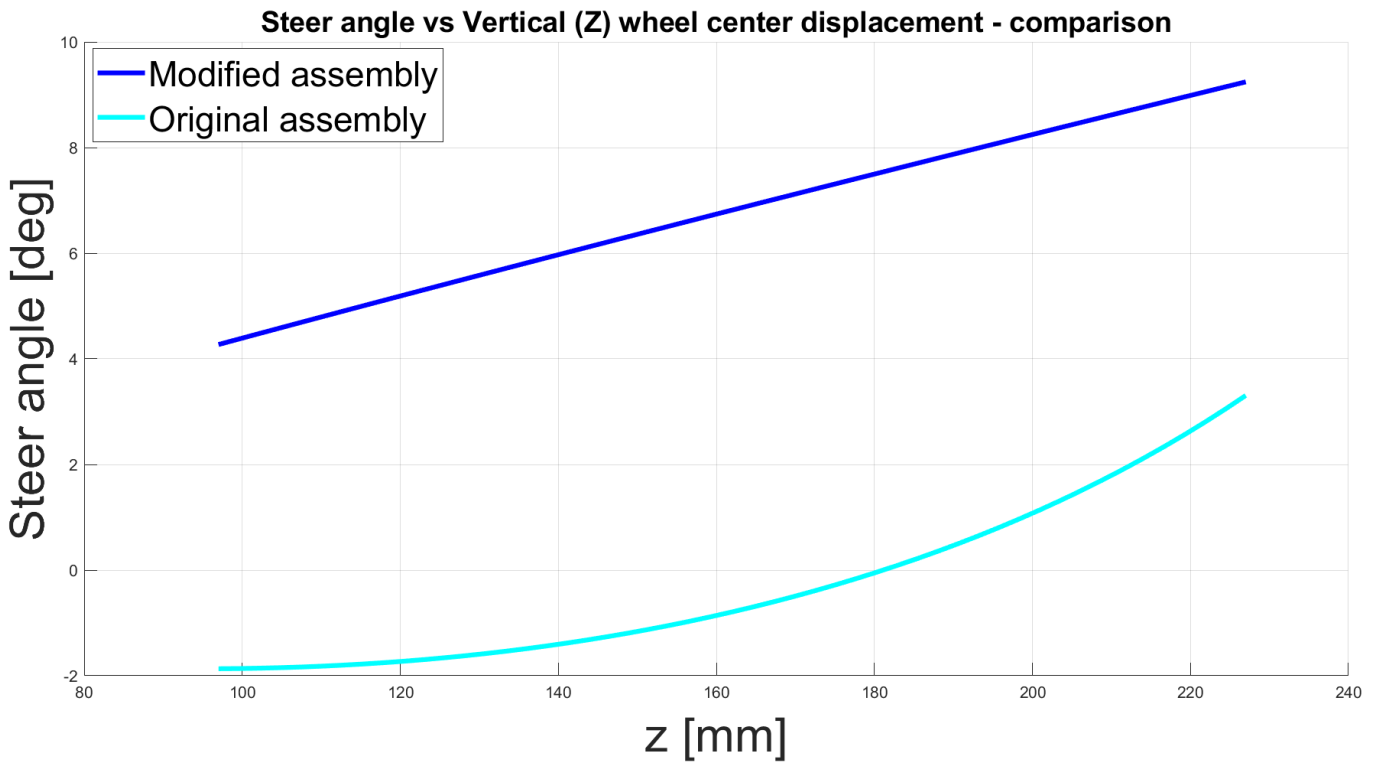


Figure 4.4.8 – Modified VS original assembly: steer angle

Considerations about the steer angle:

- Starting from the lower point of the bouncing, for the same z value of the wheel centre, the difference is around six degrees, and it is constant for all the wheel travel. This difference is imputable to the difference in the tie rod coordinates.
- The two suspensions have a different trend: linear in the modified suspension, parabolic in the original one.

## 4.5 Simulation's results

The purpose of the tests performed on MSC/Adams Car is to understand if there is correspondence between experimental and numerical data. To do that, results are compared to one another. To better understand the difference in the slope of the curves, which is not always evident, it is computed the angular coefficient of each curve, then reported in the tables below the graphs.

*Wheel travel in longitudinal direction*

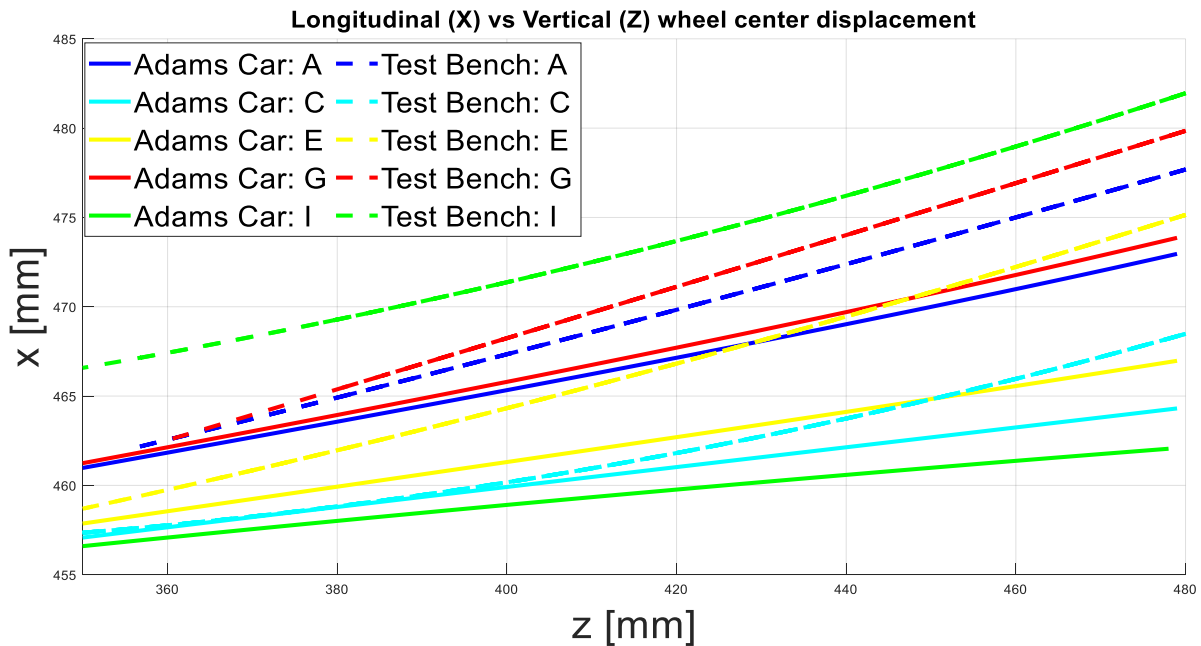


Figure 4.5.1 – Test Bench VS MSC/Adams Car: longitudinal wheel travel

Comments about the graph above:

- Mounting position “A”, “G”, “E”, “C”: for all these four mounting positions, experimental and numerical curves have the same starting point but then they diverge. It means that during the bouncing, test bench suspension suffers more a shift in x direction than the virtual suspension. The difference is about 5 mm, so it can be considered negligible.
- Mounting position “I”: in this position, the suspension has a behaviour different from the others. There is a relevant difference, equal to about 10 mm, between the starting point of the real suspension and the starting point of the model. Moreover, it diverges more, leading to a difference at the end of the test equal to 20 mm.
- The disposition of the curves, except the green one, shows a coherence between Test Bench and MSC/Adams Car.

The divergence between the curves can be underlined by analysing their slope.

The table here below shows that the slope of the test bench curves is higher than MSC/Adams Car ones.

TEST BENCH		MSC/ADAMS	
Curve	Slope	Curve	Slope
A	0.12	A	0.09
C	0.06	C	0.06
E	0.07	E	0.07
G	0.14	G	0.1
I	0.12	I	0.04

Table 4.5.1 – Slope comparison

Wheel travel in lateral direction

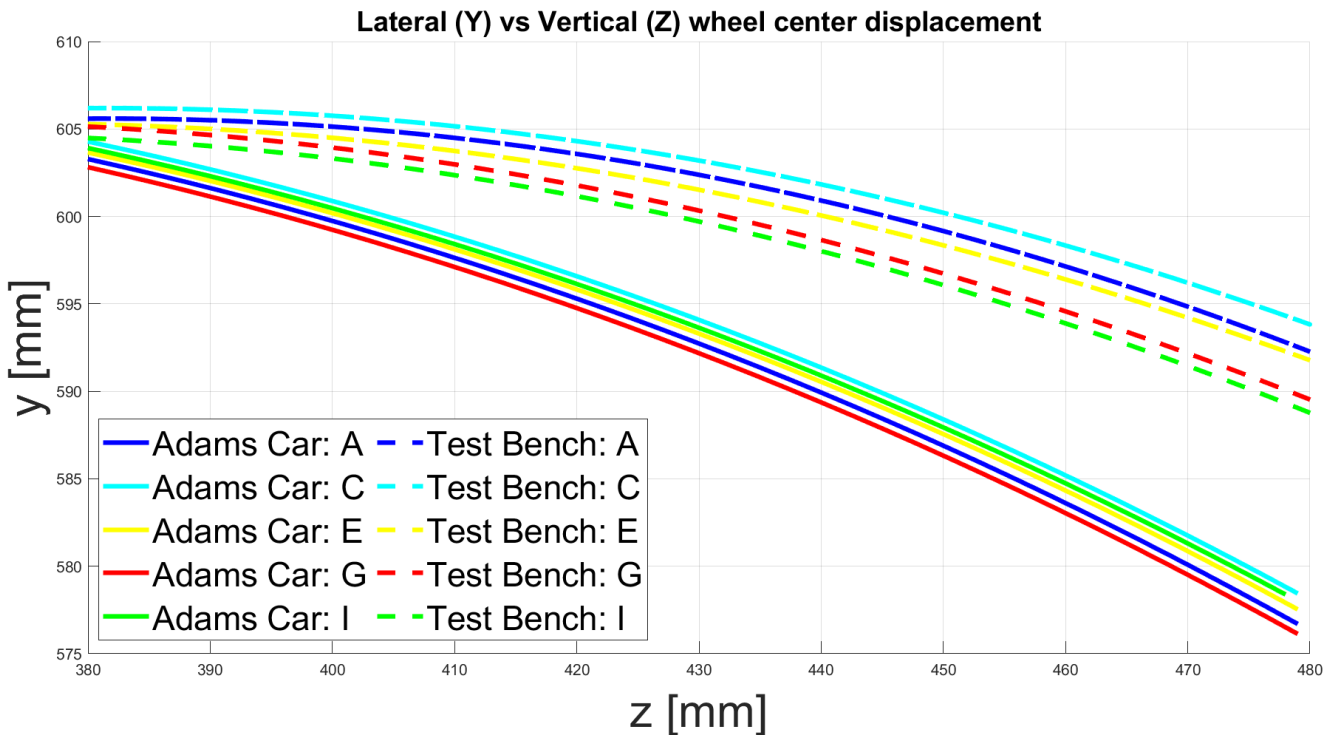


Figure 4.5.2 – Test Bench VS MSC/Adams Car: lateral wheel travel

Comments about the graph above:

- As it happens for the test bench curves, also the ones related to MSC/Adams Car simulations have almost overlapped each other. This behaviour is particularly evident for the virtual model, while the real case is a little bit different. In fact, test bench curves have the same starting point, but the ending point is not coincident. As for what concerns the longitudinal wheel travel, also in the lateral direction there is divergence between curves. It means that, at high z values, the mounting position influences the wheel centre position in y coordinate.
- The other relevant difference is the slope of the curves, as it is possible to note in the tables below. In MSC/Adams Car model, the bouncing leads to a high displacement in lateral direction. The wheel centre moves of about 30 mm while test bench suspension moves only 10 mm. This behaviour is independent from mounting position.

TEST BENCH		MSC/ADAMS	
Curve	Slope	Curve	Slope
A	-0.14	A	-0.23
C	-0.13	C	-0.23
E	-0.17	E	-0.23
G	-0.18	G	-0.23
I	-0.19	I	-0.23

Table 4.5.2 – Slope comparison

Camber angle

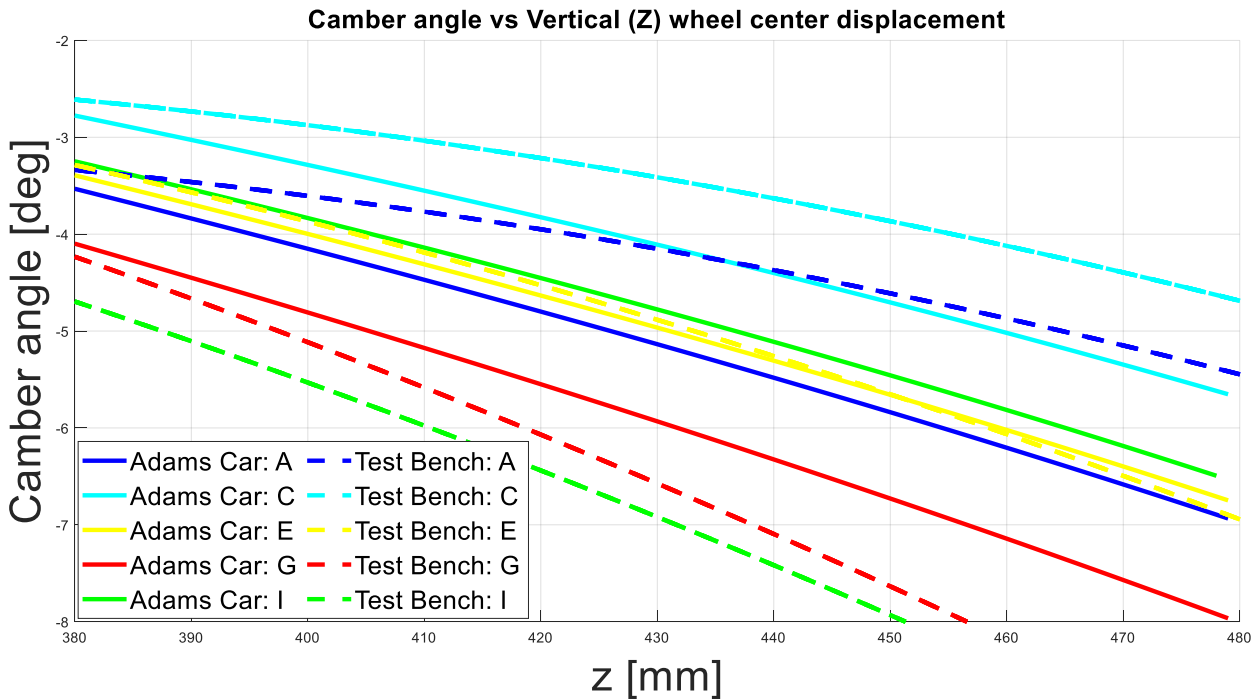


Figure 4.5.3 – Test Bench VS MSC/Adams Car: camber angle

Comments about the graph above:

- Mounting position “E”: this is the central mounting position and in this case the curves are perfectly coincident. The starting and the ending points are the same and the trend is almost equal.
- Mounting position “C” and “A”: these two upper positions lead to a divergence between real suspension’s curves and virtual ones. In detail, during the bouncing, the 3D suspension model, undergoes to a greater variation in camber angle compared to what actually happens.
- Mounting position “G”: this is the lower position, and it shows the opposite behaviour in respect to the upper positions. In fact, again, the two curves (real and numerical) start from the same camber angle value but then they diverge. What is different is that, in this case, the experimental curve suffer for a higher camber angle variation and not the numerical one, as in the previous case.
- Mounting position “I”: this position causes some problems. As in the longitudinal wheel travel case, also camber angle has not a coherent trend in respect to the others, since in this case the two curves start from two different camber values. Apart from this offset (equal to 1.5 degree), the behaviour is equal to the one related to “G” mounting position. They diverge and, also in this case, the real camber angle varies more than the numerical one.

Camber angle variation allows to keep itself constant in respect to the ground, leading to precise driving of the vehicle.

TEST BENCH		MSC/ADAMS	
Curve	Slope	Curve	Slope
A	-0.02	A	-0.03
C	-0.02	C	-0.03
E	-0.03	E	-0.03
G	-0.05	G	-0.04
I	-0.05	I	-0.03

Table 4.5.3 – Slope comparison

Caster angle

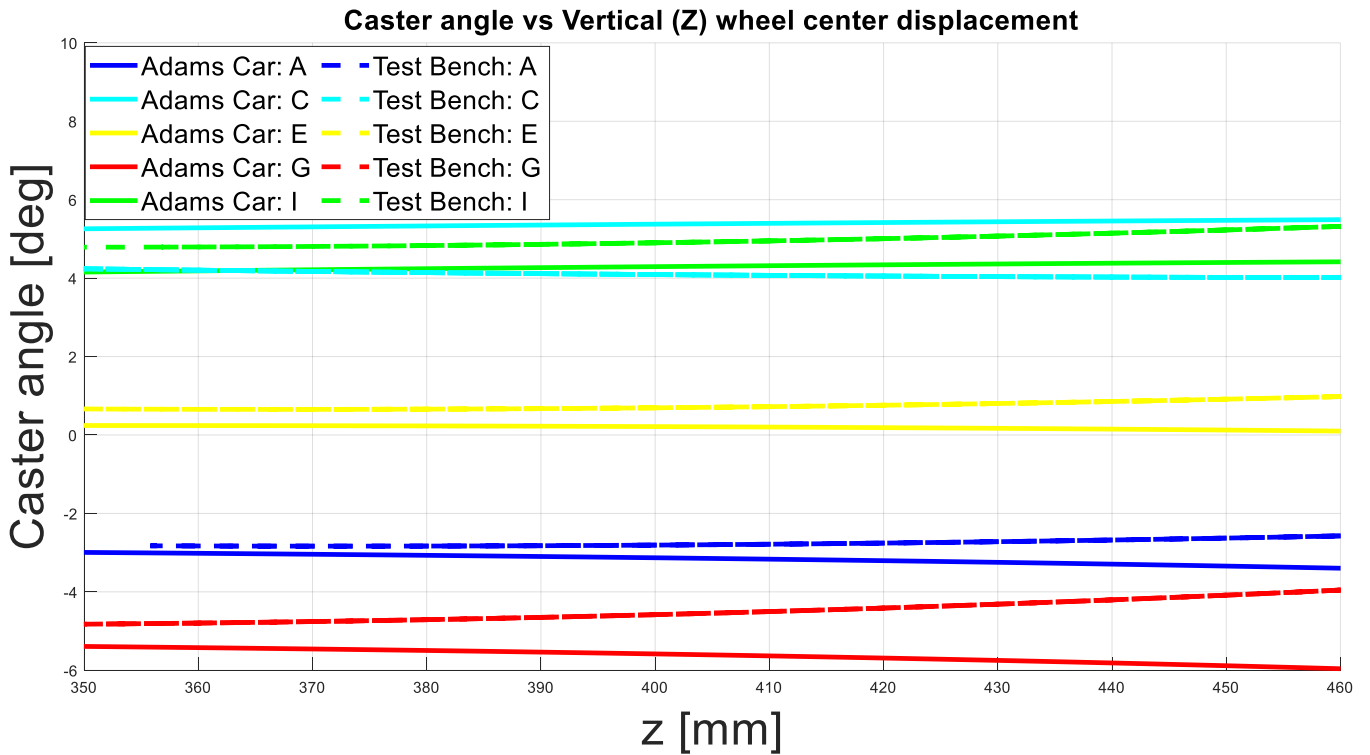


Figure 4.5.4 – Test Bench VS MSC/Adams Car: caster angle

Comments about the graph above:

- Mounting position “A”, “G”, “E”, “C”: for all these four mounting positions, experimental and numerical curves have almost the same starting point but then they diverge a little bit. It is the same situation already seen for the other quantities, but in this case in minor measure.
- Mounting position “I”: as for the other quantities, also for what concerns the caster angle this position leads to an abnormal result. There is a bigger offset between experimental and numerical curve in respect to the other mounting positions.
- All the curves show that caster angle remains unvaried during the bouncing, especially in MSC/Adams Car. In test bench simulations instead, it changes of less than one degree.

TEST BENCH		MSC/ADAMS	
Curve	Slope	Curve	Slope
A	0.00	A	0.00
C	-0.07	C	0.00
E	0.00	E	0.00
G	0.04	G	0.00
I	0.01	I	0.00

Table 4.5.4 – Slope comparison

Steer angle

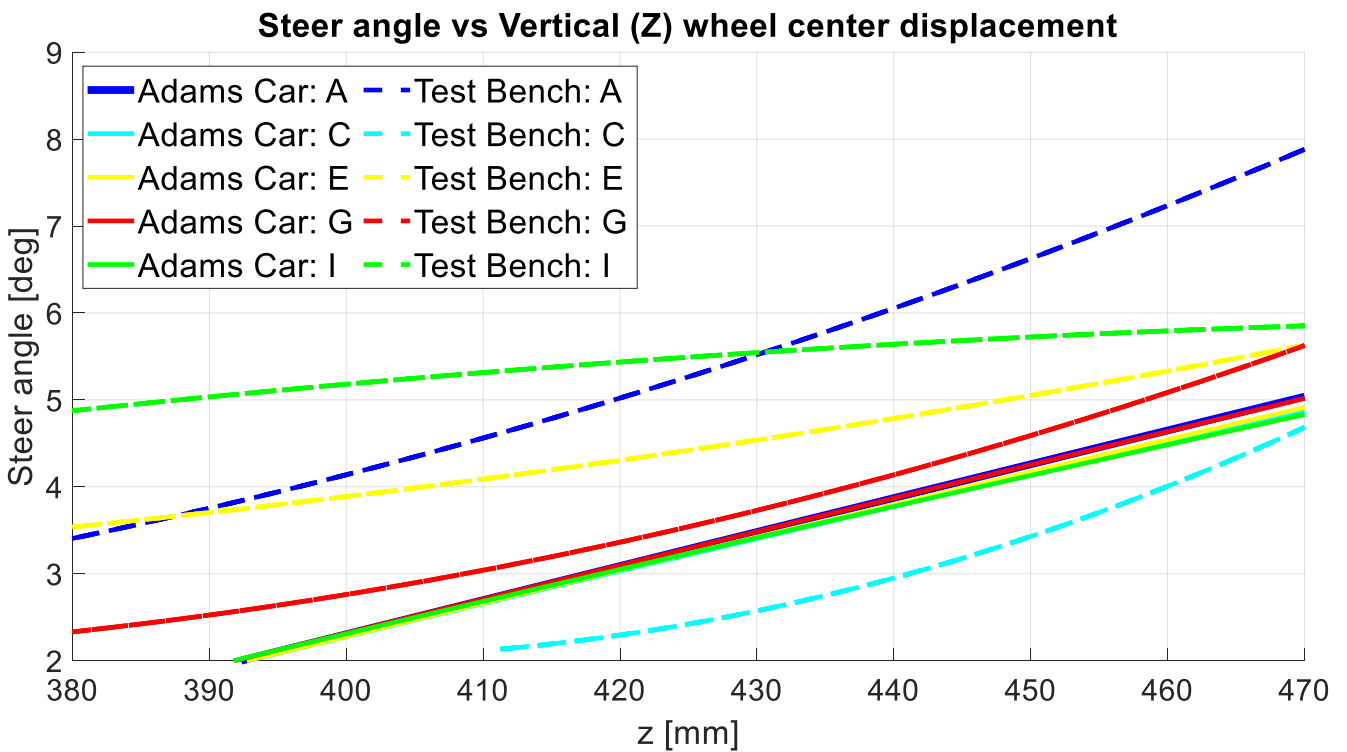


Figure 4.5.5 – Test Bench VS MSC/Adams Car: steer angle

Comments about the graph above:

Steer angle is the only quantity which does not show coherence between numerical and experimental data. This problem is imputable to a failure acquisition of the data in the test bench.

- In MSC/Adams Car, the trend is clear and equal for all the five mounting positions: all the curves start from the same steer angle value, have the same slope and so it is equal also the steer angle variation due to bouncing, equal to 3 degrees.
- In test bench, curves disposition does not make sense. It does not follow a logic, nor the virtual trend. The only thing that is coherent, except for mounting position “I”, is the growing behaviour: steer angle increases by raising up suspension’s wheel centre, but with a very low slope. In light of this, it is possible to say that the test bench gives not reliable results for what concerns this quantity.

TEST BENCH		MSC/ADAMS	
Curve	Slope	Curve	Slope
A	0.06	A	0.04
C	0.05	C	0.04
E	0.03	E	0.04
G	0.05	G	0.04
I	0.01	I	0.04

Table 4.5.5 – Slope comparison

## 4.6 Roll centre influence

The graph below shows that the real steer angle has a different behaviour compared to the expected one. In an ideal situation, as shown below, the steer angle is constant, and it is equal to zero.

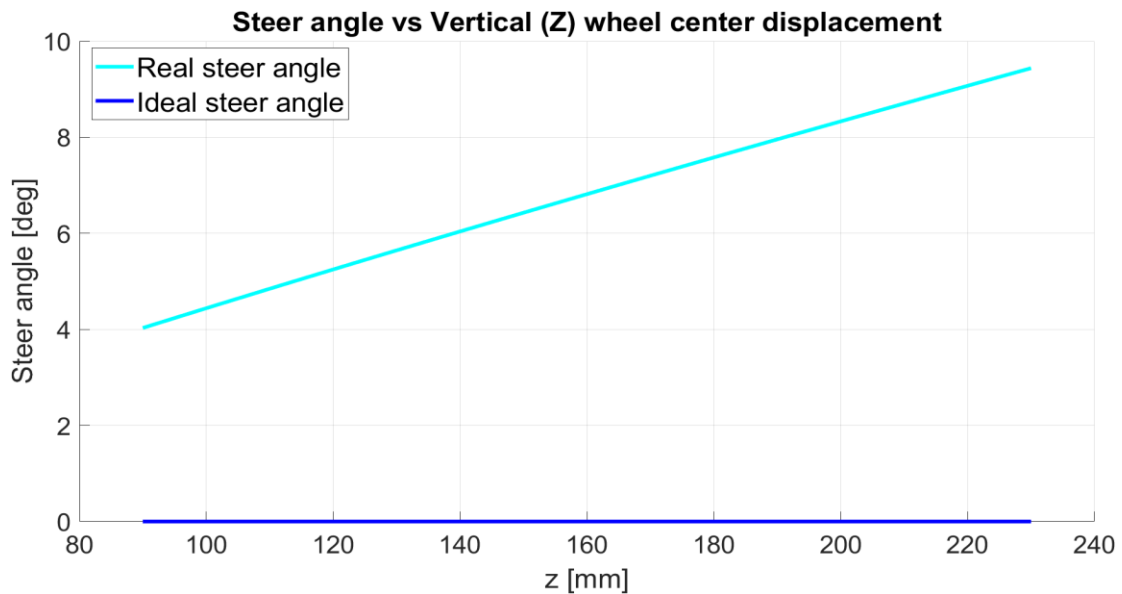


Figure 4.6.1 – Ideal VS Real steer angle

The purpose of this chapter is to explain the nature of this difference. To understand it, it is necessary first to know what “roll centre” is. In the following picture it is possible to see some geometrical points:

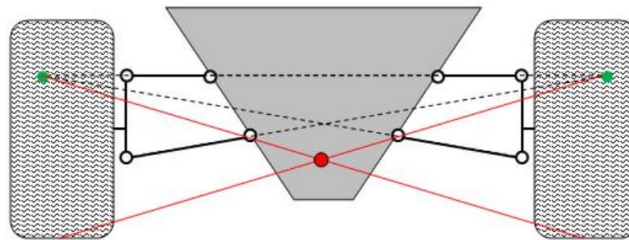


Figure 4.6.2 – Geometrical points [15]

By continuing the lines relative to the lower and the upper control arms, it will be found an intersection point. This point, highlighted in green, is the suspension *instantaneous centre of rotation*. It is a fixed point, and it is the only one the suspension can rotate around [3].

Once both the centres of rotation have been spotted, by tracing the lines that connect them with the contact patch between tyres and ground, the *roll centre* is obtained. It is a theoretical point in which forces between sprung and unsprung masses are exchanged. The importance of this point is all about it since roll motion and therefore lateral dynamics of the vehicle depends on it [15].

Its height can be modified by varying suspension’s arms inclination. For this reason, during the bouncing of the suspension due to vehicle movement, roll centre position could change. The design of the suspension should be done to reduce this variation as much as possible.

On each axle can be spotted a roll centre, therefore, two axes’ vehicles present two different roll centres. It is different also the variation they are subjected to. In detail, on front axle it can vary between 0 and 100 mm, on the rear axle instead it varies more, between 50 and 150 mm [15].

By connecting the roll centres of the two axles, the *roll axle* can be obtained. It is the axis around which the vehicle rotates when subjected to a lateral acceleration.

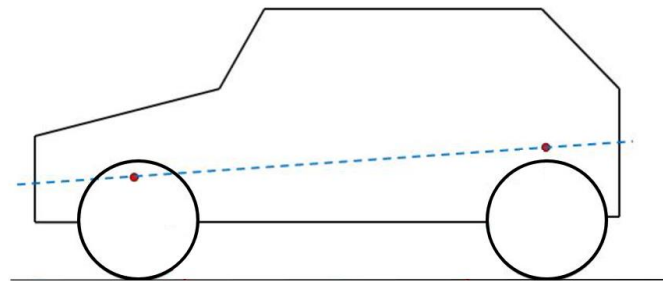


Figure 4.6.3 – Roll axle [15]

Once the roll centre concept is clear, it is possible to get it on MSC/Adams Car suspension model. With the same procedure described above, it is found the instantaneous centre of rotation of both the original and modified suspensions, identified by the red point. In yellow it is drawn also the tie-rod virtual extension.

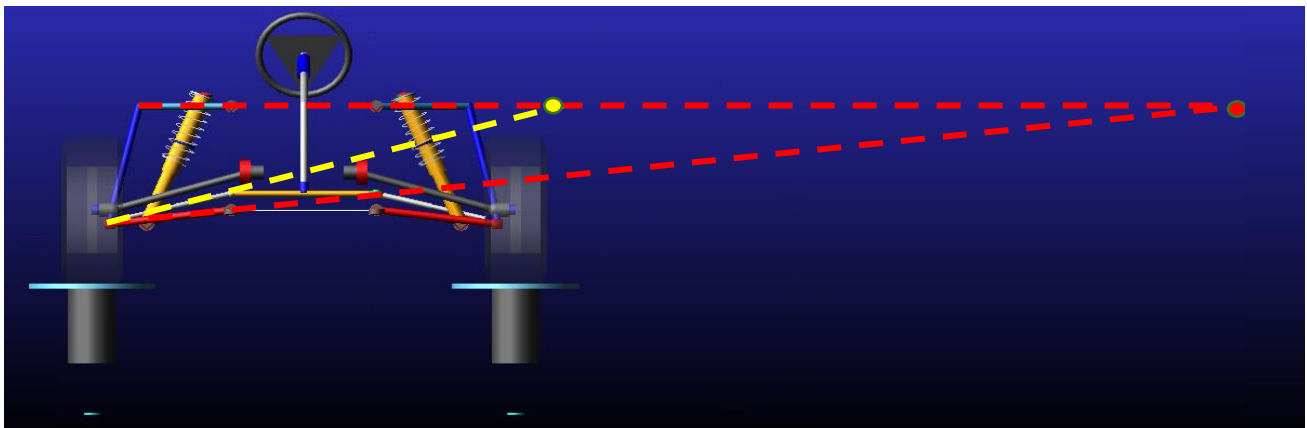


Figure 4.6.4 – Modified suspension's centre of rotation

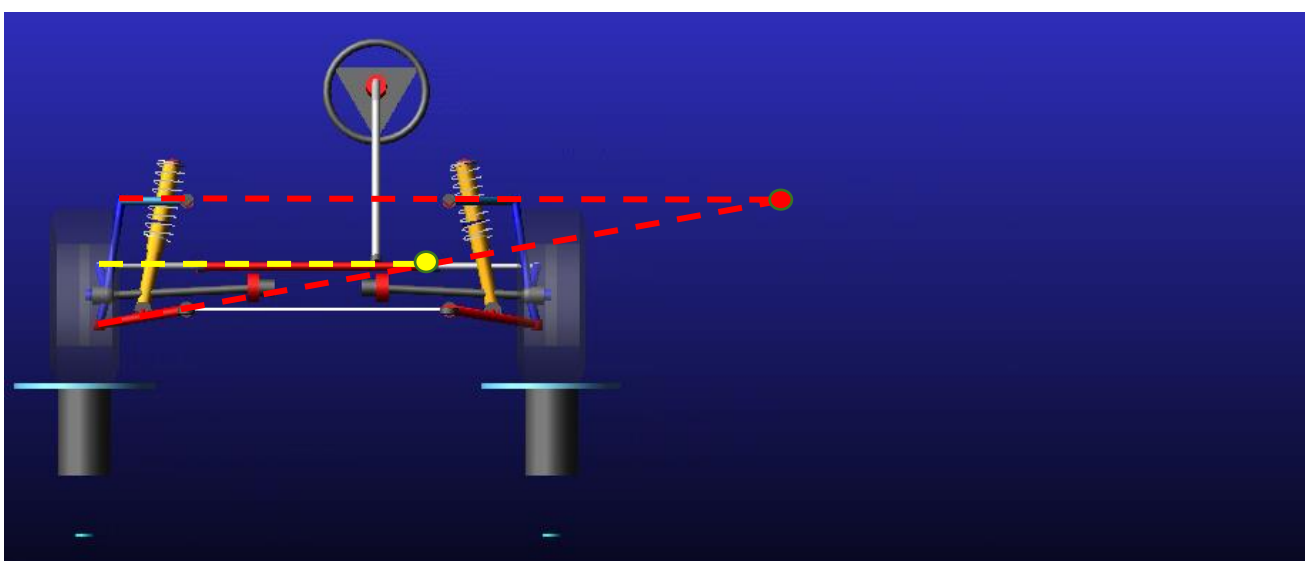


Figure 4.6.5 – Original suspension's centre of rotation

As the pictures above show, because of its geometry, the suspension under analysis does not have the convergence point between lower arm, upper arm, and tie-rod. The variation of the steer angle during wheel centre bouncing can be assigned to this reason.

The consequent hypothesis is that, by varying the steering tie-rod inclination, the steer angle variation during bouncing would consequently change. In detail, by reducing tie-rod slope, the theoretical line which represents the tie-rod extension moves progressively toward the instantaneous centre of rotation, until it reaches it.

Since it is not possible to modify the real suspension, tests are carried on exclusively on MSC/Adams Car model.

The first step is to reduce the inner tie rod z coordinate, by keeping fixed the z coordinate of the outer point. In this way, inclination is reduced, as shown in the picture below, relative to the modified model:

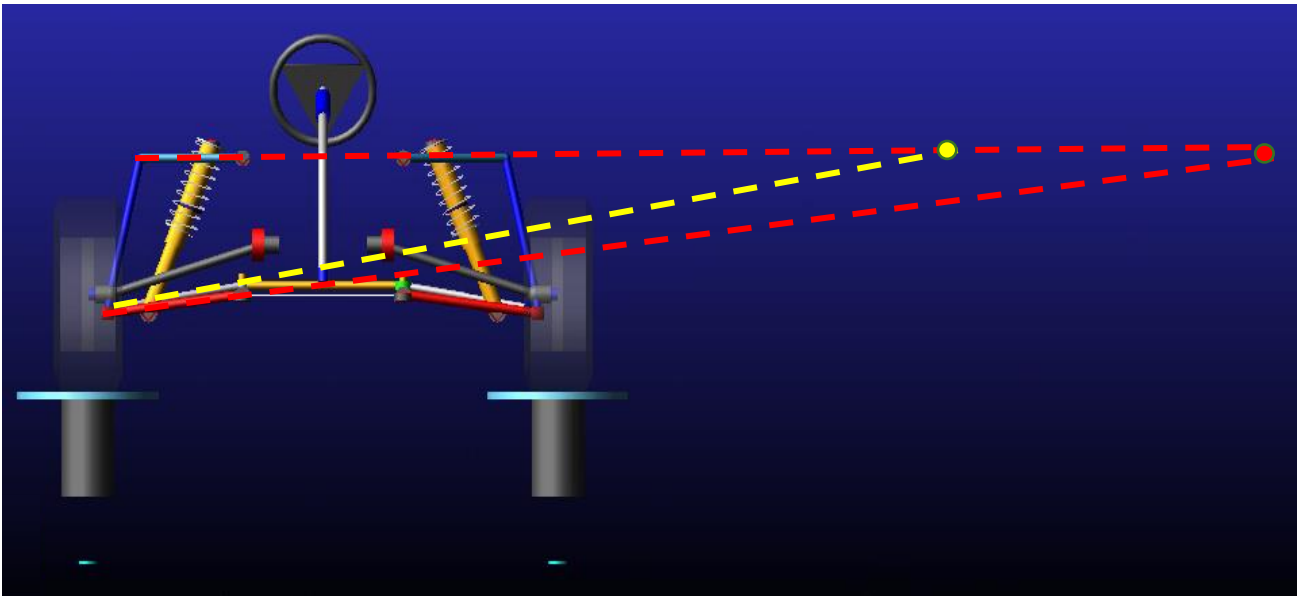


*Figure 4.6.6 – Modified suspension's new tie-rod inclination*

With this new geometrical configuration, it is run a simulation with the same boundary conditions of the previous one. As it was expected, this simulation gives as result a reduction in the steer angle variation.

Here below is reported a plot in which it is possible to compare the curves related to the ideal situation (renamed “ideal template”), the previous test (renamed “test bench template”) and the test performed with the new configuration (renamed “new configuration template”).

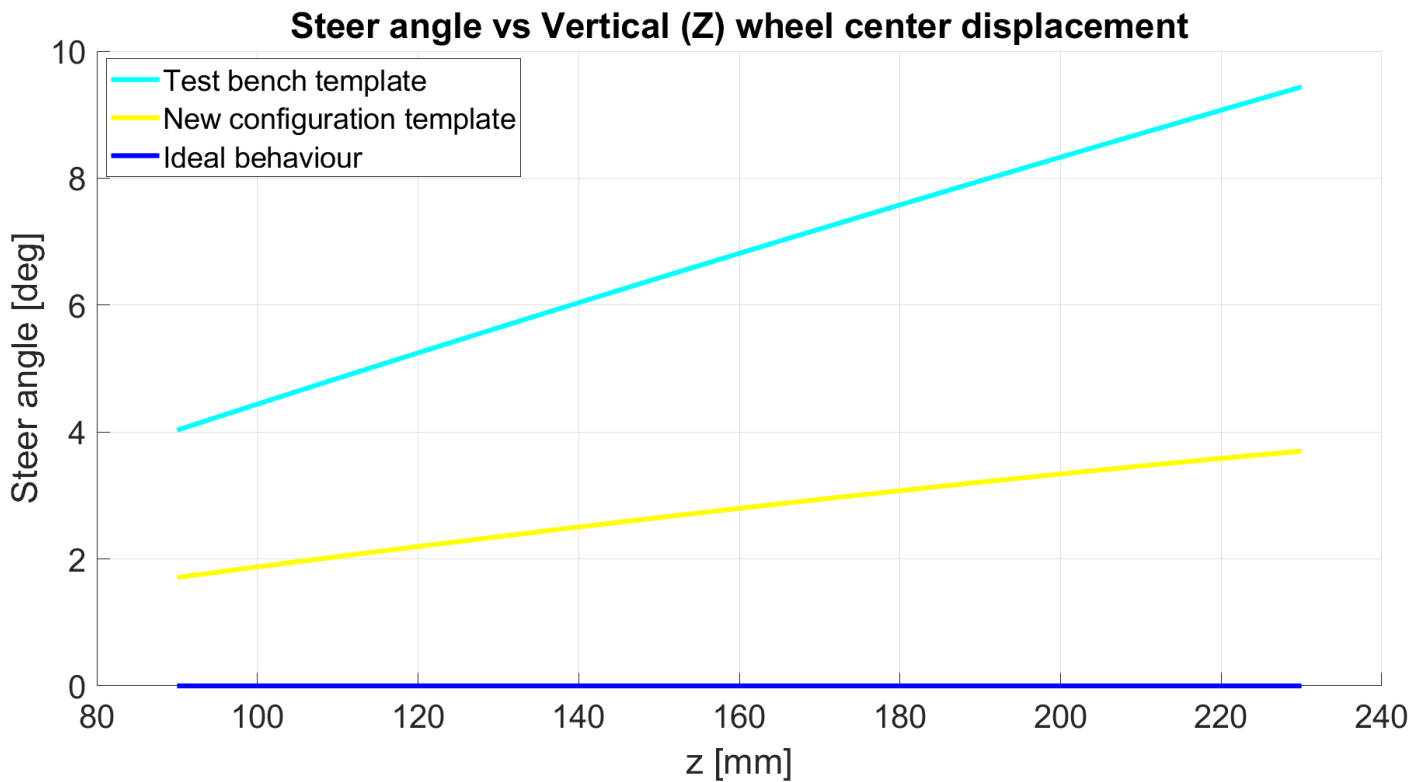


Figure 4.6.7 – Steer angle behaviour

It is possible to note that the steer angle value at the starting point has decreased. Also, its variation diminishes, passing from five to two degrees.

The following tests are performed by decreasing more and more tie-rod inclination, and as consequence the steer angle behaviour moves closer and closer to the ideal case.

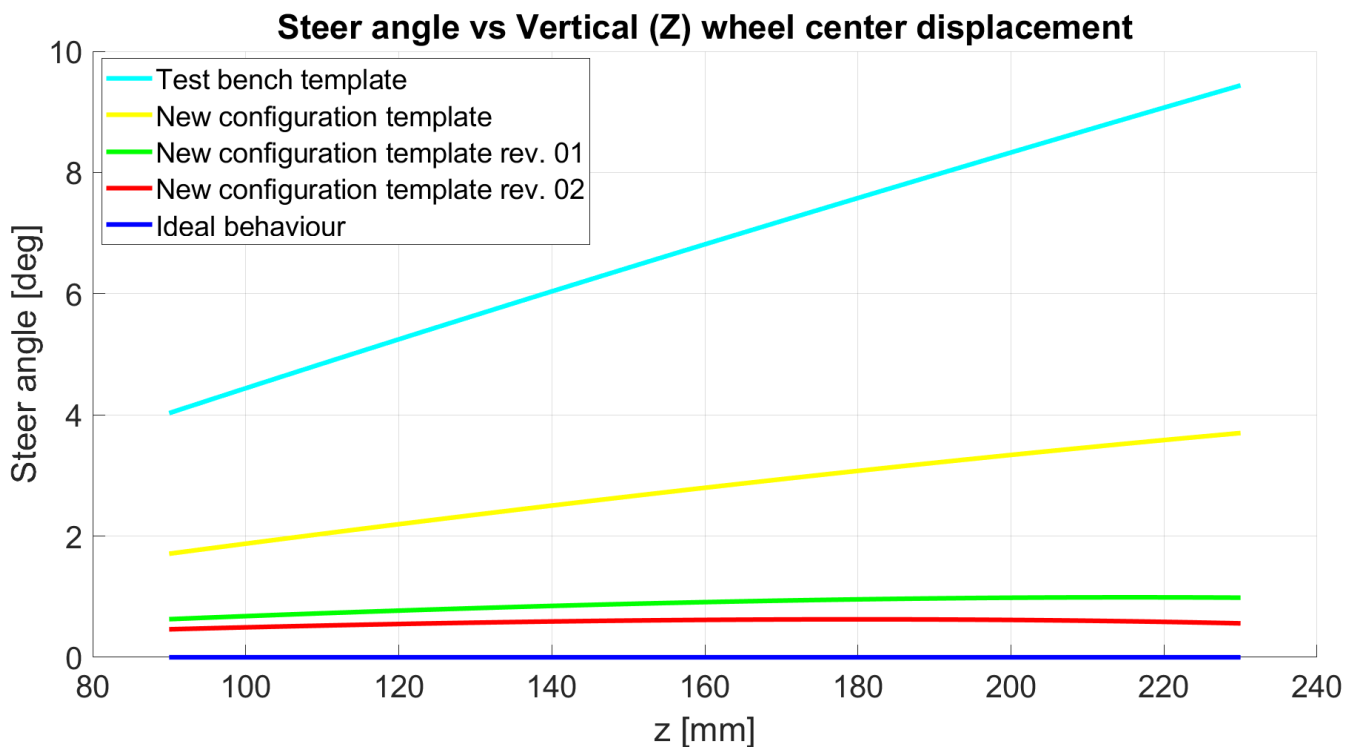


Figure 4.6.8 – Steer angle behaviour

Eventually, to reach the ideal behaviour, the coordinates of the instantaneous centre of rotation are computed. It is done by finding the intersection point between the extension of the upper and lower arms, and the obtained results are:

- $x = -370$
- $y = -3650$
- $z = 785$

By knowing these coordinates, it is possible to find the required coordinates of the tie-rod inner point so that its prolongation exactly intersects the instantaneous centre of rotation.

The following picture shows the ideal template:

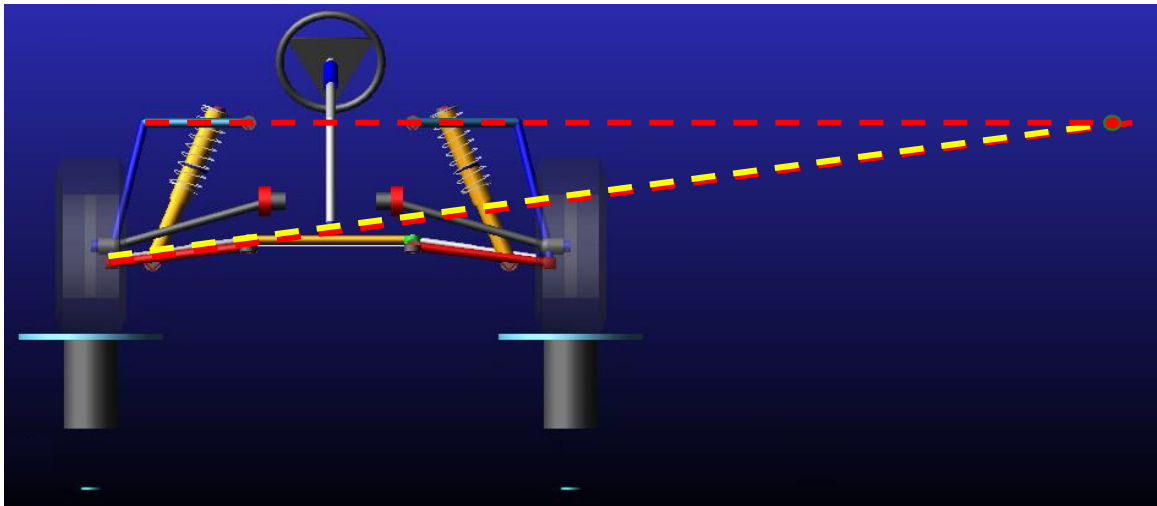


Figure 4.6.9 – Ideal template

The simulation performed with this template confirms what was assumed: the steer angle behaviour in this tie-rod configuration reproduces the ideal trend. The only difference is that it is not perfectly constant during all the bouncing, but it slightly varies because of the non-ideal characteristics of the suspension.

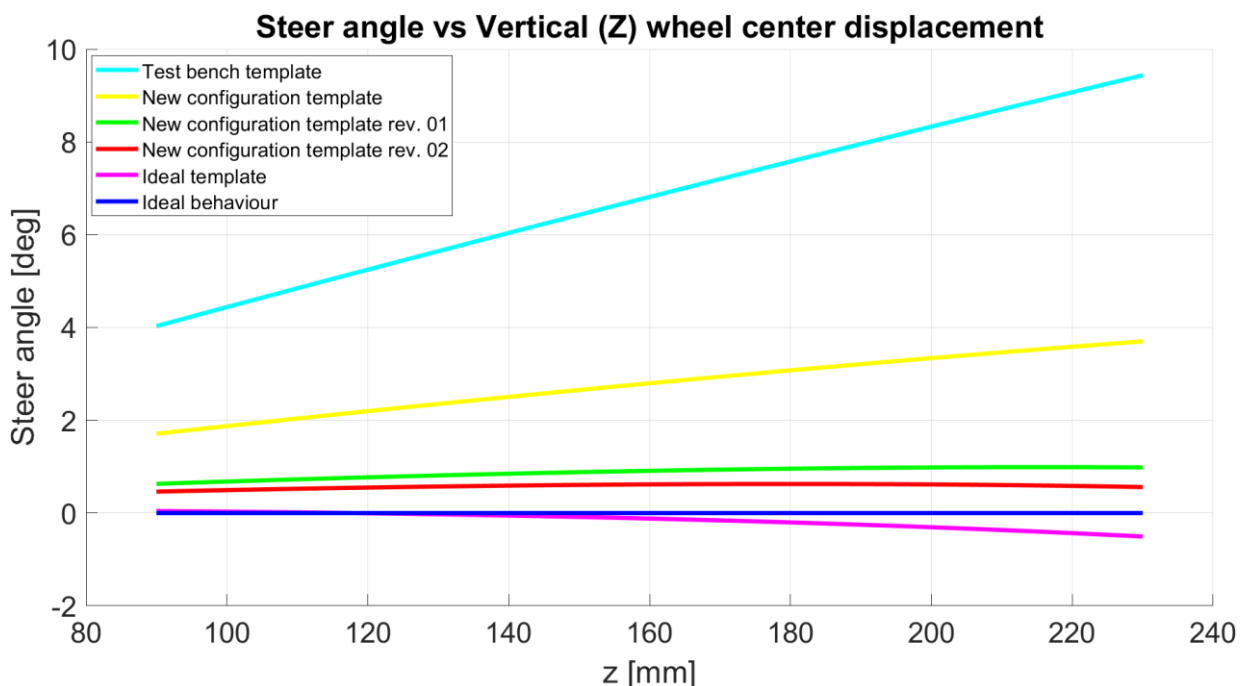


Figure 4.6.9 – Steer angle behaviour

## 5. Choice from catalogue for the construction of an electric motor

### 5.1 Introduction

As already anticipated in the introduction of the thesis, the aim of this chapter is to present the sizing of an electric motor. It is intended to replace the manual work done to operate the jack and to simulate the bouncing of the suspension. The lifting and lowering of the system are done by means of a pantograph cricket. It is a mechanical system, which is actuated by means of a screw. The movement is managed with a cranking. By rotating it clockwise, the suspension rises up, the other way around, if the rotation is counter-clockwise, the suspension is lowered. This spin is done manually, and the idea is therefore to design an electric motor to manage the rotation, so that the movement becomes smoother and more repeatable.

To have a connection between the jack and the motor shaft, since the link is like the one showed in the picture 5.1.1, several solutions are possible:

- Keying of a hook on the shaft at the output of the electric motor.
- Use of an intermediate metal profile coupled by pins both on the jack and on the crankshaft.
- Grinding of the final part of the shaft, until a square section is reached, which allows the assembly of a 24-socket wrench.

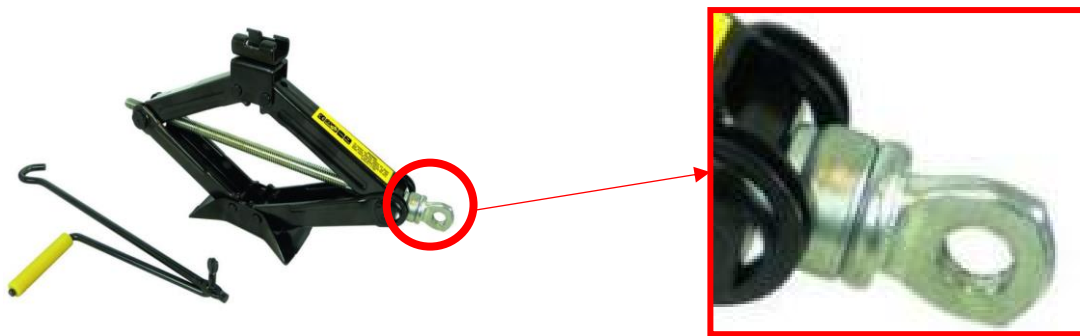


*Figure 5.1.1 – Pantograph cricket [16]*

Considering this last point, a quick solution could be the assembly of a socket wrench directly on a drill, which would also allow an easy reversal of the direction of rotation.

Instead, to use a dedicated electric motor, an advantageous choice in terms of utility is a motor powered by direct current. The latter, in fact, compared to alternating current motors, have a higher speed of inversion of the direction of rotation, which is a fundamental characteristic for simulating the bouncing. On the other hand, however, it will be necessary to use an inverter to convert alternating current into direct one.

## 5.2 Electric motor

Electric motor is a machine that allows the conversion of electric energy into mechanical energy. It is composed by two parts: the stator and the rotor.

The first one is the fixed part of the motor, and it has, inside a chassis, a ferromagnetic core consisting of a certain number of windings. By means of alternating voltage, these windings are excited, and this causes the generation of a rotating magnetic field.

The rotor, instead, is the rotating part of an electric motor. It is located inside the stator and its composition is the same of the fixed part, it means that it has a ferromagnetic core wrapped in windings. Differently from the stator, it is powered with direct voltage.

The interaction between the two magnetic fields causes the generation of the torque.

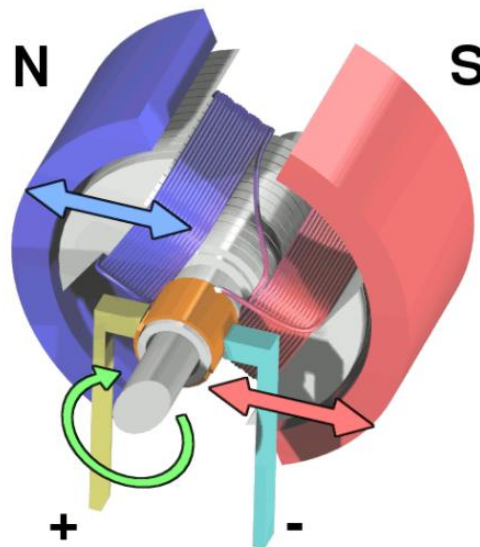


Figure 5.2.1 – Electric motor scheme [17]

These motors can be either direct (DC) or alternating current (AC). Here below are highlighted some differences:

- An AC motor can be powered through a three-phase power, while a DC motor can only exploit single-phase power from batteries or cells.
- DC motors enjoy the automatic start, differently from the AC motors.
- In an AC motor, the frame is fixed, and the magnetic field rotates. In a DC motor it is the opposite.
- AC motors are used for large applications, while for smaller applications it is preferable a DC motor.

For the sizing of the electric motor, it is necessary to know: the forces involved, the rotational speed of the jack, the output power, and the output torque.

Involved forces:

The first step is to compute the weight force, starting from the masses. These are obtained considering the relation between the volume, obtained by the 3D cad, and the density, known by knowing the material of the suspension.

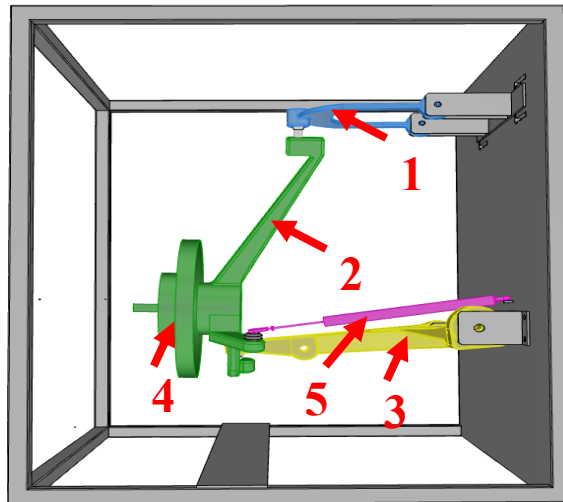


Figure 5.2.2 – Suspension parts mapping

$$V_1 = 387338.11 \text{ mm}^3 = 3.87 \cdot 10^{-4} \text{ m}^3$$

$$V_2 = 1850266.90 \text{ mm}^3 = 1.85 \cdot 10^{-3} \text{ m}^3$$

$$V_3 = 2457121.71 \text{ mm}^3 = 2.46 \cdot 10^{-3} \text{ m}^3$$

$$V_4 = 3358600 \text{ mm}^3 = 3.36 \cdot 10^{-3} \text{ m}^3$$

Parts 1 and 3 are made of Aluminium alloy, which density is  $\rho_{aluminium} = 2700 \frac{kg}{m^3}$ . It follows that:

$$m_1 = 1.1 \text{ kg}$$

$$m_3 = 6.7 \text{ kg}$$

Part 2 is instead in cast-iron, which has a density equal to  $\rho_{castiron} = 7800 \text{ kg/m}^3$ . The mass will be then:

$$m_2 = 14.4 \text{ kg}$$

The wheel is simulated by a plywood wheel, whose density is  $\rho_{wood} = 410 \frac{kg}{m^3}$ . Its mass is therefore:

$$m_4 = 1.4 \text{ kg}$$

The masses of the three potentiometers directly supported by the suspension could be neglected but, since their exact values are reported in the datasheets, it was easy to obtain them, which sum is:

$$m_5 = 0.3 \text{ kg}$$

The total mass of the system is given by the sum of all these values:

$$m_{tot} = 23.9 \text{ kg}$$

The resulting weight force is therefore:

$$F_p = 234.5 \text{ N}$$

Since both the upper and the lower arms are hinged to the test bench, the jack actually supports a lower force. To be able to know the real weight, the suspension is schematized with three different free body diagrams, as shown below:

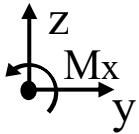


Figure 5.2.3 – Coordinate system

1) **Upper control arm**

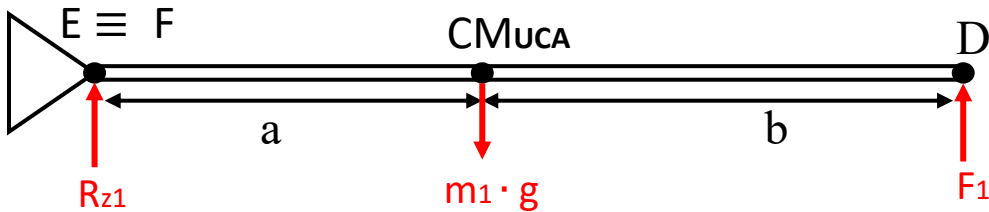


Figure 5.2.4 – Upper control arm free body diagram

2) **Lower control arm**

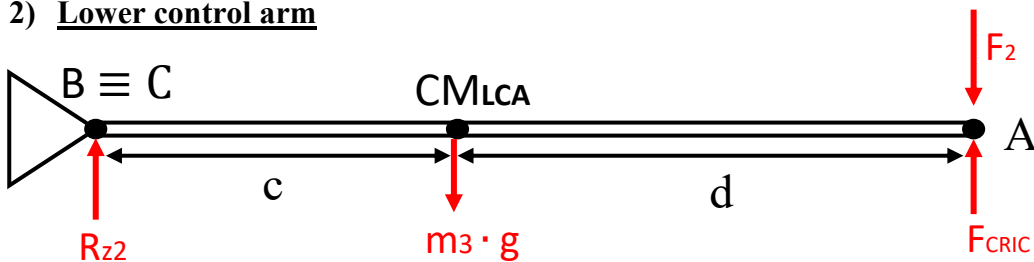


Figure 5.2.4 – Lower control arm free body diagram

3) **Wheel + central part + potentiometer**

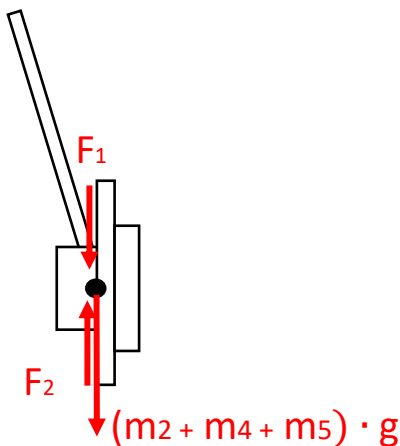


Figure 5.2.5 – Wheel and central part free body diagram

The centre mass position is instead obtained by MSC/Adams Car model. It follows:

$$a = 141.35 \text{ mm}$$

$$b = 207.65 \text{ mm}$$

$$c = 203.50 \text{ mm}$$

$$d = 253.90 \text{ mm}$$

Equations for translational and rotational static equilibrium:

1)

$$\uparrow) R_{z1} + F_1 - m_1 \cdot g = 0 \quad (5.2.1)$$

$$\text{E} \curvearrowleft -m_1 \cdot g \cdot a + F_1 \cdot (a + b) = 0 \quad (5.2.2)$$

2)

$$\uparrow) R_{z2} - m_3 \cdot g - F_2 + F_{CRIC} = 0 \quad (5.2.3)$$

$$\text{B} \curvearrowleft -m_3 \cdot g \cdot c - F_2 \cdot (c + d) + F_{CRIC} \cdot (c + d) = 0 \quad (5.2.4)$$

3)

$$\uparrow) -F_1 - (m_2 + m_4 + m_5) \cdot g + F_2 = 0 \quad (5.2.5)$$

Solving the system above, forces values are found:

$$F_1 = 4.4 \text{ N}$$

$$F_2 = 162.3 \text{ N}$$

$$F_{CRIC} = \mathbf{191.5 \text{ N}}$$

The jack therefore actually sustains the 80% of the real weight.

### Rotational speed of the jack

For the computation of the velocities, five of the several tests performed are analysed. In detail, it is computed the speed for each of them by knowing the time taken for the wheel to rise by a known number of millimetres and it is later averaged. Here below the results:

- 1)  $\frac{170 \text{ mm}}{50 \text{ s}} = 3.40 \frac{\text{mm}}{\text{s}}$
- 2)  $\frac{138 \text{ mm}}{45 \text{ s}} = 3.10 \frac{\text{mm}}{\text{s}}$
- 3)  $\frac{104 \text{ mm}}{32 \text{ s}} = 3.25 \frac{\text{mm}}{\text{s}}$
- 4)  $\frac{110 \text{ mm}}{39 \text{ s}} = 2.82 \frac{\text{mm}}{\text{s}}$
- 5)  $\frac{167 \text{ mm}}{47 \text{ s}} = 3.55 \frac{\text{mm}}{\text{s}}$

$$V_m = 3.22 \frac{\text{mm}}{\text{s}} = 0.00322 \frac{\text{m}}{\text{s}}$$

### Output power

Knowing both the force and the speed, multiplying them, it is computed the power:

$$P = F_{CRIC} \cdot V_m = 191.5 \text{ N} \cdot 0.00322 \frac{\text{m}}{\text{s}} = 0.62 \text{ W}$$

To be able to compute the required output power, it must be taken into account also the friction, which causes losses. The efficiency for a screw is lower than 0.5, therefore the torque delivered by the electric motor must be higher.

Assuming, to be conservative, an efficiency equal to:  $\eta = 0.4$ , the required torque is:

$$P_m = \frac{P}{\eta} = \frac{0.62}{0.4} = 1.54 \text{ W}.$$

### Output torque

In order to ascertain the torque, it is now necessary to calculate the rotation speed of the jack, schematized below.

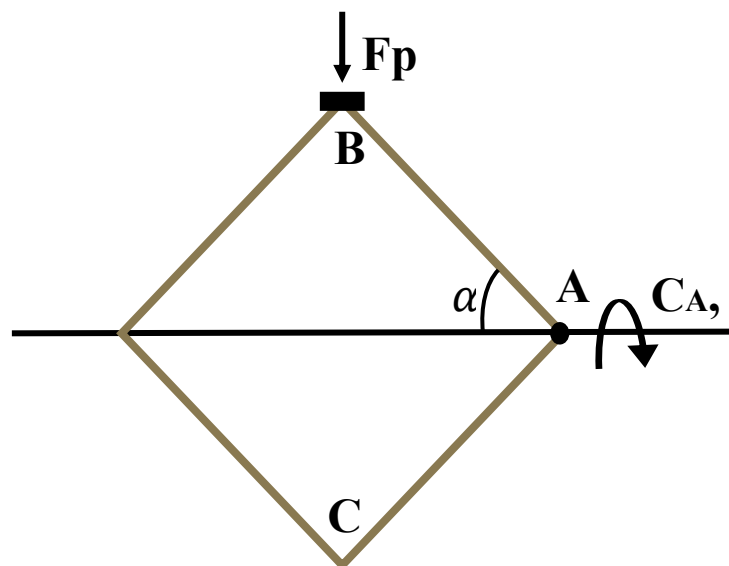


Figure 5.2.6 – Jack free body diagram

Since point B has a velocity which depends on the geometry of the jack, that continuously changes, it is chosen a position according to which the wheel centre stands in the middle of the excursion. It means that it is distant 415 mm from the origin in vertical direction. In that instant, point B stands at about 198 mm.

**Data:**

$$AB = AC = l = 0.14 \text{ m}$$

$$v_B = 3.22 \frac{\text{mm}}{\text{s}}$$

$$h = 0.195 \text{ mm}$$

$$\frac{B\hat{A}C}{2} = \alpha$$

From the geometry of the jack, it follows:

$$l \cdot \sin\alpha = \frac{h}{2} \rightarrow \alpha \approx 45^\circ \tag{5.2.6}$$

$$v_{A/B} = \omega_{A/B} \cdot l \tag{5.2.7}$$

$$v_{A/C} = \omega_{A/C} \cdot l \tag{5.2.8}$$

$$\vec{V}_A = \vec{V}_B + \vec{\omega}_{A/B} \cdot \vec{l} = \vec{V}_C + \vec{\omega}_{A/C} \cdot \vec{l} \tag{5.2.9}$$

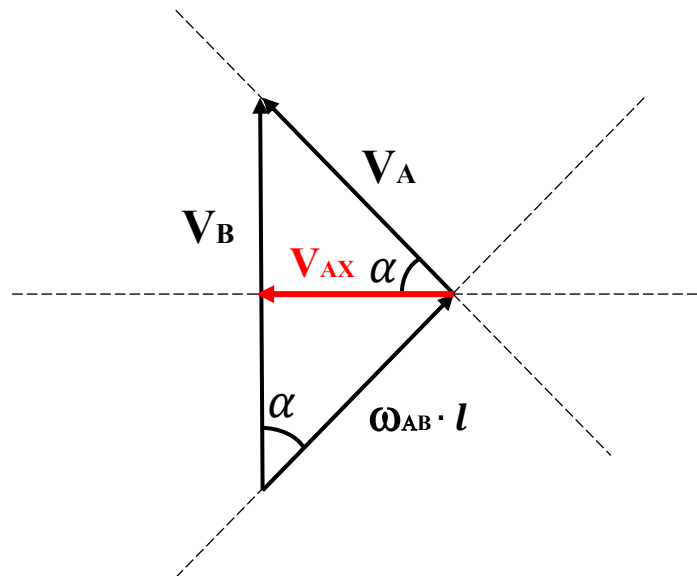


Figure 5.2.7 – Velocity triangle

This triangle is built knowing that point B velocity has only a vertical component and that point A velocity relative to point B is perpendicular to AB segment.

$$V_A = V_B \cdot \sin\alpha = 2.28 \frac{\text{mm}}{\text{s}} \tag{5.2.10}$$

It follows that:

$$V_{AX} = V_A \cdot \cos\alpha = 1.6 \frac{\text{mm}}{\text{s}} \tag{5.2.11}$$

Considering the thread pitch,  $p$ , equal to 2 mm, dividing the horizontal component of the speed by it, it is obtained the angular speed:

$$\omega_m \approx 5 \frac{\text{rad}}{\text{s}}$$

As confirmation for this result, angular speed is computed also by considering that for each test, the crank was turned 40 times and that the time spent for each lifting/lowering of the suspension was about 47 s. By dividing these two values, it is obtained once again an angular speed  $\approx 5 \text{ rad/s}$ . Now that also angular speed is known, it is possible to compute the output torque:

$$C = \frac{P_m}{\omega_m} = 0.30 \text{ Nm} = \mathbf{300 \text{ Nmm}}$$

To confirm that what was calculated is correct, some checks are made:

1) *Suspension's weight computation:*

Using a hook scale, the suspension is weighed. It results in a weight of 18 kg. Considering that about 20% of the weight is supported by the hinges, and considering the inaccuracy of the measurement, the computed weight can be confirmed.

2) *Torque computation:*

Since it was not available a torque wrench with a high enough sensibility, an indirect measurement was made. By mounting the crank to the jack, some masses were added to the end of the crank, until the value which makes it rotate was reached. By considering the imprecision of the measurement, this test was repeated several times. By averaging the various results, it was obtained a mass of 0.16 kg, corresponding to 1.57 N. This is the value of the force applied to the end of the crank. The arm, measured by means of a meter, is 20 cm. The resulting torque value is equal to 0.31 Nm, which perfectly confirms what has been calculated.

Here below it is reported the trend of point A velocity in horizontal direction, in relation to  $\alpha$  angle.

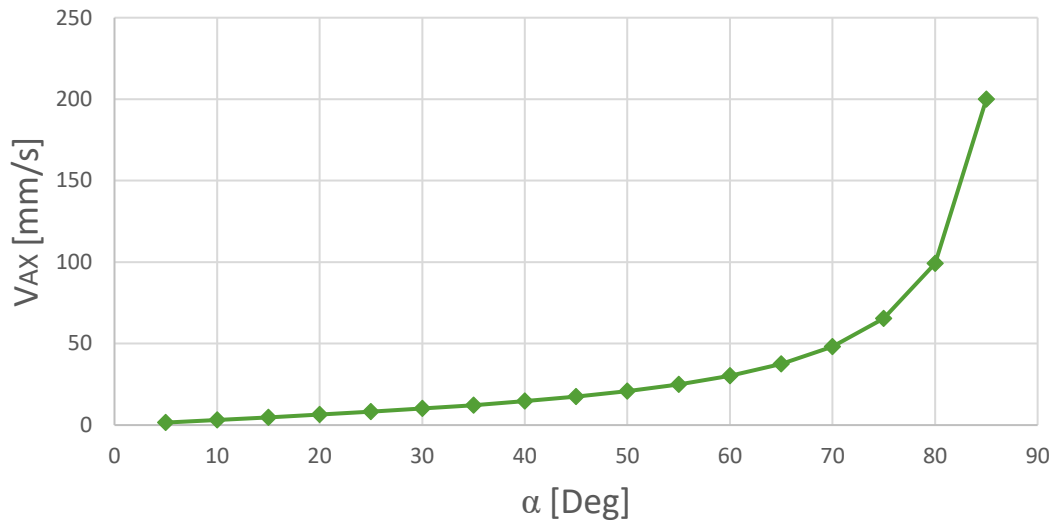


Figure 5.2.8 –  $V_{AX}$  VS  $\alpha$

The interesting range is  $30 \text{ deg} < \alpha < 60 \text{ deg}$ , angle values for which the wheel centre stands between 350 mm and 480 mm, which represent the lower and the upper limits. Going over these limits, the test bench does not react in the correct way, so they are not taken into consideration.

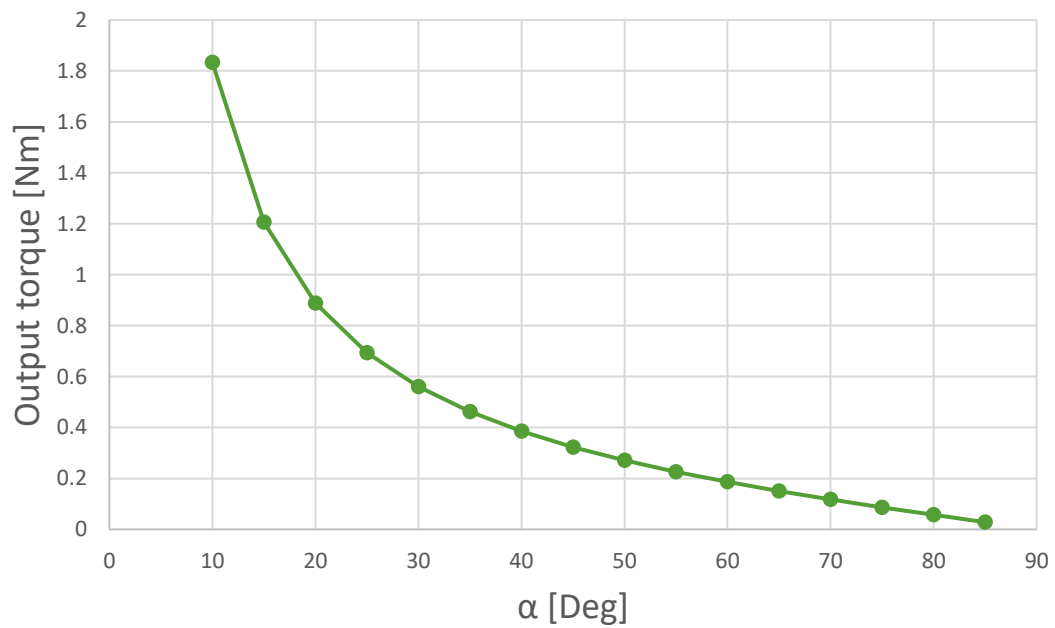


Figure 5.2.9 – Torque VS  $\alpha$

The graph above highlights that, for lower  $\alpha$  values, the required torque increases. The maximum value is 1.8 Nm. Considering a safety factor of 1.5, it would be appropriate to have a maximum derivable torque equal to 2.7 Nm.

Since the required power is very low, the motor angular speed might be increased. Consequently, also the suspension lifting/lowering speed would raise, and bouncing would be much plausible.

A more realistic speed would be ten times higher than the one used till now. It means that for  $\alpha = 45$ , as in the previous case,  $\omega_M$  would be equal to  $55 \text{ rad/s}$ .

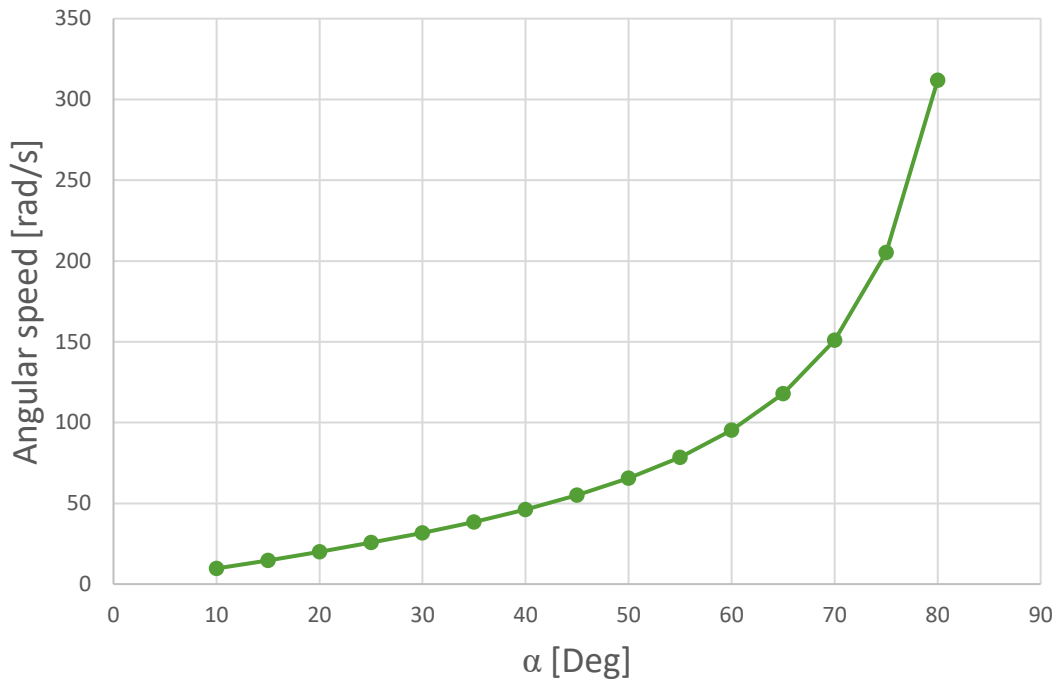


Figure 5.2.10 – Angular speed VS  $\alpha$

Under this assumption, the higher speed reached is about  $300 \frac{\text{rad}}{\text{s}}$ . The output torque is not affected by this variation and the power consequently rises to  $16.8 \text{ W}$ .

In conclusion, here below the summary of the necessary characteristics:

Angular speed	$\omega_m$	300 [rad/s]
Output torque	$C_m$	2.7 [Nm]
Potenza	$P_m$	16.8 [W]

Table 5.2.1 – Characteristics summary

Knowing these values, it is possible to choose from a catalogue an electric motor which respect these requests.

## 6. Conclusions

The aim of this thesis was to understand how a double wishbone suspension reacts to a bouncing motion in terms of camber, caster, and steer angles. The idea was to simulate a real situation in which a car runs into small obstacles as bumps, gutters, or, in general, unevenness of the road.

The importance of the study presented in this thesis is confirmed by the fact that comfort, handling, and safety are strongly affected by the suspension behaviour.

For what concerns *camber angle*, which aim is to increase the adherence, it not only depends on the driving due to suspension and steering movement, but also on the mounting position of the upper control arm. In the simulations done, its variation is, as an average, around 4 degrees, but, for some different mounting positions, it is lower. The most relevant aspect is that, in the analysed suspension, independently from the chosen mounting position, the camber angle value is too large, ranging between -3 and -8 degrees, while the optimal range is  $-0.5 \div -3$ . This can be assigned to the upper arms, considerably shorter than the lower ones. When cornering, the tire tends to deform towards the centre of the curve and there would be grip only on the outside of the tire. A negative camber angle which is within the optimal range, compensates for this behaviour, increasing adherence and thus improving driving. On the other hand, if it is too much negative, there would be an uneven and premature wear of the tire and moreover, compromising driving stability. The mounting position that comes closest to the request is the one identified with the letter C.

The second angle under analysis is the *caster angle*, which the speed necessary to return to the straight position depends on. While cornering, it positively influences camber angle, by making it more negative on the outside wheel and the other way around on the opposite one. To obtain a better driving feeling, it should be in the range  $+3 \div +5$  degrees. Considering this, there are only two mounting positions that comply with this requirement, C and I.

As a last point, attention focuses on the *steer angle*. Its study on the test bench was not easy because of inaccuracies of the potentiometer, but MSC/Adams Car simulations gave good results. An ideal steer angle must have a constant value as the height of the wheel centre varies, but, according to the simulations, its value changes by about 3 degrees for a wheel centre variation in vertical direction of 80 mm. Analysing the geometry of the suspension, the cause of this problem lies on the fact that, due to the way it is built, there is not convergence in the instantaneous centre of rotation between the lower arm, the upper arm, and the tie-rod. For this reason, the subsequent analysis is performed with a variation of the geometry on MSC/Adams Car model: the coordinates have been changed so that the convergence point was reached, leading to an almost ideal behaviour of the steering angle. Another important point to underline is that none of these quantities particularly suffer from hysteresis. It means that the suspension behaves almost in the same way both while lifting and lowering.

To have results that better reflect reality it is still necessary to improve the activation system of the jack. For this reason, the possibility of using an electric motor has been studied, obtaining the necessary values of speed, torque, and power.

## 7. Reference

- [1] PoliTO Suspension Test Bench, 2020.
- [2] [https://it.wikipedia.org/wiki/Sospensione\\_\(meccanica\)](https://it.wikipedia.org/wiki/Sospensione_(meccanica))
- [3] “Motor Vehicle Mecanics” and “Dynamic Design of Machines” personal notes
- [4] <https://www.f-tech-motorsport.com/>
- [5] <https://www.suspensiondesigner.com/kpi-static-camber/>
- [6] [http://street.umn.edu/VehControl/javahelp/HTML/Definition\\_of\\_Vehicle\\_Heading\\_and\\_Steering\\_Angle.htm](http://street.umn.edu/VehControl/javahelp/HTML/Definition_of_Vehicle_Heading_and_Steering_Angle.htm)
- [7] [https://en.wikipedia.org/wiki/Steering\\_ratio](https://en.wikipedia.org/wiki/Steering_ratio)
- [8] [https://www.researchgate.net/figure/A-front-wheel-steering-FWS-vehicle-and-the-Ackerman-condition\\_fig1\\_224929833](https://www.researchgate.net/figure/A-front-wheel-steering-FWS-vehicle-and-the-Ackerman-condition_fig1_224929833)
- [9] <https://www.moogparts.eu/blog/double-wishbone-suspension.html>
- [10] [https://en.wikipedia.org/wiki/Double\\_wishbone\\_suspension](https://en.wikipedia.org/wiki/Double_wishbone_suspension)
- [11] <https://www.moogparts.eu/blog/double-wishbone-suspension.html>
- [12] <https://www.omnicalculator.com/physics/car-mass-center>
- [13] <https://en.wikipedia.org/wiki/Wheelbase>
- [14] MSC/Adams Car
- [15] <http://meccanicadelveicolo.com/2017/08/14/posizione-centro-rollio/>
- [16] <https://www.amazon.it/CARPOINT-0613002-Martinetto-Losanga-1500Kg/dp/B002VXC0AW>
- [17] [https://it.wikipedia.org/wiki/Macchina\\_in\\_corrente\\_continua#/media/File:Electric\\_motor\\_cycle\\_1.png](https://it.wikipedia.org/wiki/Macchina_in_corrente_continua#/media/File:Electric_motor_cycle_1.png)